Republic of Iraq
Ministry of Higher Education
and Scientific Research
University of Babylon
Faculty of Materials Engineering
Department of Metallurgical Engineering

Effects of Cold Rolling on corrosion and Wear Behavior of Magnesium Biomaterial Alloy

A Dissertation
Submitted to the Department of Metallurgical Engineering at the Faculty Materials Engineering / University of Babylon in Partial Fulfillment of the Requirements for the degree of Master in Materials Engineering / Metallurgical

By

Zaid Ali Hadi Abbas

(B.Sc. in Metallurgical Engineering - 2003)

Supervised by

Prof. Zuheir Talib Khulief (PhD)

2023 A.M **1444 A.H**

بسم الله الرحمن الرحيم

نَرْفَعُ دَرَجَاتٍ مَنْ نَشَاءُ وَفَوْقَ

كُلِّ ذِي عِلْمٍ عَلِيم

صدق الله العلي العظيم

سورة يوسف (76)

Supervisor Certificate

Confirm that the Dissertation titled

“Effects of Cold Rolling on corrosion and Wear Behavior of Magnesium Biomaterial Alloy”

has been conducted by

(Zaid Ali Hadi Abbas)

Under guidance at the Department of metallurgical Engineering, College of Materials Engineering/ University of Babylon/ as part of the necessary criteria for the completion of a Master of Science degree in Materials Engineering.

Signature:

Name : **Prof. Zuheir Talib Khulief**

(Supervisor)

Data : /11/2023

Examination Committee Certification

We certify that we had read this dissertation entitled **(Effects of Cold Rolling on corrosion and Wear Behavior of Magnesium Biomaterial Alloy).** And as an Examination Committee, examined the student (**Zaid Ali Hadi Abbas)** in its contents and that in our opinion it meets the standard of a dissertation and is adequate for the award of the Degree of Master in Material's Engineering / Metallurgical.

Prof. Dr. Ali Hubi Haleem
Committee Chair
Date: /11/2023

Asst. Prof. Dr. Nabaa Sattar Radhi
Committee Member
Date: /11/2023

Asst. Prof. Dr. Ali Mezher Resen
Committee Member
Date: /11/2023

Prof. Dr. Zuheir Talib Khulief
Supervisor
Date: /11/2023

Approval of Department
of Metallurgical Engineering
Head of Metallurgical Engineering Department

Approval of Department
of Metallurgical Engineering
Dean of College of Materials Engineering

Prof. Dr. Haydar H. J. Jamal Al Deen
Date: /11/2023

Prof. Dr. Abdul Raheem K. Abid Ali
Date: /11/2023

Dedication

Heartfelt appreciation and gratitude to all those who have contributed to the completion of this work.

Zaid AlHasmot

2023

Acknowledgments

All thanks to GOD for his grace and mercy that enabled us to complete this work.

I want to express my utmost gratitude to my supervisor,

Prof. Zuheir Talib Khulief

For his invaluable guidance, expertise, and unwavering support throughout the process and constant encouragement have played a significant role in shaping the trajectory of this study.

All sincere gratitude to the College of materials engineering staff for constantly providing assistance.

I am also grateful to my family and friends who supported me and stood by me at all stages. They were supportive, a source of strength and inspiration to me, for which I am very grateful and grateful.

Zaid AlHasmot

2023

ABSTRACT

The selection of magnesium as futuristic biomaterials is due to the high-specific strength characteristic, lightweight, elastic modulus closer to that of cortical bones and highest biocompatibility.

This research includes studies the effect of different cold work (rolling), on the bio-corrosion, wear properties of magnesium alloys (AZ31) and (AZ91). The first process accomplished by heat the samples to (250^{o}C for AZ31 and 400^{o}C for AZ91) and then cooled in the furnace to obtain an alloy free from any structure deformation or internal stresses. The second process is rolling samples with different thickens redaction (5, 10, 15, 17) percentage. Microstructure analysis for the sample by using an optical microscope and SEM to remark the microstructure effect of cold work.

The Wear test carried out for the samples; this test is performed by sliding on samples in the simulated body fluid (SBF). Bio-corrosion test accomplish for the samples by immersing the samples in simulated body fluid (SBF) and measuring the corrosion rate value for each sample by liner polarization test, Electrochemical Impedance Spectroscopy (EIS), pH degrees, hydrogen evaluated, ion released, and the antibacterial test.

The results from the wear test reveal that wear resistances of as received samples is the lowest than compared with the cold work samples. The results from the corrosion test exhibited a high corrosion rate value for as received sample and low corrosion rate value for cold work samples for AZ91 alloy, while the corrosion rate value for as received sample low compart with the corrosion rate value for the cold work samples for AZ31 alloy.

The Table of Contents

Table of figures

List of tables

Chapter One

Chapter One

Introduction

1.1 Overview

A goal of third-generation biomaterials is to elicit very particular molecular reactions from cells. Bioactive materials from Third-generation biomaterials designed to be resorbable from the live body represent. The previously ideas of bioactive materials and biodegradable materials are both convergence.

The initial generation of biomaterials aimed to establish a balance of functional qualities that mimicked the original tissue without provoking a negative reaction from the host. Biomaterials have been around since the 1950s and 1960s, but it is not until the second generation that designed to cause a specific response in the tissues they transplanted in it. The Figure (1-1) shows the stages of development of generations of biomaterials [1].

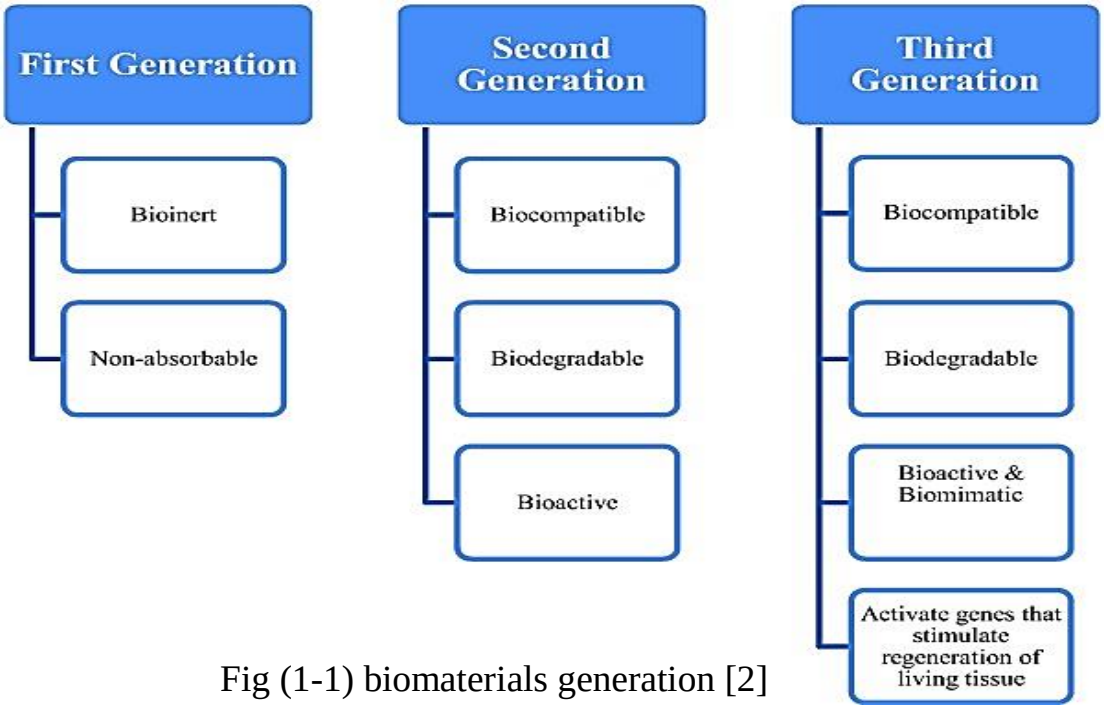

Fig (1-1) biomaterials generation [2]

The third generation of biomaterials aims to promote functional tissue regeneration by building. The use of this biodegradable substance may help doctors save time and reduce the possibility that a patient will need to go through surgery again. Figure (1-2) shows the behaver of metal from different generation in tissue. Several different materials are in use today; magnesium alloys are the focus of this research (AZ31 and AZ91). The need for lightweight, unique, and easily machined materials found in magnesium alloys [1].

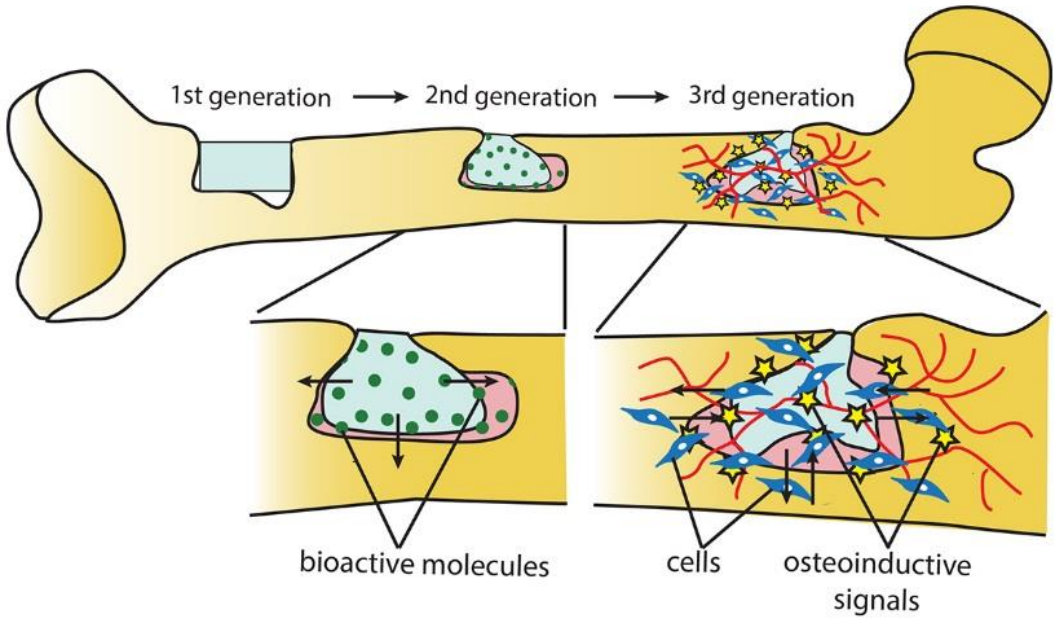

Fig (1-2) biomaterials generation with it behaver with tissue [3]

Magnesium alloys have great machinability and forging ability, making it possible to produce even the most difficult die-cast components with relative ease. Cast or solid magnesium alloy parts may be machine and weld using inert fuel. Magnesium alloys are highly sought-after materials because of their exceptional unique qualities, such as their low density (1.74 g/cm^3) [4].

A major problem of magnesium alloys is the low corrosion resistance. Instead of forming a passive film to protect against corrosion as aluminum does, it has broken down completely. Magnesium and magnesium alloys have had their corrosion resistance improved upon in several ways since it is view as one of the material's fundamental flaws.

Yet, the magnesium alloy strong reactivity in corrosive conditions may find use in the biological realm [4].

Implants placed in hard tissues (temporary implant) nowadays always made of permanent materials such titanium alloys, Nitinol (55Ni-45Ti) or stainless steel. There may be consequences such as endothelial dysfunction, prolonged local inflammation, and pain. A second operation need to implant removed. As the human body is capable of mending and replacing injured tissue over time, a degradable implant Figure (1-3) would be the best course of therapy since it would give a physiologically less invasive temporary support and repair while the injured tissue healed. When its function has accomplished, this implant will naturally remove and expelled by the body Figure (1-4) show the degradable of implant in the body [5].

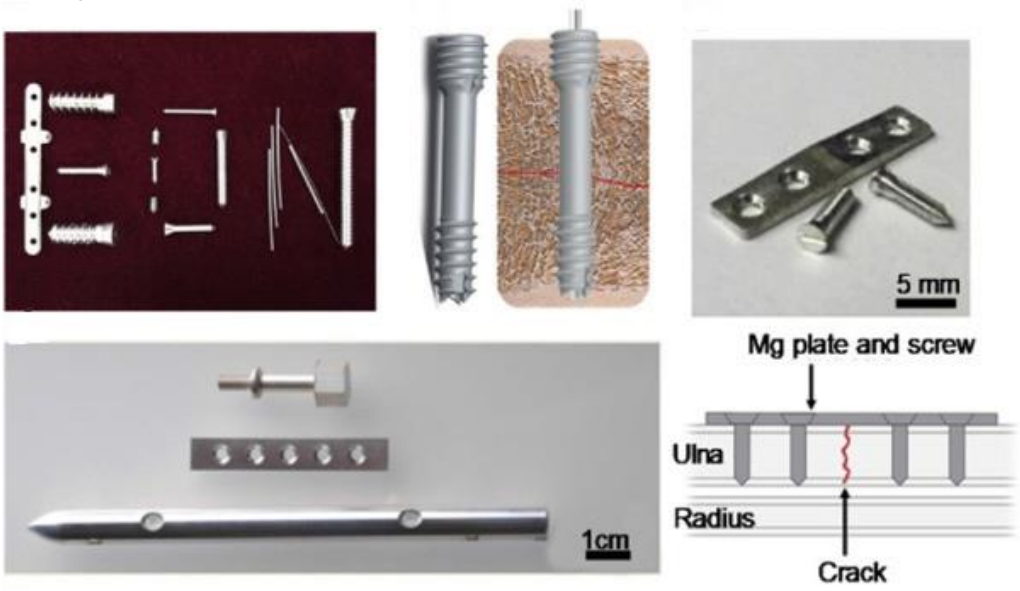

Fig (1-3) medical device from magnesium and mg alloys [5]

Fig (1-4) Implant naturally degraded in body with time. [5]

Magnesium also has benefits with other implant. Here is a list of them:

a- The density of natural bone is 1.75 g/cm^3, which is the same as the density of magnesium (Mg) at 1.74 g/cm^3.
b- Alloying may increase the strength of an Mg to as much as 330 MPa in wrought magnesium alloy.
c- The Young's modulus of Mg (41-45GPa) its value is close that of natural bone (3-20GPa) [5].

Magnesium is an innovative and practical biomaterial. Because of their low density, specific strength, elastic modulus that is similar to the bone, excellent biocompatibility, and acceptable deteriorating properties. Magnesium-based materials provide a promising alternative for load-bearing uses, making them a prime candidate for orthopedic implant design [6].

Based on this, we conclude that third generation biomaterials have great potential as surgical implants. Therefore, the manufacturing and formation processes that occur on these materials will affect their activity within the organism. As a result, the effect of cold rolling on the performance of biomaterials was an important factor to study (corrosion resistance and wear) [6].

1.2 Magnesium-Based Biomaterial

With the discovery the magnesium metal in 1808 by Sir Humphrey Davy, Edward C (physician). Huse is employed magnesium wires on patients in 1878 as ligatures to bleeding stop. Much of the first studies on magnesium, conducted by Frank Witte, focused on the element's potential biological uses. Magnesium's fragility discouraged its usage in biomedical applications for quite some time, since surgeons opted instead for more corrosion-resistant materials. For several reasons discussed below magnesium is an intriguing biomaterial for use in orthopedics [7].

A) Magnesium and it is alloys can be design to degrade in such a way that they disappear from the body when their useful life in the body has finished, without causing any damage. There is less of a chance that the patient will have the implant removed after the tissues have healed [8].

B) There is no evidence of systemic or local toxicity, according to proponents of the idea that pure iron and magnesium are highly biocompatible [9].

C) The daily-recommended consumption of Mg for humans is between (240 – 420) mg, which is seventeen to fifty times more than that of iron (8 to 18) mg/day. This gives Magnesium and his alloys a major edge over other prospective metallic biomaterials [10].

D) Magnesium and it is alloys have a tensile strength of 160-250 MPa, which is 3 to 16 more than that of polymers, which range from 16 to 69 MPa [11]. Magnesium (41-45GPa) elastic modulus is lower than iron (211.4GPa), but it is more in line with natural bone (30-20GPa) than other. The similarity between the bone and magnesium in elastic modulus may considerably reduces the effect of early implant failure, especially for orthopedic reasons [12].

E) Bone development stimulated by magnesium compounds, which allow for a permanent connection between the implant and the bone around it and complete regeneration the bone after implant degeneration [13].

These properties available in magnesium and its alloys made it one of the important and prominent materials in the third-generation biomaterial [13]. Therefore, in this study will discuss two basic alloys in surgical implants AZ31 and AZ91. And study the effect of cold rolling on their properties and their impact on their use for surgical implants.

1.3 Study Objectives

1. Study the effect of different cold work percentage on the microstructures of the (AZ31 and AZ91 Mg alloy) for biological uses for its compatibility with the human body.

2. Investigating the corrosion behavior of (AZ31 and AZ91 Mg alloy) at different cold work percentage in simulated body fluid (SBF).

3. Study the hardness of (AZ31 and AZ91 Mg alloys) at different cold work percentage.

4. Study the wear resistance of (AZ31 and AZ91 Mg alloys) at different cold work percentage.

5. Investigating the antibacterial behavior of (AZ31 and AZ91 Mg alloys) at different cold work percentage.

Chapter

Two

Chapter Two

Theoretical Part and Literature Review

2.1 Biomaterial

A commons (biomaterials) refers any materials that come into direct touch with a live body [5]. However, biomaterials have defined in slightly different ways according to several subject experts. The National Institute of Health Consensus Development Conference (USA), states that a biomaterial is defined as "any substance (other than drugs) or combination of substances, natural or synthetic, that are used as a whole or as a part of a system to replace or assist part of an organic or tissue, which can be used for any period of time". In Materials Science, a biomaterial is defined as "a material that has been engineered to take a form which can be used alone or as part of a complex system in intimate contact with living body, by control of interactions with components of living systems" [14].

There are two main types of materials used for bone implants: bio-inert and biodegradable [15].

Bio-inert materials used in medicine since quite time, figure (2-1) artificial implant in human body; however, they are not without their downsides. One major problem with bio-inert implants is that they have to permanently place inside the body unless there would be the need for implant removal through secondary surgery in cases. Such as loss its properties. These secondary surgeries in general are unfavorable because of the associated cost and risks for the patients [16].

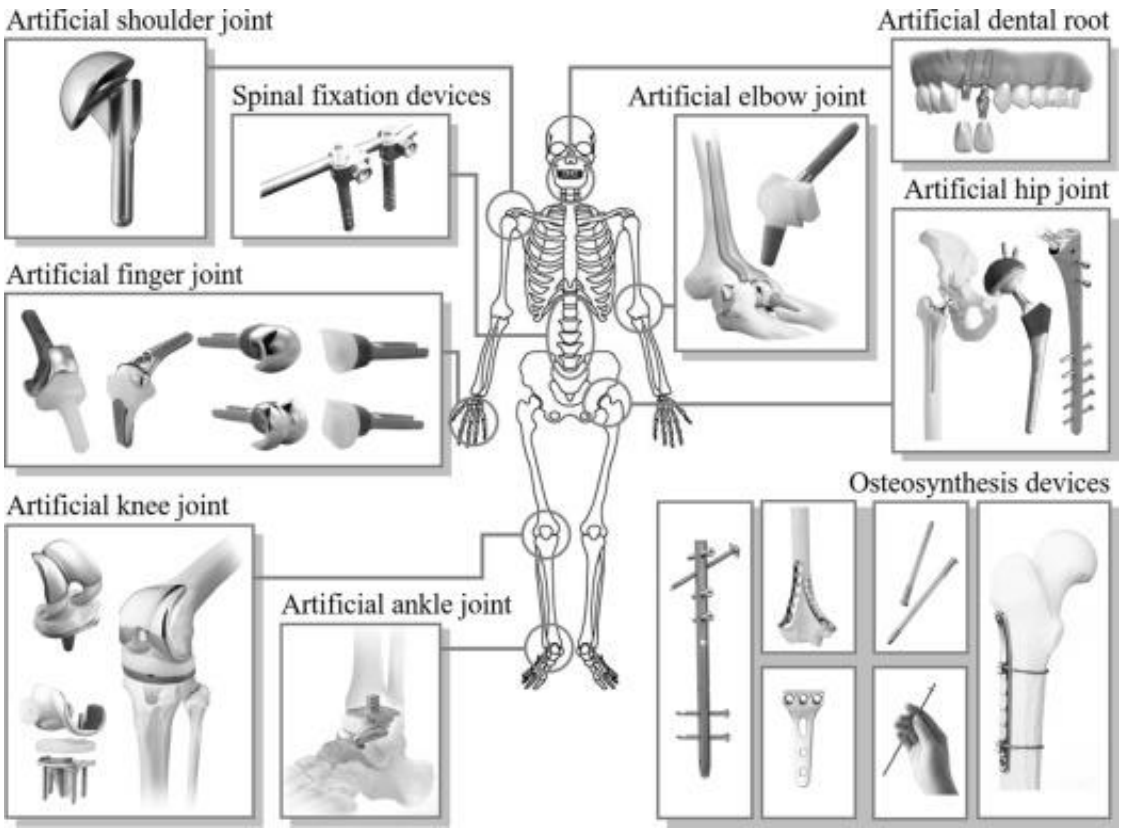

Figure (2-1) artificial implant in human body [16]

In response, biodegradable materials have alternatively introduced due to their unique degradable properties. By degrading over time, implants may gradually lose their mechanical integrity, sparing the surrounding bone and soft tissue from the damaging effects of stress shielding. Moreover, there would be no need for implant removal since the implant should degraded over time. In general, biodegradable materials are categorize into metals, polymers, and ceramics [17].

2.2 Biodegradable materials

Researchers have paid a lot of attention to the function that biodegradable biomaterials play in the healing of severe bone deformities. Biodegradable scaffolds can be used to treat bone defects by acting as bridges for new bone to grow across, as well as a place for growth factors and cells to do their physiological work, before being absorbed by the body and dissolved. Polymers, ceramics, and metals are examples of conventional biodegradable materials that have been utilized to heal bone defects for quite some time. These materials provide the foundation for creating a new generation of biodegradable materials, notwithstanding their many flaws. In the twenty-first century, there are many different types of biodegradable material, such as cell-based goods and new intelligent micro-nano materials, thanks to the fast growth of contemporary science and technology. Simultaneously, there are several advances in manufacturing methods for biodegradable materials [18].

Biodegradable materials are mostly made up of, biodegradable ceramics, biodegradable polymers and biodegradable magnesium-based materials, as per the present state of study. Figure (2-2) Type of biodegradable materials for bone implant in human body [18].

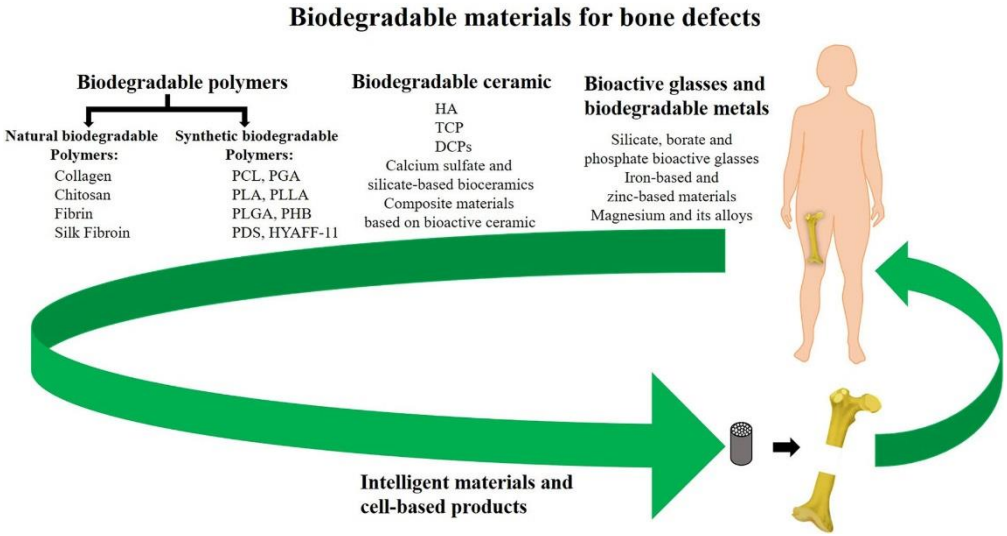

Figure (2-2) Type of biodegradable materials for bone implant [18]

2.2.1 Biodegradable ceramics

Due to their mechanical compatibility, biocompatibility, and exact chemical composition [19], bio-ceramics have seen widespread usage in recent decades for the replacement and repair of injured tissues. Scientists have a preference for biodegradable ceramics for bone tissue engineering. Their primary use is in the treatment of bone deformities and the restoration of broken bones. tri-calcium phosphate (TCP), Hydroxyapatite (HA), and di-calcium phosphate (DCP) are now the most popular biodegradable ceramics utilized today. Biocompatible, corrosion-resistant, and biologically active, biodegradable ceramics are advantageous in many ways [20]. The main benefit is that they are progressively absorbed by the body, destroyed by cell-mediated mechanisms, and solution-driven until they are eventually replaced by new bone structure. However, there are drawbacks to biodegradable materials as well, such as their weakness compared to non-absorbable ceramics and their poor fracture toughness, brittleness, and severe stiffness [21].

2.2.2 Biodegradable polymers

When many monomers are joined together by covalent bonds, the resulting macromolecule is called a polymer [22]. When it comes to repairing bone deformities, the degradability of biodegradable polymers has made them a favorite among researchers [23]. Polymers may be broken down into two categories: natural and synthetic. Due to their bioactivity, biodegradability, and biocompatibility, natural biodegradable polymers including silk fibroin, collagen, fibrinogen, hyaluronic acid and chitosan have been widely researched as bones defect healing materials. However, they may also be immunogenic [24], denatured [25] during processing, and have poor mechanical characteristics because of their high water solubility.

Synthetic polymers, whose characteristics may be tailored via design and synthesis, provide for good biomaterials. However, the acidic breakdown products of certain synthetic polymers degraded in vivo speed up the pace of implant deterioration and trigger inflammatory responses [25].

2.2.3 Bioactive Glasses

The 45S5 glass is created by Professor Hench in the early 1970s [26] using the system P2O5 (6%) - CaO (24.5%) - Na2O (24.5%) - SiO2 (45%). Since then, bioactive glass (BAG) has come into the spotlight for its usefulness in mending broken bones [27]. The 45S5 produced a chemical strong interaction with the hosted bone after implantation and exposure to bodily fluid because a HA layer comparable to the hosted bones grew on the glass surface [28]. Silicate BAG, on the other hand, has a high propensity to crystallize, a sluggish breakdown rate that cannot keep up with the pace of new bone production, and an inability to be fully converted into HA. As a result, silicate BAG has never been without its drawbacks when used for bone regeneration and repair [29].

2.2.4 Biodegradable Metals

Implants made of metals like titanium, cobalt-chromium alloys, and stainless steel have a history use in orthopedics surgery, particularly for bone restoration [30]. These materials have the potential to be used to heal bone defects, but their various drawbacks, such as stress-shielding effects and non-biodegradability, prevent this from happening routinely. Research into biodegradable metals has flourished in recent years owing to the materials' high biocompatibility and ease of degradation [31, 32]. In particular, magnesium, iron, zinc, and their alloys are the most extensively researched biodegradable metals.

The biocompatibility of these metals with human cells and tissues has been established by several research [33- 35]. At the same time, these metals are important for sustaining normal body function of human. As they are stronger, biodegradable metals are more appealing; they corrode progressively in vivo, with the right host reaction, and disintegrate entirely following bone tissue repair [36]. Biodegradable metals divided:

(A) Magnesium based (pure Mg, Mg-Zn, Mg-Ca, Mg-Al alloys) [37- 38].
(B) Iron based (pure Fe, Fe_ Mn alloy, Fe_ W alloys) [39-40].
(C) Zinc based (pure Zn, Zn_ Mg alloy) [41].
(D) Other biodegradable metals (Sr_ based, Ca_ based) [42].

Several biodegradable materials (metals, polymers, and ceramics) shown in Figure (2-3) along with their corresponding relationships between yield stress and Young's modulus [43]. In comparison to other biodegradable alloys, Mg-Zn-Ca bulk metallic glasses (BMG) have a higher yield stress, making them one of the strongest biodegradable materials. Mg-Zn have a Young modulus that is nearly to that of cortical bones (E = 3-20 GPa) than do most crystalline (Cryst) Mg-based alloys or synthetic hydroxyapatites.

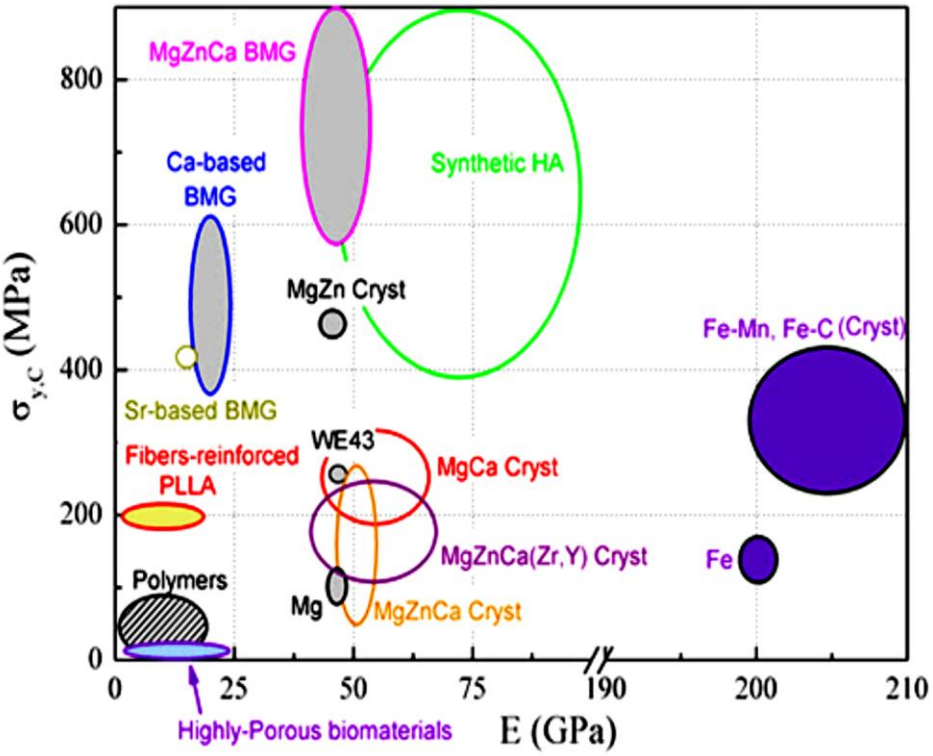

Figure (2-3) the compressive yield stress (y) and the bending stiffness (E) of the biodegradable implant materials currently in use [43].

2.3 Magnesium-based Alloys as Biodegradable Metals

In general, Mg-based alloys are attractive biomaterials due to the following characteristics:

(A) Mg-based alloys have beneficial biological qualities since they appear naturally in the human body (a total of 25 g, with 50-60% found in bone). The average person gets between 380 and 850 milligrams (mg) of magnesium per day from foods including grains, nuts, and dark green vegetables. The kidneys are able to eliminate the extra Mg efficiently [44].

(B) Excellent mechanical characteristics: Compared to biodegradable polymers and ceramics, Mg-based biodegradable metals are stronger, making them suitable for loadbearing applications.

(C) Elastic modulus (E) compatible with bone: The modulus of elasticity of Mg based metal (45 GPa) is more similar to that of bones than that of titanium alloy (110 GPa), stainless steel (200 GPa), or Co alloy (230 GPa).
(D) Mg-based metals (1.7-2.0 g/cm^3) have density similar to natural bone (1.8-2.1 g/cm), in comparison to materials like titanium alloy stainless steel (approximately 7.8 g/cm^3), (Ti-6Al-4V) (4.42 g/cm^3), hydroxyapatite (3.156 g/cm^3)and biodegradable polymers(PLLA) (about 1 g/cm^3).
(E) Mg alloys have the special feature of promoting bone formation by increasing proliferation of cells and the adhesion through the production of magnesium-containing calcium phosphate [45].

It is important to remember, nevertheless, that Mg-based alloy characteristics change with temperature. As the patient's body temperature tends to vary depending on different factors such as age and gender [46], Kirkland et al. [47] performed a comprehensive study on the influence of temperature on the behavior of degradation Mg-based alloys. They observed that corrosion rate significant increase in (approximately 50%) with a slight increase temperature from 37°C to 40°C.

2.3.1 Magnesium Based alloys

Because of its low density of 1.745 g/cm^3, pure magnesium (Mg) is one of the lightest structural metals. This alloy is weak and brittle at room temperature because pure Mg has an (HCP) structure [48-49].

Magnesium, when cast in gravity, has a limited tensile strength of merely 90 MPa and a limited yield strength of merely 21 MPa. The magnesium powder, even when at room temperature, is very flammable. The inclusion of alloying metals like Aluminum (Al), Zinc, and others improves these qualities and makes Mg alloys suited for structural purposes. Most metals alloyed with aluminum because of its widespread application [50]. When

aluminum added to an alloy, the material becomes stronger, harder, and more suitable for casting. More than 6% wt. of aluminum recommended improving corrosion resistance, strength, ductility, and heat treatability of the alloy [51].

The creation of the Mg-Zn intermetallic and the subsequent refinement of grain size are both attributed to zinc [52], the second most prevalent alloying element. Furthermore, Zn alloying reduces the destructive corrosion impact of impurities like Fe and Ni [53].

By forming the intermetallic compound and refining the grain size, a combination of Zn and Al is more efficient in increasing room temperature strength. Nevertheless, when Al concentrations are at 6-7%, adding more than roughly 1% wt. of Zn is not preferable since it leads to hot shortness (a tendency to separate along grain boundaries when stressed at temperatures around the melting point). In order to improve the alloy's overall strength, Zn may couple with additional alloying elements including Ca, Zr, and Th [50-51].

By forming a thin, thick CaO coating on the surface of the melt, adding Calcium to pure Mg reduces the surface tension of the molten metal, improves the grain structure, and eliminates the oxidation issue that arises during heating [45-46]. Nevertheless, When the Ca content is beyond the solubility limit (1%wt), an excessive amount of the Mg_2Ca intermetallic complex are produce, reducing the alloy's corrosion resistance. [54]. Adding manganese (Mn) to alloy decreases its resistance of corrosion due to formation of intermetallic compounds with corrosive impurities (iron and heavy earth metals). When coupled with aluminum, Mn very low solubility in solid solutions reduced to 0.3%wt [4, 55, and 56].

Alloying with silver (Ag) improves in general magnesium (Mg) alloys mechanical characteristics by increasing their age hardenability with the addition of Cu; the alloy's high-temperature strength is improved. Nevertheless, the corrosion characteristics of the alloy might be negatively impact by the addition of more than 0.05%wt Cu. Zirconium (Zr) is add to an alloy to enhance its microstructure by refining the grains [4].

By generating Mg2Si particles that cling to grain boundaries, Silicon (Si) boosts the molten metal's overall fluidity [54, 56].

Rare earth elements (REE) finally form precipitates in the Mg alloy that greatly increase its strength and hardness at high temperatures. In addition, the micro porosity and weld cracking lessened because this element limits the freezing range of the alloy. Along with honing the granularity [57].

In addition, Zn alloying reduces the detrimental corrosion impact brought on by impurities like Fe and Ni [58]. The development of an intermetallic compound and the refinement of the grain size make a combination of Zn and Al superior for increasing the room temperature strength. Nevertheless, when Al concentrations are at 6-7%, adding more than 1%wt of Zn is not preferable since it leads to hot shortness (a tendency to separate along grain boundaries when stressed at temperatures around the melting point). Other alloying elements, including as Ca, Zr, and Th, May added with Zn to boost the alloy's overall strength [56].

2.3.2 Magnesium alloy element Alloying

Ultra-pure Mg has the highest corrosion resistance of any alloying strategy [59]. When the number of secondary phases grows, more alloying elements are introduced, which encourages the formation of a local galvanic cell at the interfaces. In figure (2-4), Mg has a high solubility limit for elements in solids. It is clear from the exhaustive list

that many elements are either insoluble in Mg or have not been thoroughly investigated [60].

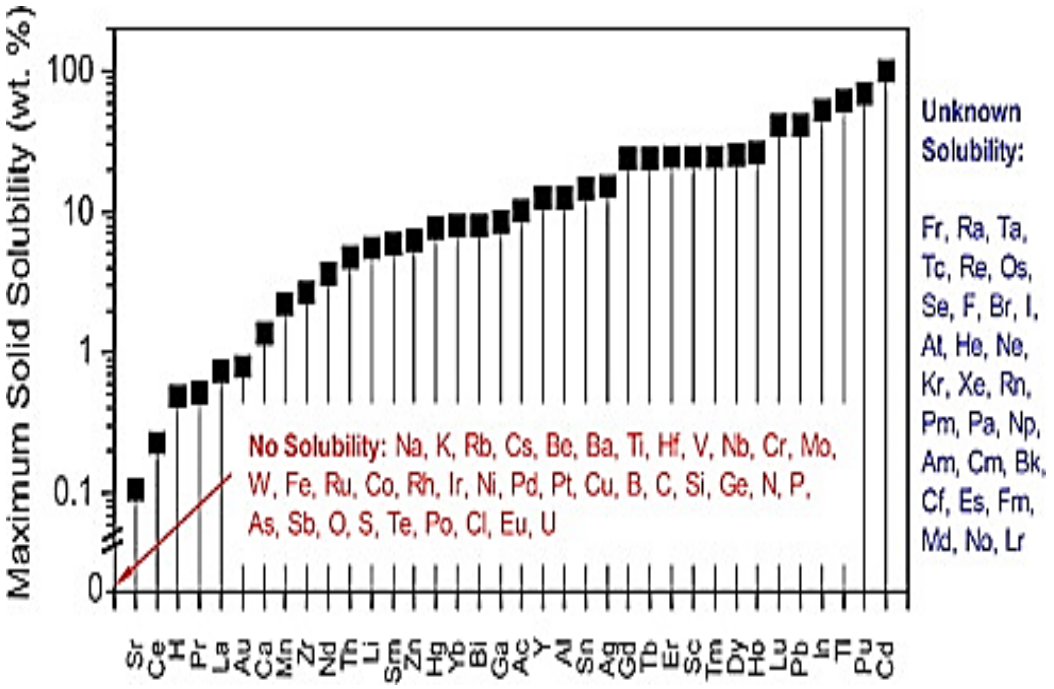

Figure (2-4) elements solid solubility in Mg [60]

As a result, the use of alloying elements to boost mechanical properties has increased (strength, elastic modulus, elongation at fracture, etc.). It has also been noted that some alloying elements may improve the corrosion resistance of standard-purity, unalloyed Mg. Three methods utilized to improve corrosion behavior:

1- Alloying is used to reduce the grain size. Grain boundaries are more prone to corrosion than the Mg matrix because they are more defective and have more internal energy. In addition to increasing the cathodic activity of the surrounding Mg matrix, these barriers serve as sites of segregation for alloying elements and second phases. This generally favors coarse grains, but in Mg alloys, the continuous distribution of such segregations in smaller grains leads

to a more homogenous corrosion behavior and acts as a corrosion barrier [61].

When it comes to resisting corrosion-assisted cracking, smaller grain sizes are better since they reduce the possibility of crack initiation and dislocation motion by increasing the number of barriers to crack propagation [36].

2- Continual presence of passivating second phases all around the Mg matrix permits the formation of an oxidative coating that shields the Mg matrix and prevents corrosion [61].

3- Added elements minimize micro galvanic corrosion by decreasing the potential difference between the second phases and the matrix or by lowering the rate at which the second phases precipitate in grain boundaries [62].

The effects of Alloying elements on magnesium alloy are briefly discussed in Table (2-1). The impact of each alloying element may be estimated by counting the alloying elements number present and calculating the proportion of each alloying element. The quantity of alloying elements used in conjunction with the proportion of elements utilized in Mg is what determines the impact of these elements [63].

This enhancement is possible via a number of alloying methods; nevertheless, it is important to determine which are safe to use. The most common alloying elements and describe their effects below. Alloying elements have effects that are very dependent on the context in which they are used.

Table (2-1) the mechanical properties effected with alloying elements [63].

No	Elements	Mechanical Properties
1	Aluminum	Increases hardness, strength, and casting capacity (fluidity), while density increases little.
2	Zinc	Improves corrosion resistance when added to Mg alloys (with Ni and Fe impurities); at 2wt% or more, there is a tendency for hot cracking.
3	Calcium	Improves thermal and mechanical properties, helps refine granulation and increases elongation resistance; reduces surface stresses.
4	Copper	Helps increase resistance to both room temperature and high temperature.
5	Manganese	Increases corrosion resistance in salt water in some aluminum-containing alloys.
6	Nickel	Increases both efficiency and maximum force at room temperature. It has a negative impact on elongation and corrosion resistance.
7	Strontium	Increases elongation resistance (used with other elements); increase bone mass and reduce the incidence of fractures.
8	Tin	Improves ductility and reduces the tendency to fracture during processing, when used with Al; Improves compressive strength and corrosion resistance
9	Yttrium and Lanthanides	Y- Increases high temperature resistance and elongation resistance when mixed with rare earth metals; increases the fluidity of alloys when casting. Ce - Improves corrosion resistance; increases plastic deformation capacity and Mg elongation and hardening ratio; reduces deformation strength. Nd - improves the strength of the material.
10	Lithium	Improvement in ductility and reduction in strength
11	Zirconium	Provides high damping strength, tensile strength, and involves high ductility
12	Titanium	Improvement in elongation
13	Silicon	Enhancement I fluidity
14	Iron	Not suitable for corrosion resistance

(a) Aluminum (AL)

Most magnesium is alloyed with aluminum because it is inexpensive, lightweight, soluble, and increases strength significantly (from 170 to 250 MPa) [37]. Not only does it prevent corrosion, but it also acts as a passivation. Almost all research on the magnesium alloys corrosion behavior has focused on (Mg Al) alloys. Researchers Song et al. [64] found that the anodic dissolving rate of pure Magnesium is greater than that AZ21 when tested in chloride solution alongside many Mg-Al alloys. Al_2O_3, MgO, and Mg $(OH)_2$ make up the three layers that make up the surface film of the specimens used in this investigation Figure (2-5). Due to the development of passivating Al_2O_3, AZ21 is more resistant to corrosion.

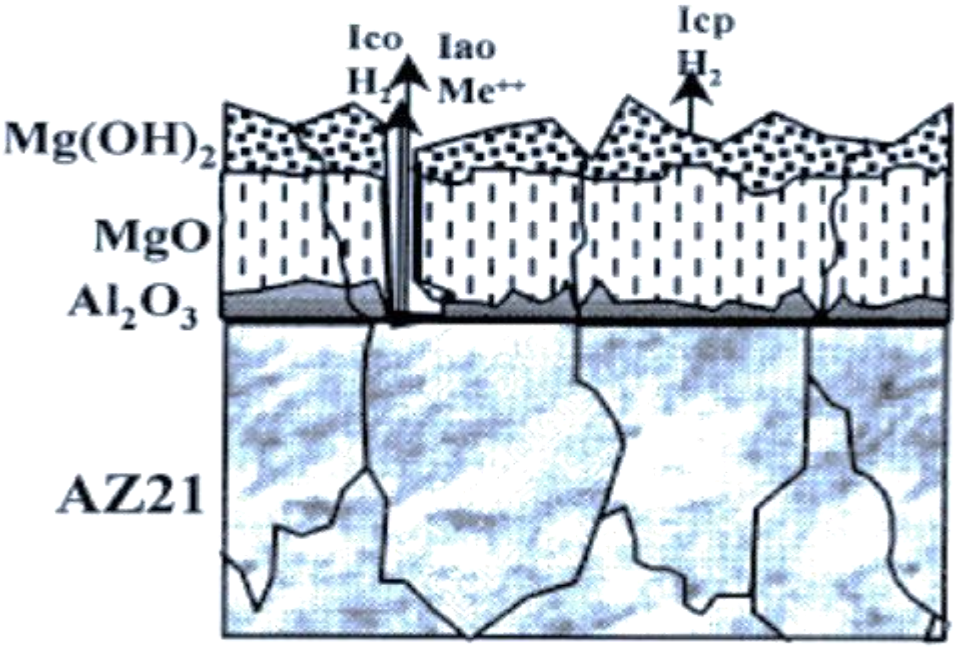

Figure (2-5) the three layers that make the surface film on AZ21 alloy [64]

High corrosion rate in AZ91 alloys may attribute to the presence of more cathodic second phases ($Mg_{17}Al_{12}$) on grain boundaries than in AZ21. Temperature-dependent on (Al) solubility in (Mg) which is around 12%wt Figure (2-6)A [65].

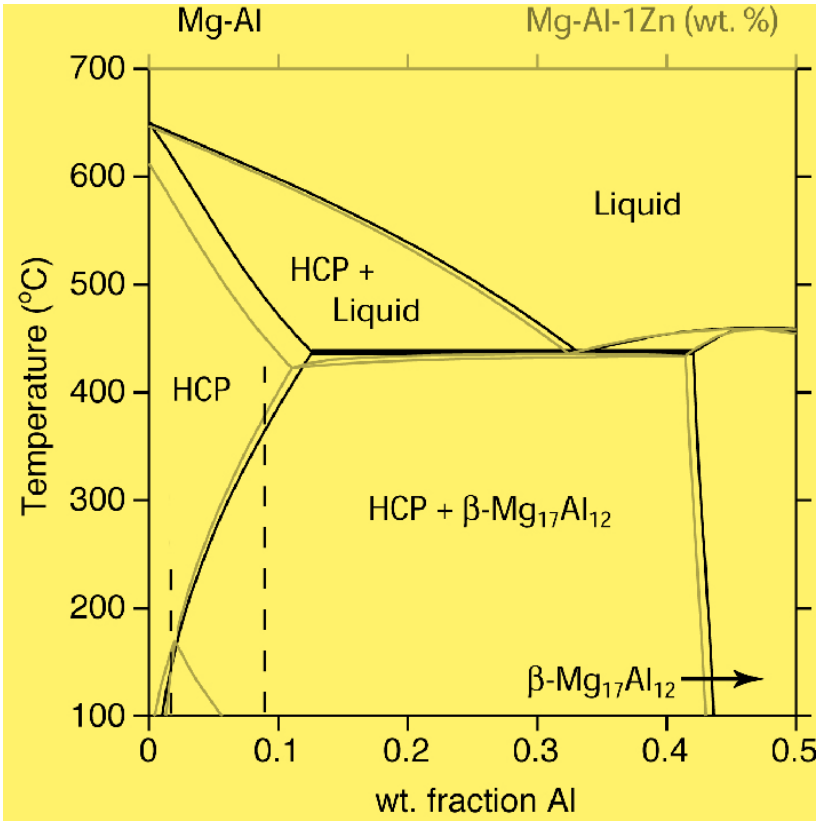

(A) Phase diagram of (Mg-AL-Zn)

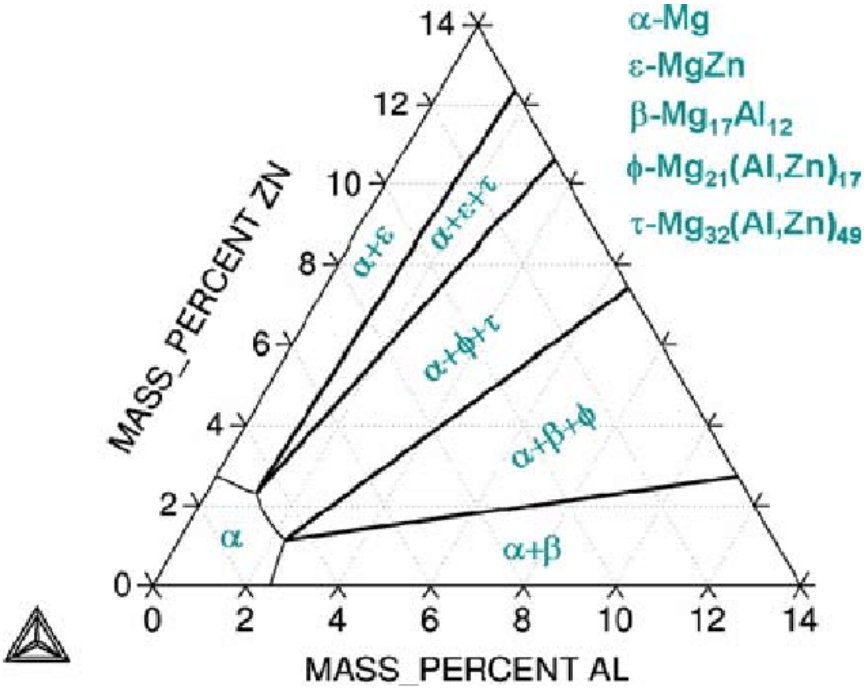

B) (A) Ternary Phase diagram of (Mg-AL)

Figure (2-6) Phase diagram of (Mg-AL-Zn) [66]

Alloys with a greater Al concentration than AZ31 second phases, as previously shown, ($Mg_{17}Al_{12}$) by Gusieva et al. [67], suggesting that adding more than 3%wt. of Al reduces the materials corrosion resistance. Other writers argued against this theory by showing that corrosion resistance really increases continuously with increasing Al content [68]. For instance, Lunder et al. [69] hypothesized that Al concentrations beyond 10%wt would further reduce the anodic dissolution. Finally, Winzer et al. [70] picked up where they left off, noting two effects of ($Mg_{17}Al_{12}$) phases on corrosion:

(1) A barrier.

(2) A galvanic cathode influence.

In respect to the number and distribution of the second phases. In low volume fractions, ($Mg_{17}Al_{12}$) exacerbates corrosion by acting as a galvanic cathode, but at large fractions, it works as a barrier and slows down corrosion thanks to its passive layer qualities and its ability to create an interconnected network [70].

These results are mechanistically intriguing, and they may be applicable to other situations involving the alloying of elements with comparable electronegativity. In spite of this, the wealth of information gained with Al alloys is not readily transferable to biological implants. Al is harmful, as shown by its long-term effects on reproduction [71], the induction of dementia [69], and the progression to Alzheimer's disease [73, 74].

(b) Manganese (Mn)

Corrosion is unaffected by Mn as a binary addition to Magnesium up to values of 5%wt [75]. Keeping the ratio of Fe/Mn at 0.032 enhanced the iron tolerance threshold in Mg-Al alloys. Absorption of iron into an intermetallic (Al Mn Fe) complex, which decreases micro galvanic because

it is less active as a local cathode [67, 76], is the most plausible mechanism explaining Fe's moderation. However, a neurological disorder called "manganism" has symptoms with Parkinson's disease, has shown produced by Mn at blood concentrations greater than 10 µg/L. [77].

(c) Zinc (Zn)

By adding 6% wt. of zinc, the strength of Mg may be increased to 280 MPa, due to Zn solid solution strengthening effect [78]. The average human body needs 15 milligrams of zinc each day [79, 80], as a trace mineral essential to numerous metabolic processes. The interaction of Zn^{+2} with hydrochloric acid is the fundamental downside of Zn biocompatibility (HCl). By the oxidation of Zn, an alloying substance, Zn^{+2} is produced,

$$Zn \text{ ------ } Zn^{+2} + 2e \qquad (1)$$

And HCl reduced according to

$$2HCl + 2e \text{ -------- } H_2 + 2Cl \qquad (2)$$

When the solid solubility limits of Fe, Cu, and Ni have surpassed, Zn increases the tolerance limit and minimizes the impacts of these three primary contaminants. Mg with Zn increases Ni tolerance by 1% wt. [81]. After the Ni and Fe tolerance thresholds met, the corrosion rate of ternary alloys can be further, reduce when adding 3% wt. Zn to Mg-Al-Mn alloys, as reported by Song and Atrens [82]. Second phases occur and corrosion resistance decreases at Zn concentrations over 3%wt. [80], resulting to localized corrosion [83]. Zn alloying has many benefits, one of which being a reduction in hydrogen evolution and Mg matrix solubility. When Zn^{+2} and Mg^{+2} ions both interact with OH free anions to create $Zn(OH)_2$, the concentration of free H_2 is lowered [85].

Hydrogen development can only be marginally slowed due to the alloying metals limited solubility of in crystalline Mg. In contrast, Mg-based glasses have higher solubility for alloying elements, which greatly reduces corrosion.

Glassy Mg60+xZn35xCa5 alloys (x = 0, 3, 6, 7, 9, 12, 14, 15) were studied by Zberg et al. [82] in SBF. Hydrogen evolution found to suppress by increasing the Zn concentration; a significant decrease in hydrogen emission seen at Zinc level of (28% wt). (Figure 2-7).

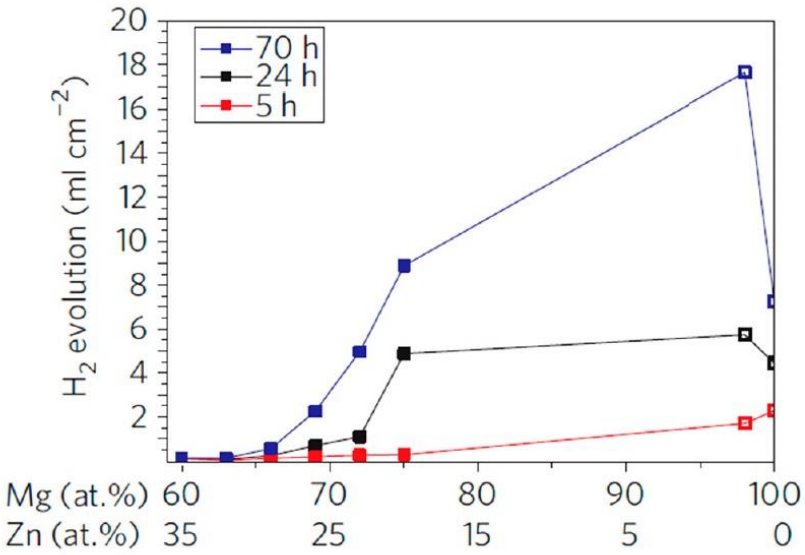

Figure (2-7) Analyzing the effect of Zn concentration on hydrogen development in Mg-Zn-Ca alloys. (86)

(d) Calcium (Ca)

Bone repair and development aided by calcium's presence in the body [87, 88]. It is a common addition to biodegradable magnesium alloy. In the presence of Ca, Mg alloy form a thin coating of hydroxyapatite (HA) on their surface, increasing their biocompatibility. Ca also enhances the mechanical characteristics of grains, making them more desirable [89]. According to Zhang and Yang [90], when the quantity of Ca increased from 0.3 to 1 % wt. in Mg-Zn-Mn alloy, grain size decreases from 175 to 51 µm.

However, corrosion resistance decreases after adding as little as 1% Ca because of formation of (Mg_2 Ca) second phase [91]. However, Bornapour et al. [92] found value in the existence of a second phase (Mg -0.3Sr-0.3 Ca) alloys showed the high resistance to corrosion compared to pure Magnesium and other alloys including Ca and Sr, despite the presence of a Ca-Sr rich second phase (Mg-0.5Sr, Mg-0.6 Ca, Mg-0.5Sr-0.6Ca, and Mg-0.3Sr-0.3 Ca).

Since less dissolution occurred due to the alignment of matrix and grain boundary corrosion potential, they concluded that this is the cause of the improved corrosion behavior. They further claim that the electro chemical barrier function of HA is maintained by just modest levels of Sr and Ca, whereas high concentrations may cause the surface layer to become non-adherent and peel off.

2.4 Magnesium alloys

2.4.1 Casting alloys

Most magnesium alloys include some amount of aluminum (often between 3 and 9 percent by weight). However, the exact ratio varies the corrosion resistance and mechanical characteristics of these alloys. More aluminum in melt (eutectic system) means higher casting properties, elongation and Tensile strength are 2-10%, 135-285 MPa respectively. Young's modulus is typically 42 GPa, and the typical density is 1.8 g/cm3. Because of its super cast ability, even for the most complicated components, AZ91 has become the most popular magnesium die-casting alloy. The important die-casting alloys [93]:

1. AZ alloys: - (Mg – AL – Zn) which have

– Excellent qualities at room temperature.

– Low creep resistance and heat resistance.

- Restricted plasticity.

2. AM alloys: - (Mg – AL – Mn) which have:

- More ductility is a result of a lack of zinc and a decrease in aluminum concentration.

- Limitation in cast ability and alloy properties at room temperature.

3. AS alloys:- (Mg – AL – Si) which have:

- Much improved creep and heat resistance by Mg-RE precipitations.

- Casting is the only method of production.

-Reduced cast ability.

2.4.2 Wrought alloys

Magnesium alloys that have been wrought display a unique quality. The tensile strength is greater than the compressive strength. Magnesium alloys that have been worked develop a stringy texture in the direction of deformation, increasing their tensile strength. Tensile strength and elongation of wrought magnesium alloys are 160–240 MPa, 180–440 MPa, and 7–40%, respectively. Because of the hexagonal lattice structure (HCP), twinning occurs more readily in compression than in tension in magnesium alloys, resulting in a decrease in strength under compression. Table (2-2) the available magnesium wrought alloys [94].

Table (2-2) the available magnesium wrought alloys [94].

Alloy	Al	Ca	Zn	Mn	Cu	Zr	Y	Nd	Th
AZ21X1	1.6-2.5	0.1-0.25	0.8-1.6	0.15 max	0.05				
AZ31	3.0		1.0	0.3					
AZ31B	2.5-3.5	0.04 max.	0.7-1.3	0.20-1.0	0.05				
AZ61B	5.8-7.2		0.40-1.5	0.15-0.5	0.05				
AZ80	8.5		0.5	0.12					
AZCOML	2.0-3.6	0.04 max.	0.3-0.5	0.15 min.	0.10				
AZM	6.0		1.0	0.3					
ZC71			6.5	0.7	1.2				
ZK40			3.5-4.5			0.45 min			
ZK60A			4.8-6.2			0.45 min			
ZM21			2.0	1.0					
ZW3			3.0			0.6			
HM21				0.8					2.0
HM31						0.7			2.0
WE43						0.5	4.0	4.0	
WE54						0.5	5.25	3.5	

In order to create a wrought alloy, the material must be hot-worked by rolling, extruding, and forging at temperatures more than 350 °C. After that, further cold-working processes are perform at low deformation rates to prevent fracture development. Magnesium and its alloys are increasingly being consider for use in high-stakes applications, and this has led to a renewed focus on wrought alloys [94].

Magnesium alloy AZ31 has high strength and ductility at room temperature, as well as being corrosion-resistant and easily welded. Medical implants, airplane fuselages, and mobile device and computer casings are just a few of the many places AZ31 may put to good use. A large range of complex vehicle parts may made from AZ31 by forming it at high temperatures [95].

2.5 Mg corrosion in simulated body environments

Human tissue is surrounded by a (Na Cl) solution that also contains trace levels of PO_4^{-3}-, Ca^{+2}, and HCO^{-3}. While carbonates and phosphates may encourage the production of protective or partly protective corrosion product layers, chloride ions tend to speed up the corrosion process. The 37 °C internal body temperature not only affects the pace of corrosion reactions but also the rate at which different Ca-phosphates precipitate out of the bodily fluids. For instance, Ca-phosphates have temperature-dependent solubility. The average blood pH is 7.4. The pH value, however, may vary somewhat from place to place. Corrosion processes are affected not only by the wide range of inorganic substances found in human fluids, but also by the presence of organic substances such biomolecules, cells, bacteria, and proteins [96].

Corrosion scenarios are notoriously difficult to predict due to the complexity introduced by the myriad of interactions between these components and the corroding Mg alloy surface and among themselves. Figure (2-8) provides a summary of some of these relationships.

The steps in Figure (2-8) procedures may be summed up as follows [97]:

1- Alkalinization, formation of H_2 (gas), and release of Mg^{+2} are the results of Mg corrosion.
2- The breakdown of magnesium (Mg) in the cathodic process releases OH^- ions, which are toxic.
3- The elevated pH encourages Ca-phosphate precipitation on the surface of the alloy.
4- The increased alkalinity has antibacterial effects.
5- When the new layers of the surface form, carbonates are integrated into them.

6- The surface of alloy's produces $MgCl_2$. After being attacked by chloride ions,

7- Proteins and cells may be found stuck to the magnesium surface. Lactic acid is produced by surface cells.

8- Mg^{+2} cations may be complexed by proteins in solution.

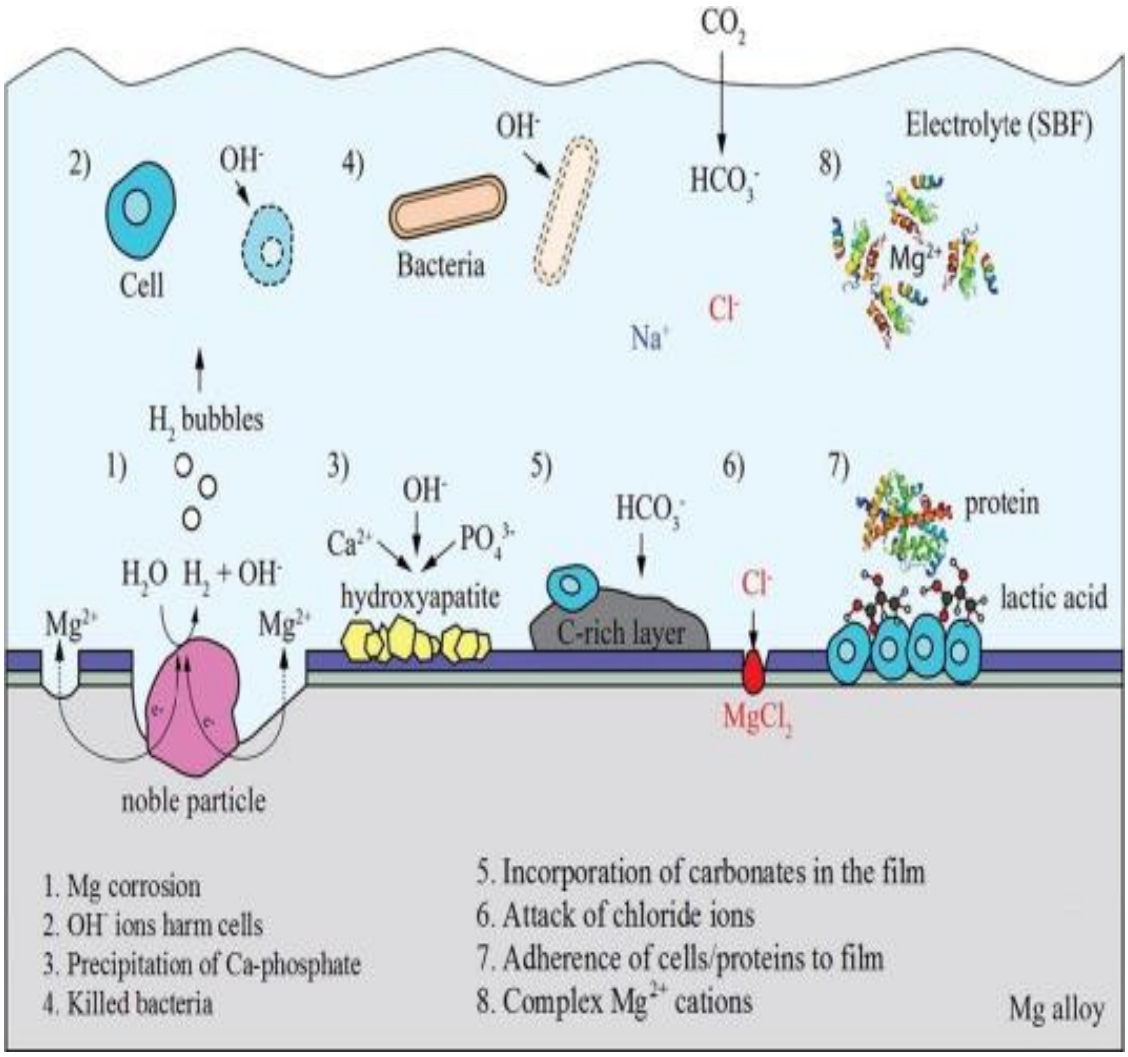

Figure (2-8) provides a summary of some of possible interactions between the implants (Mg and Mg alloys) and living tissue [97]

2.6 Corrosion of Magnesium in vivo vs. vitro environments.

Mg alloys corrosion in artificial biological fluids is a complicated process, as mentioned above. Hydrodynamic circumstances, amino acids, proteins, cells, temperature, pH and the presence of a large number of inorganic ions are all factors to be taken into account. Despite the abundance of research aimed at disentangling the effects of a single variable, the interdependence of various variables makes it difficult to pin down the underlying processes [98].

There may be more than one operating mechanism at work in many of the parameters that affect corrosion of Mg alloys. Proteins, for instance, may adsorb to surfaces in addition to complicated metal cations. One of the two operating mechanisms may be predominate depending on the context of the system. If we include in vivo considerations, the picture gets much more convoluted. Data of behavior Mg alloys on the vivo, particularly systematic and direct comparisons of in vivo and in vitro degradation is currently scarce.

In a recent review [98], the authors attempted a thorough examination of the relevant literature. Compared to in vitro value (0.1 to 2 mm/year (0.05 $mg/cm^2/day$)), the range of values for corrosion rates in vivo is narrower (0 to 1.5 mm/year (0.7 $mg/cm^2/$ day)). Furthermore, in vivo corrosion rates were 1-5 times lower than in vitro rates for all alloys. Corrosion rates studied in the lab rely significantly on the electrolyte used to replicate conditions seen in the body. The reduced corrosion rates reported in vivo have been attributed to a number of factors, including the presence of proteins and cells and a lower chloride content in human plasma compared to most synthetic mediums. The authors noted that factors such as the implant's anatomical location and the surgical technique might affect its degrading behavior after implantation. Thus, the explanation of the

observed differences in corrosion rates remains a mystery due to a lack of knowledge regarding the precise in vivo circumstances.

Long-term in vivo and vitro in deterioration of Mg alloys coating with Ca-phosphate reported in a recent study [99]. Differences in attack morphology discovered under the coverings. In vitro, the onslaught is almost homogeneous, but in vivo, it much localized. The implant/tissue contact thought to be the cause of the reduced diffusivity seen under in vivo settings.

2.7 Cold-rolling process in Magnesium alloys.

Magnesium alloys have garnered a lot of interest in recent years because of their exceptional weight-saving characteristic. However, its limited room-temperature ductility and workability prevented it from being widely used. The lack of appropriate slip mechanisms for arbitrary deformation, as required by Von Mises' criteria [100], may be to blame. As a result, twinning is typically crucial in helping organisms adapt to the stress they are under. Since both dislocation slip and twinning result in local lattice rotation during plastic deformation and since this rotation in turn affects the texture development during straining, these two mechanisms continually compete with one another. Magnesium, which has a less symmetrical crystal structure, is particularly sensitive to this. Dislocation slip in Mg and its alloys exhibited clear anisotropy, as expected for a material with a close-packed hexagonal (HCP) structure (c/a=1.624). At ambient temperature, the critical resolved shear stress (CRSS) of basal slip was only about one-hundredth that of non-basal slip [101]. As a result, non-basal slip systems that result in inhomogeneous plastic behavior are generally avoided in favor of basal slip systems. This might have an impact on mechanical qualities and the delicate equilibrium between twinning and

slide. Basal slip and 1012 twinning are often initiated at ambient temperature to allow the plastic deformation that invariably resulted in a robust basal texture [102].

2.8 Characteristics of Bio-Corrosion

Biodegradable implants have interesting medical uses. They aid in tissue healing in a less invasive manner and may potentially be gradually removed or absorbed by the body. As compared to permanent implants, they are preferable since the latter might cause behavioral incompatibilities between the implant and the body, as well as physical irritation and long-term inflammatory reactions, necessitating further surgical intervention. Polymer-based biodegradable implants dominate the market, although metal implants are on the rise. In terms of mechanical strength, they provide a better solution. Biodegradable implants are becoming an increasingly important area of study in medicine because they have the potential to dissolve naturally after the bone tissues have heal, either absorption, consumption, or expulsion from the body. The bulk of commercially available biodegradable materials are made of ceramic materials or polymeric; nevertheless, when used as load-bearing parts, these implants have inadequate mechanical strength. For example, compared to already approve biomaterials, Magnesium alloys provide a number of advantages. To begin, the high strength-to-weight ratio of magnesium alloy makes it an ideal choice for load-bearing implants and a material that displays adequate mechanical integrity. Magnesium's elastic modulus and compressive yield strength are more similar to those of natural bone than those of other metallic implants, and higher than that of ceramic biomaterials fracture toughness. (Table 2-3) [103].

Table (2-3) Properties of various implant materials [19]

Material	Density (g/cm^3)	E (GPa)	Compressive yield strength (MPa)	Fracture toughness ($MPa.m^{1/2}$)
Natural bone	1.8-2.1	3-20	130-180	3.6
Mg	1.74-2.0	41-45	65-100	15-40
Ti alloy	4.4-4.5	110-117	758-1117	55-115
Co-Cr alloy	8.3-9.2	230	450-1000	/
Stainless steel	7.9-8.1	189-205	170-310	50-200
Synthetic HA	3.1	73-177	600	0.7
PLA	1.25-1.29	2.2-3.3	/	/

New bone growth and remodeling will be less inhibit, and "stress shielding effects" will reduced or eliminated. Second, magnesium may have some mild effects on the human body. For human metabolism, Mg is an important mineral, and it found in abundance in bone tissue. Magnesium is 4th most abundant cation in the human body, with a normal adult weighing 70 kg having 1 mol of Mg. Around half of the body's magnesium is kept in the bones. Magnesium, having a very low standard electrode potential, would slowly dissolve and be absorbed after implantation in the human body (-2.37 V). Mg2+ ions are either taken in by neighboring tissues or released in body fluids. As compared to permanent implants, temporary ones may save healthcare costs and patient morbidity by eliminating the need for a second treatment to remove the implant. Last but not least, magnesium may be found for very little cost in the earth's crust and ocean. A third of the cost of titanium is what you will pay for this. High corrosion rates in magnesium and magnesium alloys are clearly unfavorable for structural applications but beneficial for biological ones. Magnesium alloys are often considered as a possible material for biodegradable orthopedic implants [19].

2.9 Toxicity of magnesium and alloying components.

Corrosion of biodegradable Mg alloys may liberate metal ions, which has been shown to produce both local and systemic toxicity in vitro. The normal range for Mg in the blood serum is 0.73–1.06 mmol/L. Adenosine triphosphate (ATP) production and enzyme activation are two of the numerous roles that magnesium plays in cellular physiology. In addition to these roles, it acts as a co-regulator of protein synthesis and a stabilizer of both DNA and RNA [28]. Increased amounts of Mg ions, caused by the implantation of Mg, may promote new bone development and have anti-osteoporotic action. An imbalance in magnesium homeostasis may cause vomiting, renal failure, and breathing difficulties. Toxic dose at 50% cell viability [28] was determined to be 73-103 mol/L in bone-related cells. Magnesium (Mg) is the least harmful of the body's plentiful elements; Due to corrosion rates and the physiological environment in the implantation sites, the quantity of alloying element employed in the production of Mg-based biomedical implants has to be adjusted. Toxic ions delivered into the body may often be tolerated at very low concentrations.

below the critical threshold level, while excessive release into the body will have undesirable side effects [104] . It is essential that biomedical implants be designed so that the localized release of metal ions below critical threshold levels can be controlled. Table (2-4) summarizes the pathophysiology and toxicology of the common alloying elements of Mg and their effects on mechanical properties [63].

Table (2-4) The effects of the alloying elements in the Mg alloy [63]

Alloying Element	Pathophysiology/toxicology
Al	Normal blood serum level 2.1–4.8 µg/L; Established alloying element in titanium implants; Risk factor in generation of Alzheimer's disease; Can cause muscle fiber damage; Decrease osteoclast viability
Zn	Normal blood serum level 12.4–17.4 µmol/L; Trace element; Essential for the immune system; Co-factor for specific enzymes in bone and cartilage; Neurotoxic at higher concentrations
Ca	Normal serum level 0.919–0.993 mg/L; Most abundant mineral in the human body (1–1.1 kg); Mainly stored in bone, teeth; Is tightly regulated by homeostasis of skeletal, renal, and intestinal mechanism.
Cu	Normal blood serum level 74–131 µmol/L
Mn	Normal blood serum level < 0.8 µg/L; Essential trace element; Important role in metabolic cycle of e.g., lipids, amino acids, and carbohydrates; Influences the function of the immune system, bone growth, blood clotting, cellular energy regulation and neurotransmitters; Neurotoxic in higher concentration (manganism).
Ni	Normal blood serum level 0.05–0.23 µg/L; Strong allergenic agent which can induce metal sensitivity; Carcinogenic and genotoxic.
Sr	140 mg in the human body; Neurological disorder
Sn	9–140 µg/L, locatedinhigherlevelsinliverandlesstoxic; Carcinogenic
Y and Lantanides	< 47 µg in blood serum level; Substituted for Ca 2+ and matters when the metal ion at the active site; compound of drugs for treatment of cancer; Basic lanthanides deposited in liver; more acidic and smaller cations deposited in bone

2.10 Literature Survey

This section preview the recent studies about bio-Mg alloys and show the literature review summery.

In 2013, Bo Song, et al. [104] studied the improving compressive and tensile properties of magnesium alloy plate by pre-cold rolling. Pre-rolling with reduction a little thickness in the transverse direction significantly improved the tensile and compressive characteristics of AZ31 plates. There was a notable reduction in the asymmetry of the yield. The introduction of extension twin borders inside the grains is responsible for this. The strain-hardening curve was also significantly lengthened in compression due to the inclusion of twin boundaries; however, this had less of an effect on the slope of the curve.

In 2014, Seyed Mohammad Arab et al. [105] studied the mechanical characteristics, Microstructure, and cold roll-ability of striped AZ31 alloy examined, along with the impacts of pass number. The grain size of a crystalline metallic material has the greatest impact on its physical and mechanical characteristics of all the microstructural factors. Repeated for numerous passes to apply larger stresses, and can be industrialized, There is a requirement for a subsequent rolling operation to provide acceptable flat specimens after ECAP has been performed on rods or bars having a square or circular cross section. One observation is that increasing the number of passes (strain) decreased grains sizes and produced a uniform microstructure. In magnesium alloys, rotational dynamic recrystallization is the primary process for grain refining. Non-basal texture and refined structure development may be linked to ECAP-induced ductility improvement. Increased activations of slips system and other plastic deformation mechanisms during cold rolling at room temperature is a result

of a more intense non-basal texture and finer grain structure . The most basic texture is not a good place to begin with rolling HCP materials. Even after the rolled specimens still showed 6 twinning, indicating that there were not 5 complete slip systems.

In 2015, Sean Johnston et al. [106] study hydrogen evolution and Mass loss were used to analyze the corrosion of Magnesium high purity (HP), ZE41, and AZ91 in a CO2-bicarbonate buffered Hanks' solution. The rate of corrosion are found to be as follows: ZE41 HP Mg AZ91. Compared to the other Mg alloys, ZE41 corroded at a substantially faster pace. Corrosion rate for AZ91 and HP Mg are similar, although HP Mg deteriorated more rapidly. As pH rose, protective coatings are more robust, and corrosion rates across the board reduced significantly. The corrosion rates of all Magnesium alloys is somewhat increased, and the corrosion morphology is uniformized, due to the sluggish fluid flow.

In 2016 Sultan Alsagabi, et al. [107] Specimens of AZ31 magnesium alloy are tested for electrochemical corrosion in room-temperature solutions of pH 4.5, 9.5, and 13.0 with additions of 0-2000 ppm of chloride. In solutions with a pH of 13 and up to 1500 ppm of chloride, cyclic polarization did not cause a loss of passivity. AZ31 corrosion in solutions with pH 4.5 and 9.5 is mitigated by adding supportive electrolytes sodium sulfate and sodium dihydrogen phosphate. The Mott-Schottky analysis revealed a duplex surface layer, with an n-type MgO1x inner layer (x = 0.024-0.05) and a p-type outer layer that grew with time at the cost of the inner layer.

In 2018 Ebrahim Tolouie, et al. [108]. Study, the effect of asymmetric cold rolling on microstructure, texture, and mechanical properties of AZ91 magnesium alloy investigated. Optical microscopy (OM), scanning electron microscopy (SEM), x-ray diffraction (XRD), tensile, and hardness tests performed. The homogenization process significantly increased the grain size of the as-cast sample. During 8% rolling, continuous dynamic recrystallization (CDRX) mechanism resulted in a relatively sharp drop in average grain size. The results indicated that the formation of extension twins during rolling led to a rotation of primary oriented grains toward texture. After 15% deformation, the created basal texture with the intensity of 4.6 mrd has almost 10-degree deviation from the normal direction. With increasing the rolling reduction, the hardness increased due to increasing the fraction of twins and intensity of basal texture. The 8% deformed sample had the maximum tensile strength and microhardness owing to the saturation of twins as well as the absence of microcracks in the microstructure. Findings showed that the as-homogenized and 8% rolled samples had the highest and lowest inhomogeneity factor (18.5 and 10.6), respectively. The failure mode was a mixture of cleavage and ductile fracture. With increasing the thickness reduction, the cleavage mode became severe due to the formation of microcrack.

In 2019 Cancan Liu et al. [109] In order to achieve a nanostructured surface layer, AZ31 and AZ91 Mg alloys were subjected to severe shot peening (SP). Transmission electron microscopy, a micro-hardness tester, and corrosion tests are used to examine the microstructure, micro-hardness, and corrosion behavior of SP-treated AZ31 and AZ91 Mg alloys. A nanoscale plastic deformation layer including -Mg grains is found on the surface of AZ31 and AZ91 Mg alloys after SP treatment. Grain

refinement and work hardening, both effects of SP treatment, clearly increased the micro-hardness in the near surface area for two alloys. By quickly forming a reasonably compact passive coating on the nanostructured surface, SP treatment increased AZ31 alloy's resistance to corrosion. Since SP treatment had only a modest impact on the size and distribution of -phases in AZ91 alloy, it is unable to significantly improve the material's corrosion resistance.

In 2020 R VAIRA VIGNESH, et al. [110]. Research the effects of SBF on magnesium alloy corrosion and wear. Characterization of the microstructure and micro hardness of AZ91 magnesium alloy. Multiple types of corrosion tests, wear tests, and a combined corrosion-wear test were performed on the foundational material. The research found the following results: AZ91 is a magnesium alloy with a microstructure made up of eutectic phases of α-Mg, β-$Mg_{17}Al_{12}$ and (α + β). The β phase dispersed throughout the matrix as large, continuous precipitates. Time spent submerged in bodily fluids increases the likelihood that hydroxyapatite will develop on the AZ91D's surface. From the Tafel, we may extrapolate a corrosion potential of 1.448 V and a corrosion rate of 4.44 mm/year. Adhesive wear test statistical modeling sheds light on the relationship between the transition load and the evolution of wear-test variables. The wear test of samples is significantly affected by SBF.

In 2023, Ebrahim Tolouie, Roohollah Jamaati [111]. Study, the effect of rolling reduction on the microstructure, crystallographic texture, and mechanical properties of the AZ91 alloy is studied. Optical microscopy (OM), scanning electron microscopy (SEM), X-ray diffraction (XRD), and tensile and hardness tests were used. The homogenization process significantly increased the grain size of the as-cast sample. The results showed that $\{10\bar{1}2\}\langle 10\bar{1}1\rangle$ extension

twinning during rolling leads to rotation of {0001}∥RD initial orientation toward {0001}∥ND basal texture. During asymmetric hot rolling up to 15%, the intensity of {0002} basal texture increased to 10 multiples of random distribution. After 15% deformation, the average grain size decreased due to the occurrence of dynamic recrystallization. It was found that by increasing the rolling reduction up to 15%, the hardness and tensile strength greatly increased owing to an increase in the fraction of twins and the intensity of basal texture. The occurrence of the CDRX mechanism and the formation of strong basal texture resulted in an excellent combination of strength and ductility for the 15% rolled sample. The as-homogenized and 8% rolled samples had the maximum and minimum inhomogeneity factor (IF), respectively. The fracture surfaces indicated that the mixture of ductile and brittle fracture is the main failure mode.

Chapter Three

Chapter Three

Experimental work

3.1 Introduction

The experimental setup, materials, methods, and tools used to conduct tests to evaluate the effects of cold work (rolling) on the Magnesium alloys used as biomaterials, corrosion and wear properties show in this chapter.

Additionally, the chapter describes the research study primary materials, cold work, corrosion, and wear tests. Additionally, it covers specifics regarding the metal preparation and immersion environment. Were put through several tests to analyze the behavior of these materials and learn more about how they perform, including microstructure, corrosion teats, antibacterial, wear and hardness testing.

3.2 Experimental Procedure (Materials and Methods)

This part specifies the raw materials, cold work (rolling), and procedures utilized during the research study. It is also includes the base material preparation and details about the operations condition and the setup used in this study, including immersion solution. Figure (3-1) summarizes all the activities took place during this study.

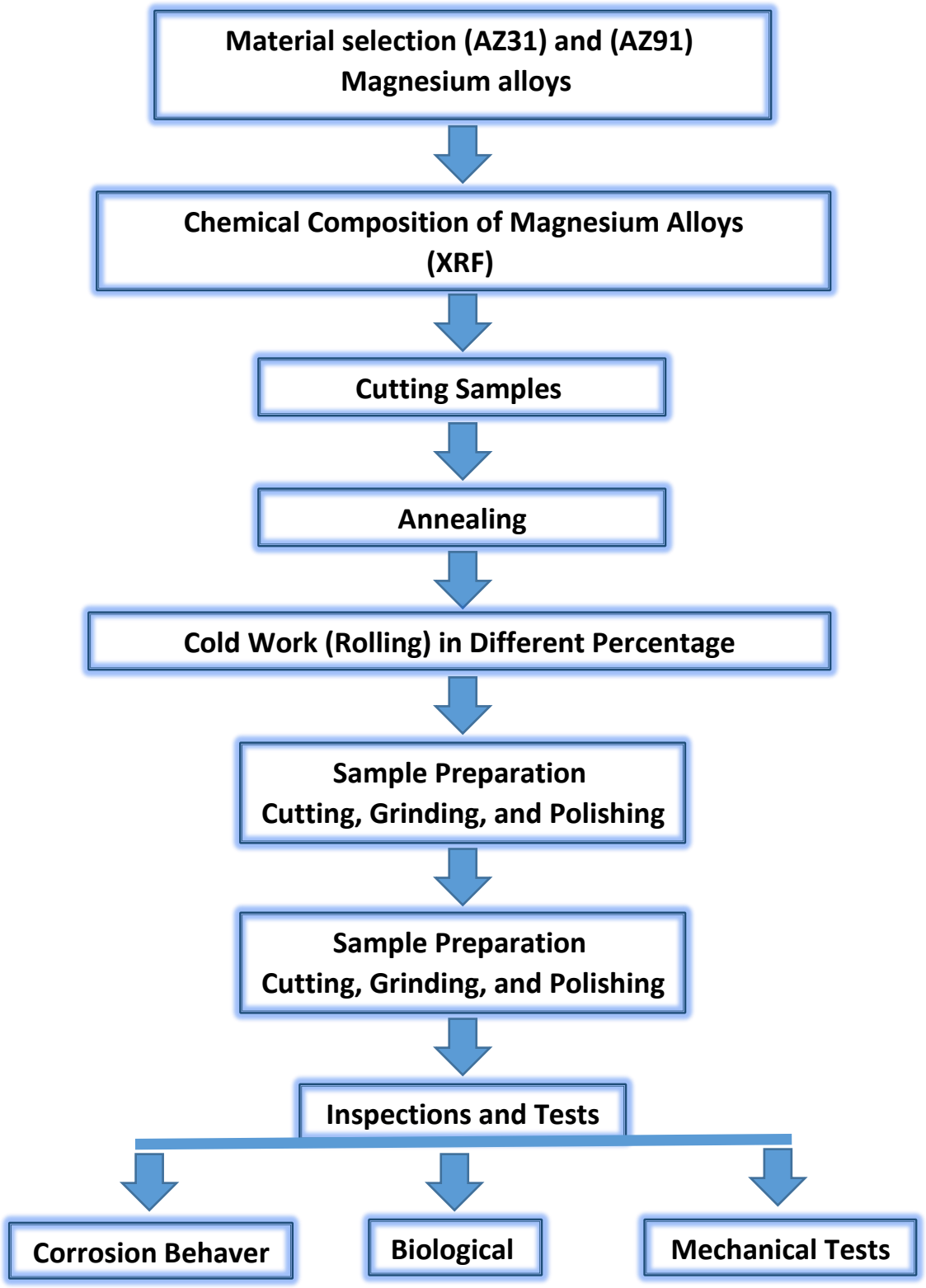

Figure (3-1) block diagram of experimental steps of the work

3.3 Materials Used in the Current Research

The chosen materials for studied in the current work is biodegradable Magnesium alloys (AZ31 and AZ91). The both of alloys used in the third generation biomaterials [36].

The AZ31 alloy is wrought magnesium alloys, typically contents aluminum (3%Al) and a zinc (1%Zn) by weight. In addition to its employment in medical implants and airplane fuselages, AZ31 alloy also used in the construction of mobile phone and laptop casings.

The second alloy is AZ91 cast magnesium alloys typically contents aluminum (9%Al) and a zinc (1%Zn) by weight. Among, AZ91 alloy is the most popular option because to its high strength and great cast-ability. For die casting, AZ91 alloy has to have better mechanical properties. AZ91 is employed for a variety of commercial applications due to its high strength/weight ratio and outstanding welding qualities in fields as diverse as automotive, electrical, medical, sports, and aerospace [112].

A Chinese company (Eternal Bliss Alloy Casting & Forging Co. LTD) has prepared the two plate of (AZ31) and (AZ91) magnesium alloy. And cut into pieces using the Vertical Milling Machine (VMC) (in the University of Technology) for samples with 200 mm length, 30mm width and 11 mm thickness.

3.4 Chemical Analysis

Chemical composition of tested materials (AZ31 and AZ91 magnesium alloys) the chemical composition analysis were done using the x-ray fluorescence (XRF) and (XRD) in the Ministry of Science and Technology. The chemicals composition of magnesium alloys obtained by x-ray fluorescence (XRF) as shown in the table (3-1) for both alloys. The results compared with the chemical analysis of Chines Company and with the ASTM specifications, as shown in the appendix (A).

Table (3-1) chemical composition

Table (3-1A): chemical composition for AZ31

Element	Al	Zn	Mn	Si	Cu	Ca	Fe	Na	Mg
Standard	2.5-3.5	0.6-1.4	0.2	0.1	0.05	0.04	0.005	0.005	Bal.
AZ31	3.25	1.23	0.15	0.08	0.04	0.003	0.004	0.003	Bal.

Table (3-1B): chemical composition for AZ91

Element	Al	Zn	Mn	Si	Cu	Ca	Fe	Na	Mg
Standard	8.3-9.7	0.3-1	0.2	0.01	0.03	-	0.005	0.002	Bal.
AZ91	9.3	1	0.1	0.01	0.02	-	0.004	0.003	Bal.

The density for AZ31 are 1.76 g/cm^3, whereas for AZ91 it was 1.8 g/cm^3 by used Archimedes method.

3.5 Heat treatments

Since the process of preparing the alloys is done through a commercial company, and to obtain an alloy free from any structural deformations or internal stresses that may affect the course of scientific research, the recrystallization process is resorted to remove any influences that the alloy might have been exposed to during manufacturing or cutting operations.

For the AZ31 alloy, sample recrystallization process accomplished by heating the samples in the furnace at (250℃) for 1 hours. and then cooled at the furnace [113].

While for the AZ91 alloy, sample recrystallization process accomplished by heating the samples in furnace at (400℃) for 3 hours. Then cooled at the furnace [114].

3.6 Specimen Preparation

3.6.1 Cold work (rolling)

A sample of (AZ31) and (AZ91) magnesium alloys has deformed by rolling in room temperature (reduce thickness of the sample by passing in the one direction of the rolling machine) to deferent ratio (5, 10, 15, and 17)% for samples of AZ31 and (5, 10, and 15)% for AZ91 alloys [115].

$$Cold\ work\ \% = \left(\frac{Initial\ Thickness - Rolled\ Thickness}{Initial\ Thickness}\right) * 100\% \qquad (1)$$

3.6.2 Preparation sample

The samples catting after rolling process, then grinding by silicon carbide (SiC) papers of 180, 400, 600, 800, 1200, 2000 and 3000 grades, respectively with using water as a lubricant. The samples then polished using diamond liquid as show in figure (3-2). After polishing stage, the samples washed by ethanol and then dry with hot air.

Figure (3-2) simple after polishing

3.7 The Examinations

3.7.1 Optical Microscopy (OM)

The samples are prepared for microstructure investigation using conventional metallographic methods. Then, the samples subjected to the chemical etching (15ml water, 100ml ethanol (95%), 6g picric acid and 30ml acetic acid) [116]. This inspection conducted at the University of Babylon's Laboratory of the Metallurgical Engineering Department of the Faculty of Materials Engineering.

3.7.2 Micro structure Examination with Scanning Electron Microscope test (SEM)

By using scanning electron microscope (SEM) in the University of Babylon - Faculty of Materials Engineering, revealed the microstructures of the samples. The sample etched by using a suitable etch solution to reveal the grain boundaries. The solution that used for etching process composed of 15ml water, 100ml ethanol (95%), 6g picric acid and 30ml acetic acid.

3.7.3 Hardness Test

The effects of cold work (rolling) on the hardness of AZ31 and AZ91 magnesium alloys investigated. A digital Vickers micro hardness tester used to conduct a micro hardness test (HVS-1000). with a holding period of 10 seconds and weights of 2 N. Three separate readings of hardness taken from various locations on the surface of each sample, and an average was then calculated. This test done in the Metallurgical Engineering Department, Faculty of Materials Engineering, the University of Babylon laboratories.

3.7.4 Corrosion Tests

All AZ31 and AZ91 magnesium alloys samples are test in the simulated body fluid (SBF). Each 1000 ml of SBF includes elements as the table (3-2) [112]. The pH of simulated body fluid (SBF) are (7.4).

Table (3-2) simulated body fluid (SBF) [117]

S. no.	Reagents	Amount in 1000 ml
1	NaCl	8.035 g
2	$NaHCO_3$	0.355 g
3	KCl	0.225 g
4	$K_2HPO_4 \cdot 3H_2O$	0.231 g
5	$MgCl_2 \cdot 6H_2O$	0.311 g
6	1.0 M HCl	39.0 ml
7	$CaCl_2$	0.292 g
8	Na_2SO_4	0.072 g
9	$((HOCH_2)_3CNH_2)$	6.118 g
10	1.0 M HCl	Appropriate amount for adjusting the pH ~ 7.4

3.7.4.1 Open Circuit Potential (O.C.P)

During this process, the free corrosion potential (E_{corr}) is determined by measuring the open circuit potential (OCP), which is also known as the equilibrium potential or open circuit voltage (O.C.V). E_{corr} is determined by recording the open - circuit potential of samples immersed in the SBF. When both the working and reference electrodes submerged in a solution of 200 cc electrolyte, the potential difference between them calculated using this method.

Every five minutes, the specimen in the corrosion solution had its O.C.P. (voltage versus time) measured. The voltage recorded every five minutes

for the duration of the test, beginning with the initial reading acquired immediately after immersion. Using a magnetic stirrer, all of the tests performed at ambient temperature and in the open air.

3.7.4.2 Potential dynamic Polarization

Magnesium alloys AZ31 and AZ91 examined to see how they fared in corrosive environments. In order to calculate the corrosion rate, the Tafel extrapolation technique has been use. The cell had three electrodes:

1- The reference electrode.
2- The counter electrode.
3- Working electrode (specimen).

It placed in containing electrolyte solution, which is SBF. At the outset of each specimen test, the open-circuit voltage recorded. The instrument (type WENKING M LAB) used, it located in the Babylon University Metallurgical Department College of Materials Engineering.

The value of corrosion rate (mm/year) can be determined from the data of this test according to [ASTM G102] as follows:

$$corrosion\,rate = K * icorr * EWD \quad (2)$$

Where:

K = $3.27 * 10^{-3}$ m.g / μA.cm.year

EW=Equivalent Weight

D = material density (g/cm^3)

i_{corr} = corrosion current density ($\mu A/cm^2$)

$$icorr = Icorr * A \quad (3)$$

Where:

I_{corr} = current of corrosion (μA)

A= the exposed surface area (cm^2)

Equivalent Weight Calculation

Only elements above one mass percent are included in the computation of equivalent weight (EW) for alloys, according to normal ASTM standard for calculating corrosion rates and related information from electrochemical experiments. As a result, in the instance of AZ31Mg alloy, magnesium (Mg), aluminum (Al) and zinc (Zn) are the only elements that really depend (show Table 3-1). As a result, equivalent weight is determined using the relationship:

$$EW = \frac{1}{\sum \frac{Mass\ fraction * Valence}{Atomic\ weight}} \qquad (4)$$

Where for AZ31 mass fraction of (Mg), (Al) and (Zn) percentage are 92.38, 3.25 and 1.23 respectively (see Table 3-1). Valence value is $^{+}2$ for both elements and $^{+}3$ for Al, atomic weight for (Mg), (Al) and (Zn) are 24.31, 26.98 and 65.38 respectively, and substituting these values give 7.999. Therefore, the AZ31 Mg alloy equivalent weight is 100/7.999 = 12.5156.

And for AZ91 mass fraction of (Mg), (Al) and (Zn) percentage are 87.34, 9.3 and 1 respectively (see Table 3-1). Valence value is $^{+}2$ for both elements and $^{+}3$ for Al, atomic weight for (Mg), (Al) and (Zn) are 24.31, 26.98 and 65.38 respectively, and substituting these values give 8.2502. Therefore, the AZ91 Mg alloy equivalent weight is 100/8.252 = 12.1209.

3.7.4.3 Electro-chemical Impedances Spectroscopy (E.I.S)

To investigate the impedance properties of a cell, electrochemical impedance spectroscopy (EIS) is a potent experimental technique that employs an alternating current (AC) signal of low amplitude. This method generates an impedance spectrum for the tested electrochemical cell by measuring its impedance over a variety of frequencies. An element in a circuit (resistor, capacitor, inductor, etc.) has an impedance, which is its frequency-dependent resistance to current flow. Figure (3-3) depicts the EIS Excitation and Response [118].

Specimen resistance to corrosion of study done in SBF. The electrochemical corrosion cell placed in the water path to maintain a temperature consistent with that of the human body (±37˚C). The test done in the Material Characterization Center (MCC).

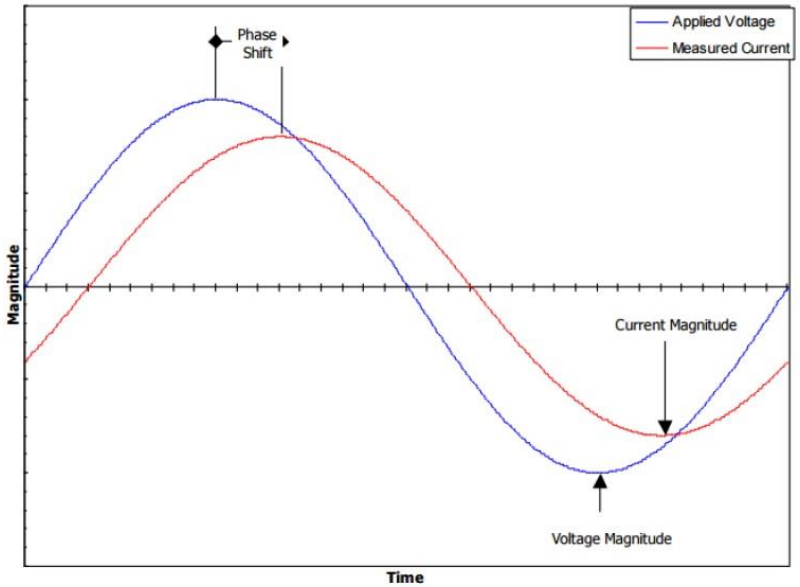

Figure (3-3) depicts the EIS Excitation and Response [118]

3.7.4.4 Ion released

AZ31 and AZ91 samples are stored in plastic containers with tight lids and exposed to the physiological medium (20 milliliters of S.B.F) for 7 days. The solutions held at 37 °C with the use of a thermostatic bath. The test done in U-science scientific lab, Al diwanya, Iraq.

3.7.4.5 pH-Measurement

To acquire pH readings, samples having a surface area of 6 cm^2 were submerged in SBF at (37°C $^{+-}$1) for 7 days. A pH meter used to determine the sample's pH value.

The specimen is floating in the fluid. Corrosion rate as determined by pH fluctuation. The pH of each solution is measure after it placed in a water bath and kept at (37°C $^{+-}$1) for a reasonable amount of time.

Since the pH of corrosive solutions fluctuates in response to prolonged immersion, this property taken into account.

3.7.4.6 Hydrogen Evolution

Samples are floating in the liquids. By keeping it in a water bath, we can keep the temperature constant at (37°C $^{+-}$1). The design of the equipment used to determine the hydrogen evolution rate in this study shown in figure (3-4) [116]. This simple device used for collecting data on hydrogen evolution.

A sample of magnesium alloys AZ31 and AZ91 submerged in an electrolyte (SBF) in a beaker. The specimen placed under the funnel to remove any remaining hydrogen from its exterior. After putting a burette atop the funnel and filling it with (SBF), the hydrogen gas released during magnesium's disintegration collected and transferred to the burette,

gradually displacing the caustic solution. Simply by measuring the level of the (SBF) in the burette, the volume of the evolved hydrogen could be determined. Work performed at a constant (37°C $^{+-}$1).

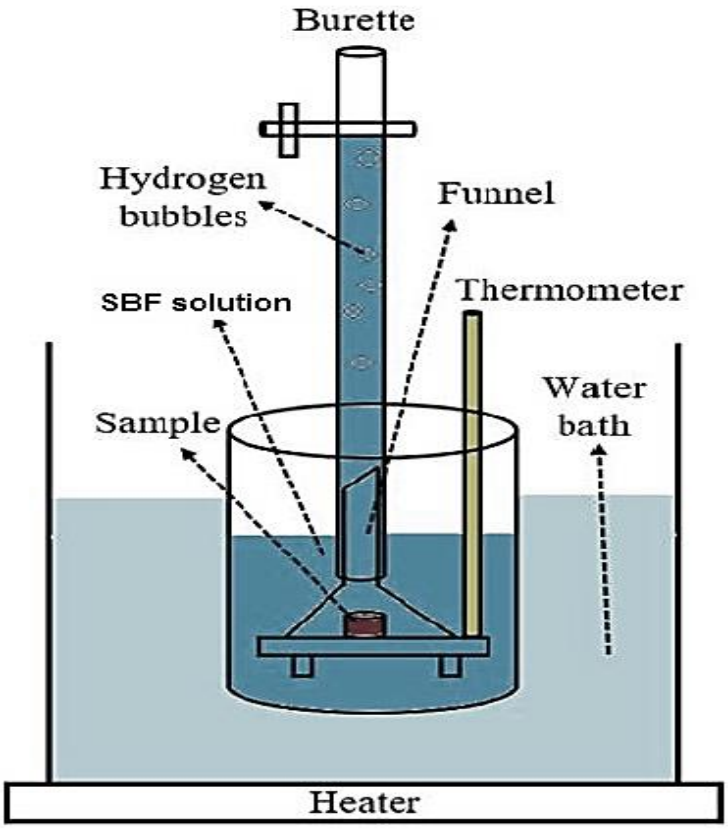

Figure (3-4) schematically measuring of the hydrogen evolution [121]

3.7.5 Biological Tests Antimicrobial Activity

Antimicrobial activity investigated using included gram-negative bacteria (Enterococcus) and gram-positive bacteria (Staphylococcus epidermidis). In diagnostic labs, spreading microorganisms on a surface of alloys samples perform the test. After that incubated at 37 ° C for 24 hrs. The inhibition areas then evaluated. The test done in the University of Babylon - Faculty of Science for Girls.

3.7.6 Wear Test

To study the Tribology behavior of samples, wet sliding wear test carried out following ASTM G99 [119] [using a wear tester pin-on-disk. To understand the effect of cold work on the responses of the alloys in terms of specific wear rate. In the tests, the radius of rotation is constant at 3 mm with a total testing time of 30 min the rate of SBF flow is 3.5ml/min. The samples rotated speed 350 rpm. Total sliding distance 197.82 m with loadings of 5N.

Wear test is performed by the wear device with stainless steel boll, in the University of Babylon - Faculty of Materials Engineering figure (3-5). Wear test is performed in laboratory at room temperature. The weight of specimen recorded before test by using a sensitive balance. This test done in wet environment-using SBF. The weight of specimen recorded after the test.

Specific Wear rate will obtain by [120]:

$$Specific\ wear\ rate\ \left(\frac{mm3}{Nm}\right) = \frac{volume\ loss(mm3)}{sliding\ distance\ (m) * Load\ (N)} \quad (1)$$

Where:

$$Volume\ loss(mm3) = \frac{\text{Weightloss(mg)}}{Density\ (\frac{mg}{mm3})} \quad (2)$$

And

$$\text{Sliding distance } SD = 2\pi rnt \quad (3)$$

Where:

r: radius the specimen to Center of the disc(cm)

n:- Number of sessions of the disk (r / min)

t:- Testing time (min).

Figure (3-5) Wear testing device

Chapter

Four

Chapter Four

Results and Discussion

4.1 Introduction

This chapter provides an in-depth discussion and analysis of the obtained experimental data. Includes a discussion of how various percentages of cold work effect the corrosion and wear behavior of third-generation biomaterial (magnesium alloys AZ31 and AZ91).

4.2 X-ray Diffraction (XRD)

Shows the XRD patterns of starting materials. Appearance of peaks corresponding to α-Mg phase and β-phase ($Mg_{17}Al_{12}$). The β-phase found to be prominent for AZ91 sample in which (Al) content more compared with AZ31. As see in figure (4-1) and (4-2).

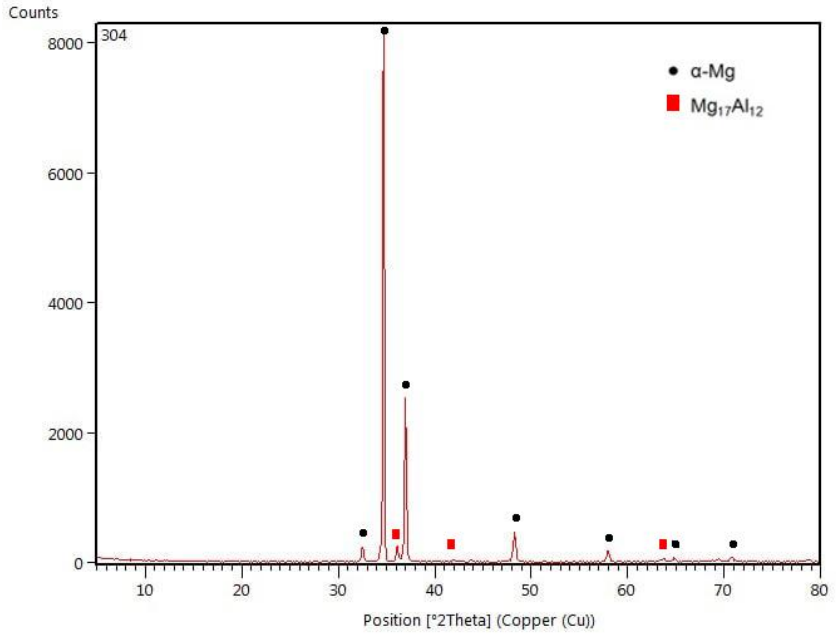

Figure (4-1) XRD for AZ31 alloy

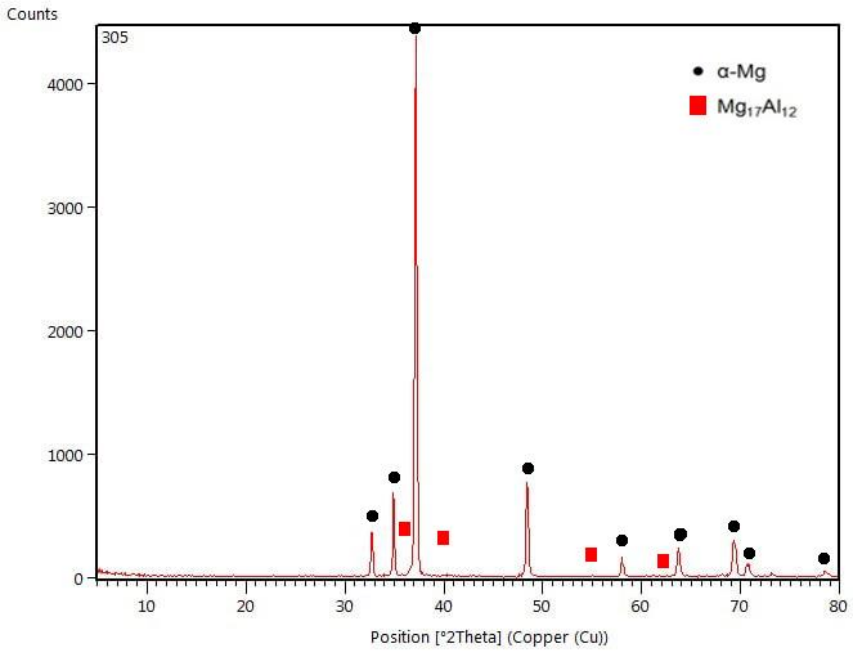

Figure (4-2) XRD for AZ91 alloy

4.3 Optical and Electron Microscope (SEM)

Initial microstructures that consist of equiaxed-grain with an average grains sizes of ~35µm for AZ31 and ~30µm for AZ91. Which can be an indication of recrystallize states of as-received materials. The AZ31 and AZ91 alloys consists of α-Mg and eutectics phases (Mg2Al3, Al8Mn5, and Al4Mn) distribute heterogeneous in the Mg matrix. The morphology off eutectics precipitate varies from block structure (~6µm) to fines particle [121]. The analyses show Aluminum and manganese as their main element, as secondary phase contain mainly Al and Mn. Promote the formation of segregation and brittle precipitate figure (4-3) and (4-4) [121].

During rolling, microstructural significant changes generated on the initial microstructures of AZ31 and AZ91 Mg alloys. Which affected by the deformations degrees. In figure (4-5), Optical Microscopes images for AZ31 alloy and figure (4-6) Optical Microscopes images for AZ91 alloy,

with different percentage cold work value from the figures remark the effect of rolling on microstructure orientation. The main microstructure generate for different deformation. Rolling at temperature (room temperature), generate microstructure with some region of small grain relatively un-deformed (~7μm) surrounded by bigger deformed grains figure (4-7) and (4-8). Where in mechanicals twin preferentially formed and intensified when the deformations degrees increase. Pointing that the max reduction thickness (between 15% - 20%) [111].

Since it generate higher grain subdivision on different region of deform sample, probably involve geometry necessary boundary and slip-induced grain boundary sliding during the grain subdivision mechanism. Which commonly originate in homogeneous plastic deformation of polycrystalline material with high anisotropy level such as Mg alloy figure (4-9).

Most deformation twins formed in the rolled alloys are {10–11} contraction and {10–11}-{10–12} double twins, rather than {10–12} extension twins. Moreover, the formed twins have a narrow width and needle-like shape, which is typical morphology of contraction and double twins. It is notable that the formed twins more homogeneously distributed in the rolled alloys. However, since deformation twinning leads to lattice reorientation [122–124]. Which indicates that more twins formed in the rolled room temperature. Since twinning are activate through atomic motion, it is strongly related to deformation temperature [125 - 127] the distributions of these twins in the two rolled alloys in this study, the twins are evenly distributed throughout the material. As the deformation temperature decreases, the homogeneity of deformation reduces because of the increased plastic instability, which eventually causes localized deformation [128–129]. . As a result, deformation twins are at room temp

causes the compressive deformation to impose relatively evenly throughout the material, which results in the formation of deformation twins uniformly across the rolled alloys.

However, on cold work deformed with reduction higher than 10%, a massive twins boundary interaction generate double-twin formation and increase the localized stresses concentrations, which is often associated with suddenly failure. Heterogeneous microstructures formed at low strain rates, with areas of tiny untwined grain surround by regions of coarse twinned grain and shear-band, whereas high strain rate promoted the production of twinning and shear bands [130].

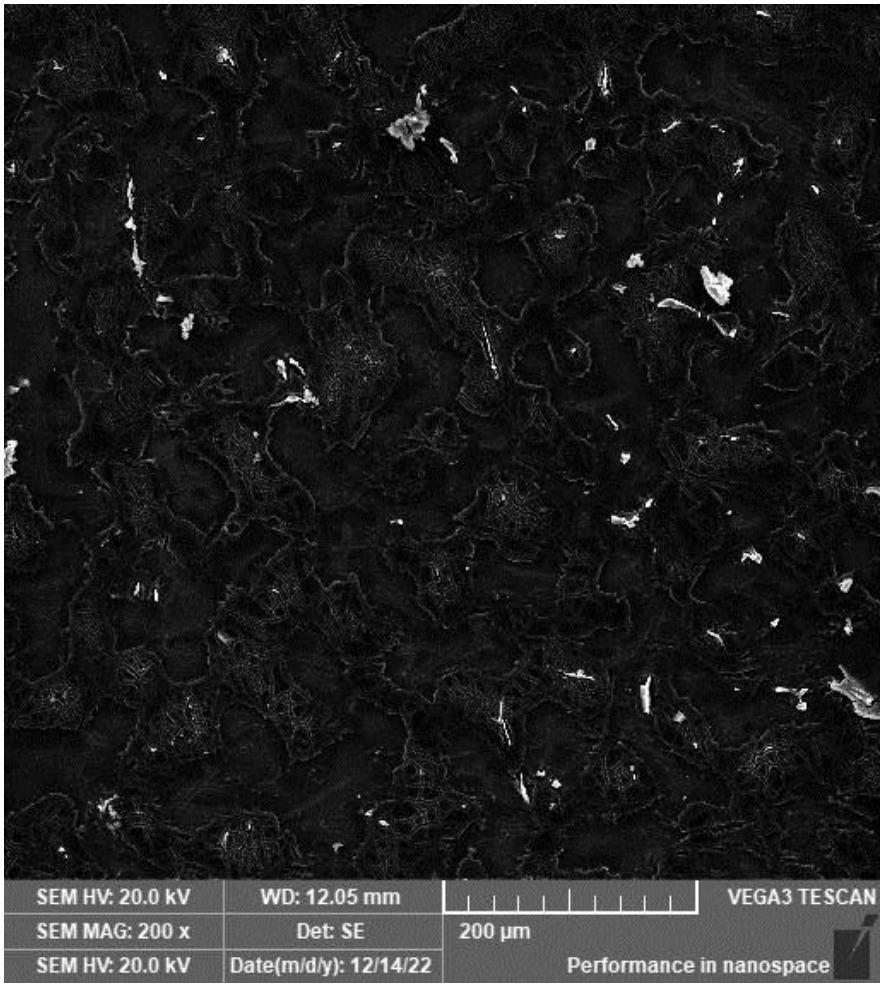

Figure (4-3) Scanning electron microscope image for AZ31

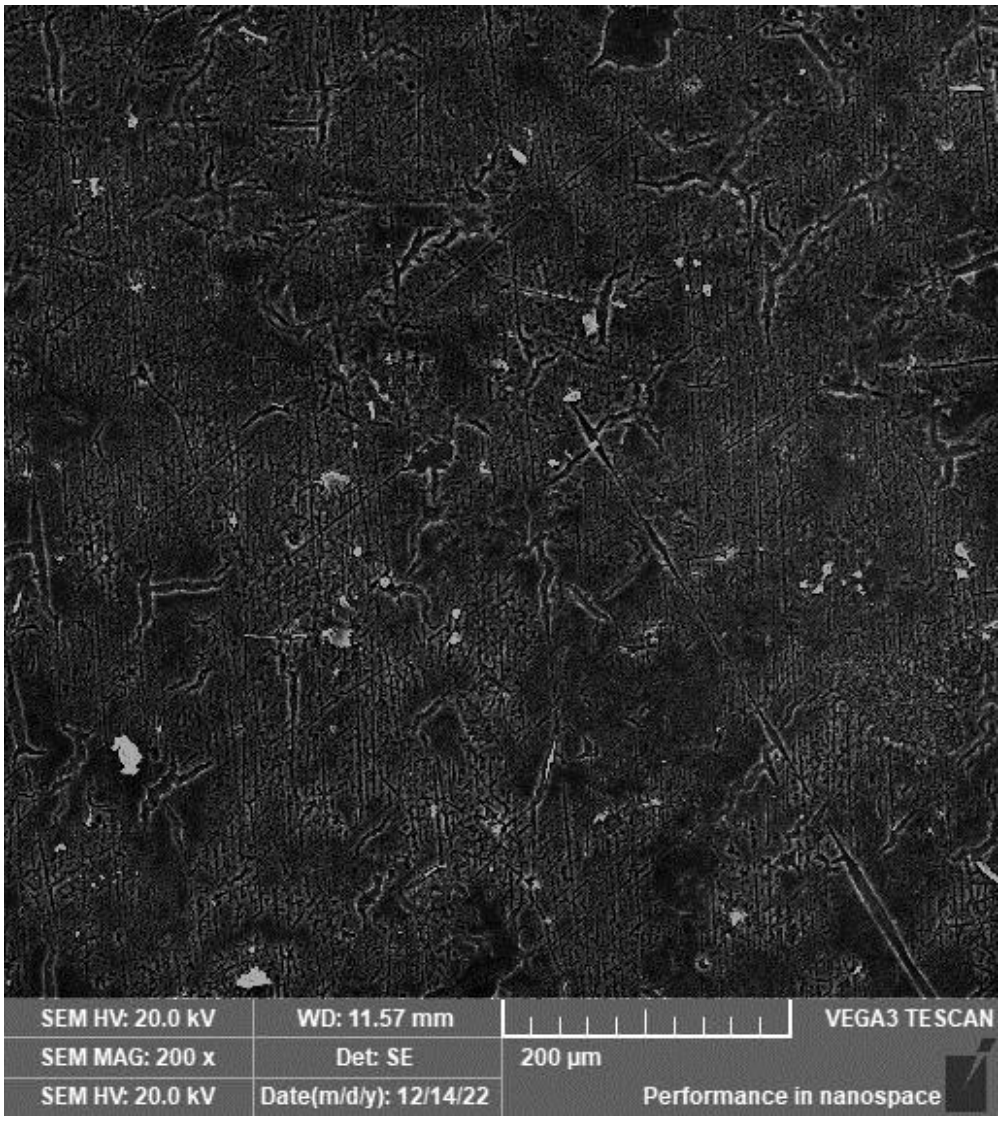

Figure (4-4) Scanning electron microscope image for AZ91

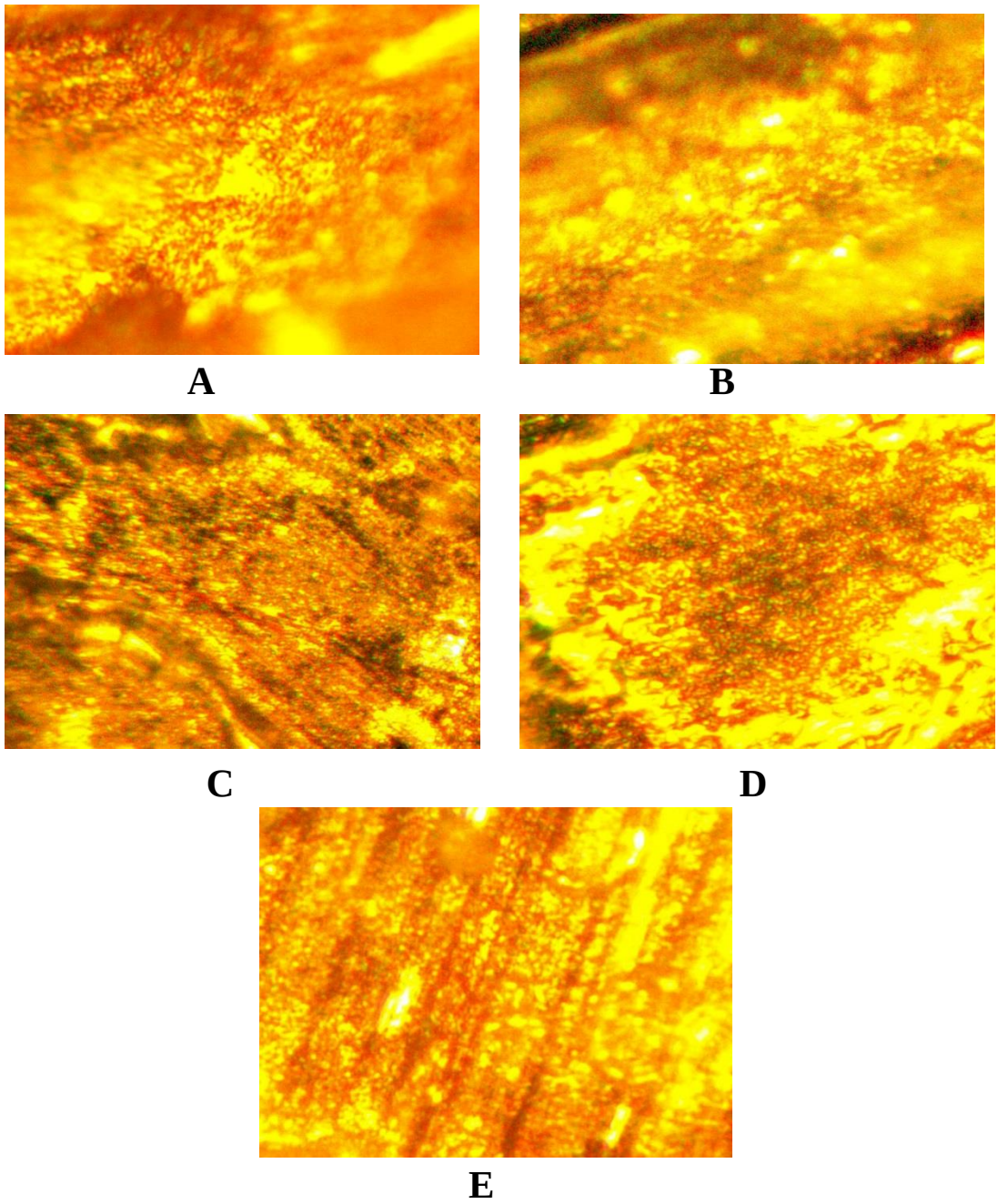

Figure (4-5) Optical Microscope image for AZ31 alloy.

A) As received alloy. B) 5% cold work . C) 10% cold work.

D) 15% cold work. E) 17% cold work

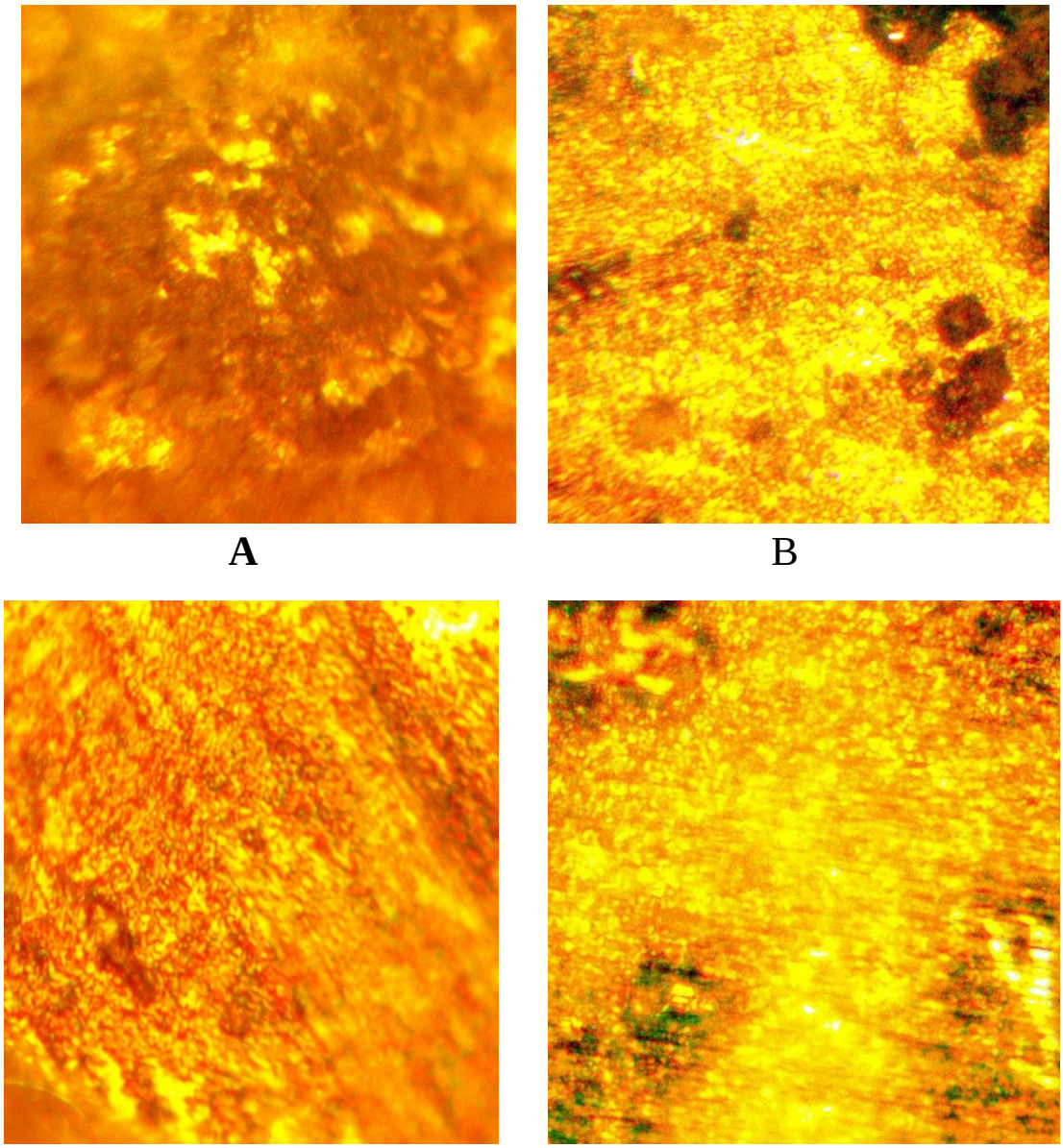

A B

C **D**

Figure (4-6) Optical Microscope image for AZ91 alloy.

A) As received alloy. B) 5% cold work.

C) 10% cold work. D) 15% cold work.

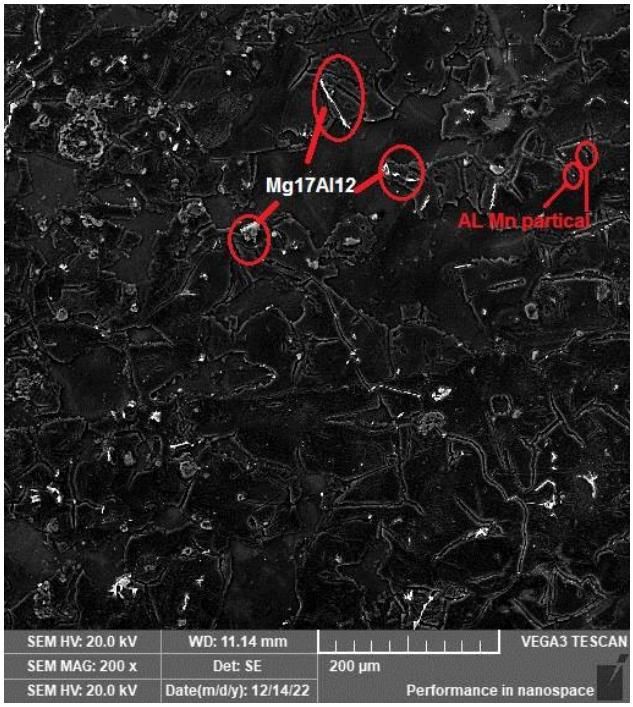

Figure (4-7) Scanning electron microscope image for AZ31 15%

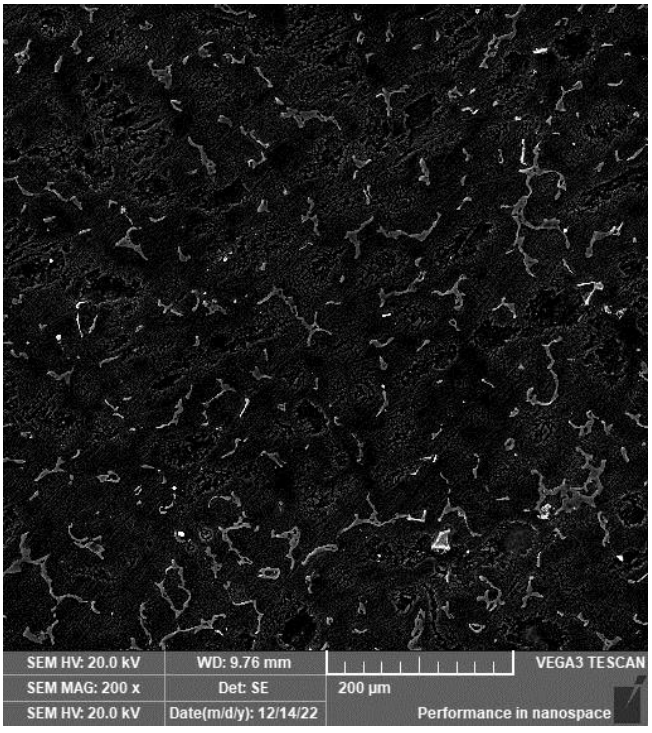

Figure (4-8) Scanning electron microscope image for AZ91 15%

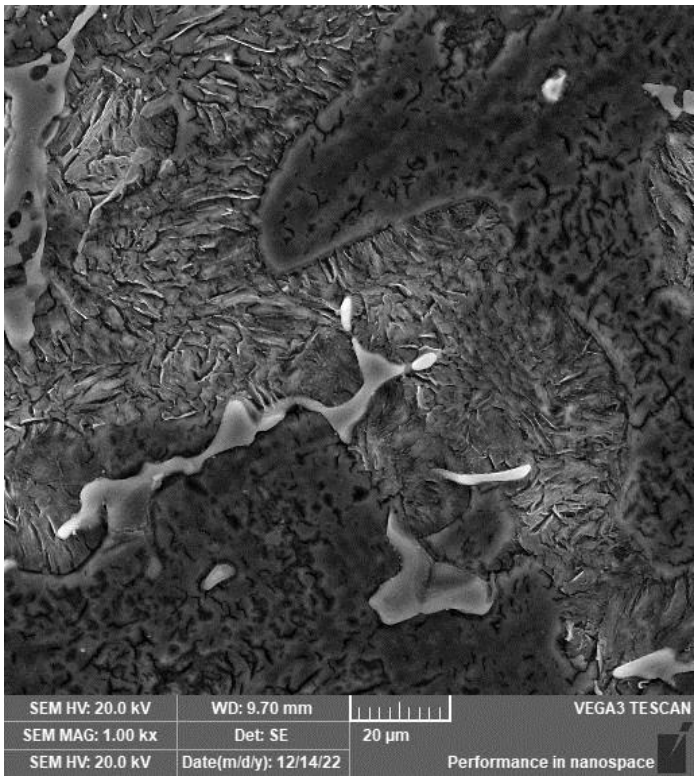

Figure (4-9) Scanning electron microscope image for AZ91 15%

4.4 Hardness Test

The impact of cold work on the hardness of AZ31 and AZ91 magnesium alloys is examined. The material hardness is measured using a Vickers hardness tester set to a holding duration of 10 seconds and weights totaling 200 g. Three separate readings of hardness are collected from various locations on the surface of each sample, and an average is then calculated.

As show in table (4-1), the hardness of both alloy increased with increase of cold work to maximum value at 10% cold work. The hardness of colds rolling sample increase from (58.7 HV to 107 HV) for AZ31 and from (102.79 HV to 122.95 HV) for AZ91. This strengthen mainly influence by

the rolling reductions and generate by the activations of various deformations mechanism, include mechanicals twins, slip on non-basal and basal plane and highs dislocation pile–ups produce at grains and small particles boundary of cold rolling. After this percentage, the alloy will have reached the highest stress energy that can be tolerated by the deformation mechanisms such as twinning and sliding levels [131]. Therefore, the alloy will have a lower hardness when increasing the forming percentage above 10%, but it will remain higher than the hardness recorded for the basic alloy before forming.

Table (4-1) the hardness test of AZ31 and AZ91 alloy

Sample	**HV kg/mm^2**
AZ31	58.7
AZ31 5%	91.23
AZ31 10%	107
AZ31 15%	103.4
AZ31 17%	88.42
AZ91	102.79
AZ91 5%	122.71
AZ91 10%	122.95
AZ91 15%	117.66

4.5 Corrosion

4.5.1 Open Circuit Potential (OCP)

Magnesium corrosion behavior is very environment dependent; in this studies using SBF as the corrosion environment, results are reported at intervals of 5 minutes for times ranging from 0 to 120 minutes. The extraordinarily negative potentials of -1585 mV and -1700 mV for AZ31 and AZ91, respectively, indicate their highly active nature. Figure (4-10) displays findings for AZ31, whereas Figure (4-11) displays results for AZ91.

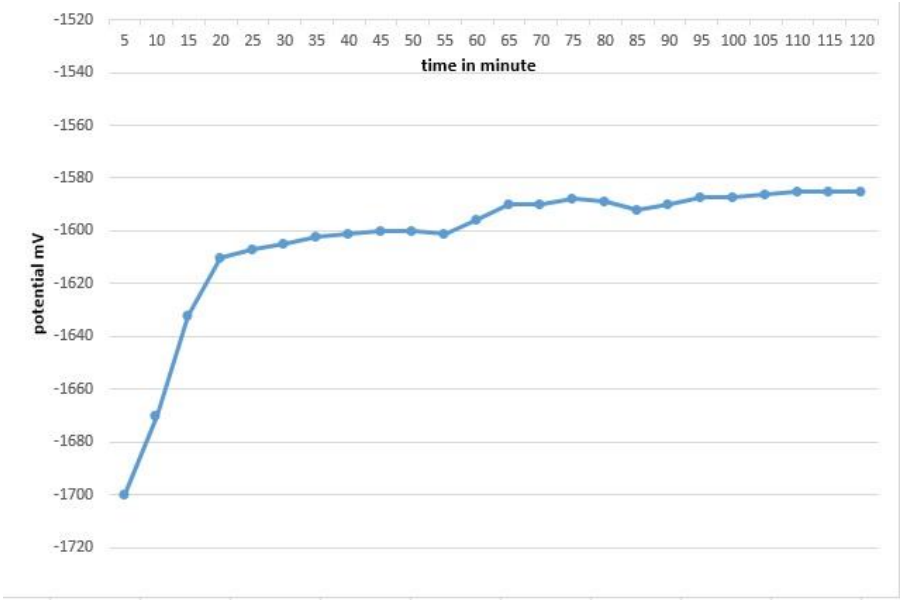

Figure (4-10) Open Circuit Potential for AZ31

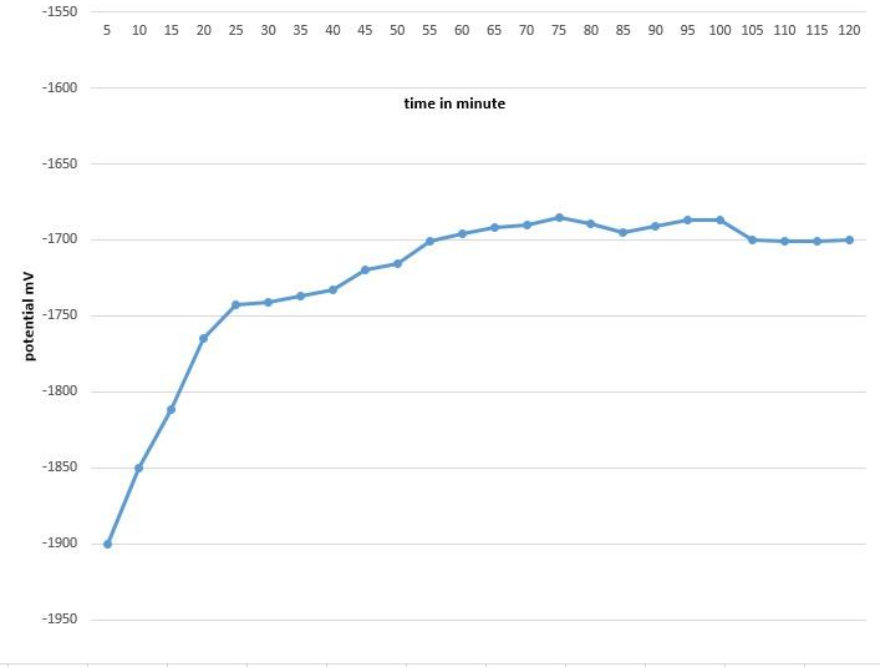

Figure (4-11) Open Circuit Potential for AZ91

4.5.2 Potential dynamic Polarization

The corrosion rate of the samples is determine by immersing them in SBF at room temperature and using the Tafel test. Such experiments may provide an approximation of the electrochemical behavior of the Mg alloys (AZ31 and AZ91) investigated in a corrosive environment. The percentage cold work impact on the corrosion parameters of corrosion current density (icorr), corrosion potential (Ecorr), and corrosion rates (CR).

As can be seen in Tafel test figure (4-12), as well as in the results for a sample of AZ31 alloy in Table (4-2), the corrosion potential of the alloy increases when it is exposed to cold forming. The alloy's activity rises because of the internal stress in it and that increase the potential energy of alloy. For AZ91 alloy, we see from the table (4-2) and the figure (4-13)

that as the formation percentage increases, the potential value decreases, with the lowest value occurring at 5% cold work and gradually increasing to the reserved alloy value at 15% formation percentage. In Alloy AZ91 the second phase ($Mg_{17}Al_{12}$) is an important factor in the corrosion process, as the base alloy in which the second phase is randomly distributed and with rolling is organized on the grins boundary, forming a barrier to corrosion to a certain extent, as this effect appears at a ratio of 5% [132].

Table (4-2) the Tafel test results for AZ31 and AZ91 alloy samples.

	$E_{corrosion}$ (mV)	$I_{Corrosion}$ (mA/cm^2)	β_C (mv\decade)	βa (mv\decade)	C.R
AZ31	-1560	15.17	-17.3	31.5	$1.09 *10^{-3}$
AZ31 5%	-1678	25.82	-18.8	12.7	$1.85 *10^{-3}$
AZ31 10%	-1684	24.33	-32.7	33.1	$1.75 *10^{-3}$
AZ31 15%	-1712	27.47	-31	22.6	$1.97 *10^{-3}$
AZ31 17%	-1684	43.60	-48.2	65.2	$3.14 *10^{-3}$
AZ91	-1801	20.91	-36.5	41.4	$1.49 *10^{-3}$
AZ91 5%	-1606	23.44	-36.1	39.8	$1.67 *10^{-3}$
AZ91 10%	-1763	27.77	-35.3	44.6	$1.98 *10^{-3}$
AZ91 15%	-1807	47.2	-36.1	41.2	$3.36 *10^{-3}$

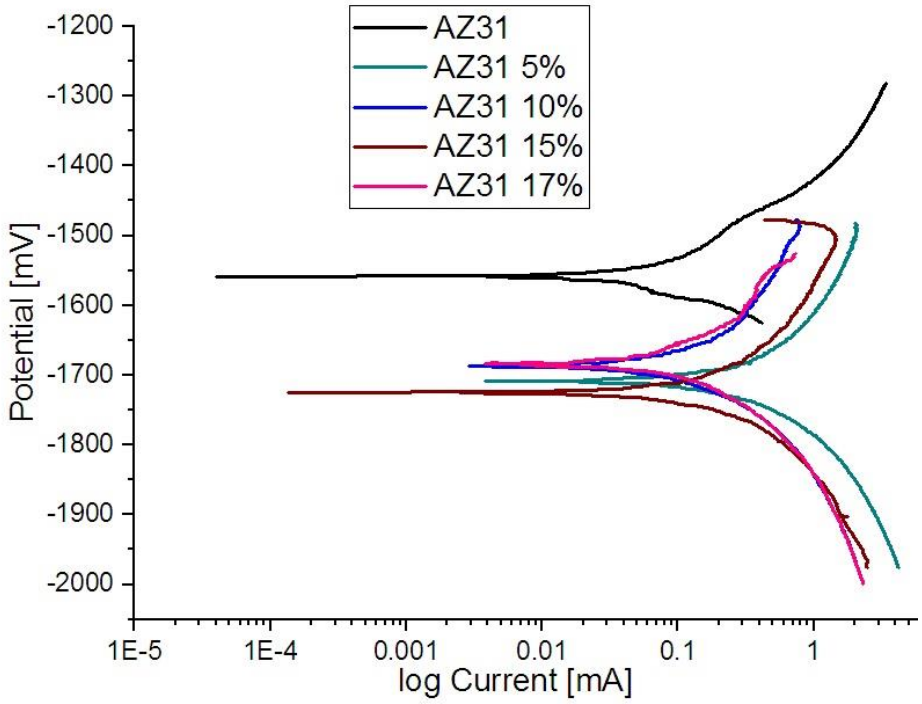

Figure (4-12) five samples of AZ31 alloy Tafel test results

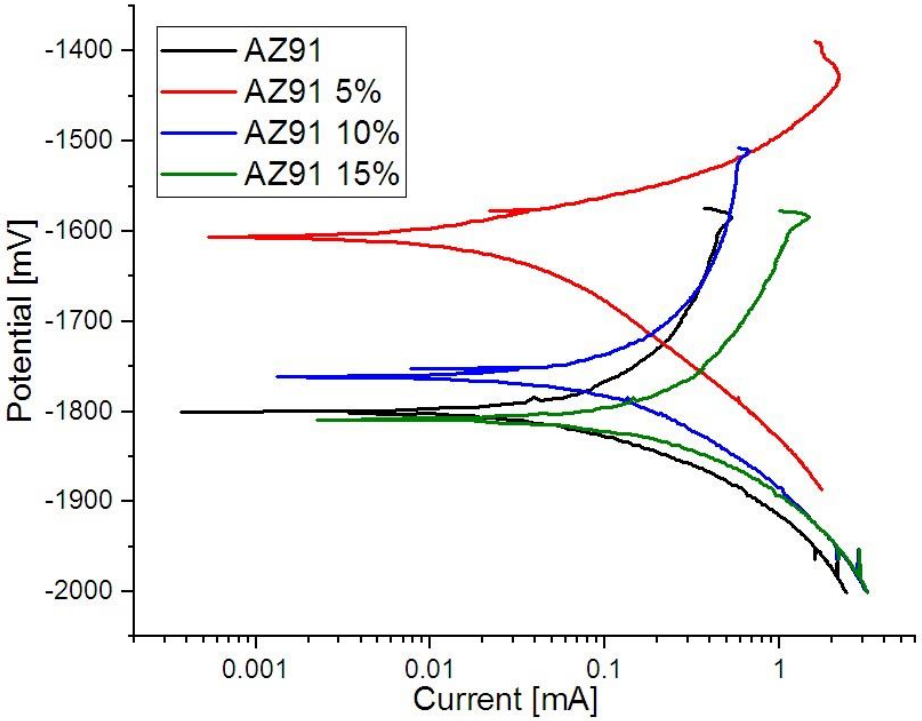

Figure (4-13) four samples of AZ91 alloy Tafel test results

4.5.3 Electrochemical Impedance Spectroscopy (EIS) test

Electrochemical characterization of the surfaces are carried out by using standard three-electrode traditional corrosion cell with SCE as a reference electrode (its potential vs. SHE is 0.242 V), two graphitics rods as the counter electrode , and the materials test as working electrode . The volume of the cell is 500 ml. The polished sample immerse in preheat simulated body fluid at 37C for 1800 s to record OCP. EIS was undertaken using a Corr Test Workstation (Corr Test, China). The frequency range is 100 kHz to 15 MHz in perturbation amplitude 10 mV at 10 points per frequency decade . All EIS tests taken for the surface OCP for two times to ensure high reproducibility.

Bode plots showed the logarithm of the impedance modulus |Z| and phase angle (θ) as functions of the logarithm of the apply frequency range and the EIS data are typical present as a Nyquist plot , where the imaginary impedance component (Z″) is plotted against the real impedance component (Z′) at each excitation frequency.

4.5.3.1 Nyquist test

It is the relationship between the resistance and resistance of solution. As shown in figure (4-14) the AZ31 5% have the highest corrosion rates because of high resistance of the obstruction of ion transfer.

In figure (4-15) the AZ91 have the highest corrosion rate because of high resistance of the obstruction of ion transfer. While the AZ91 10% have the lower corrosion rate.

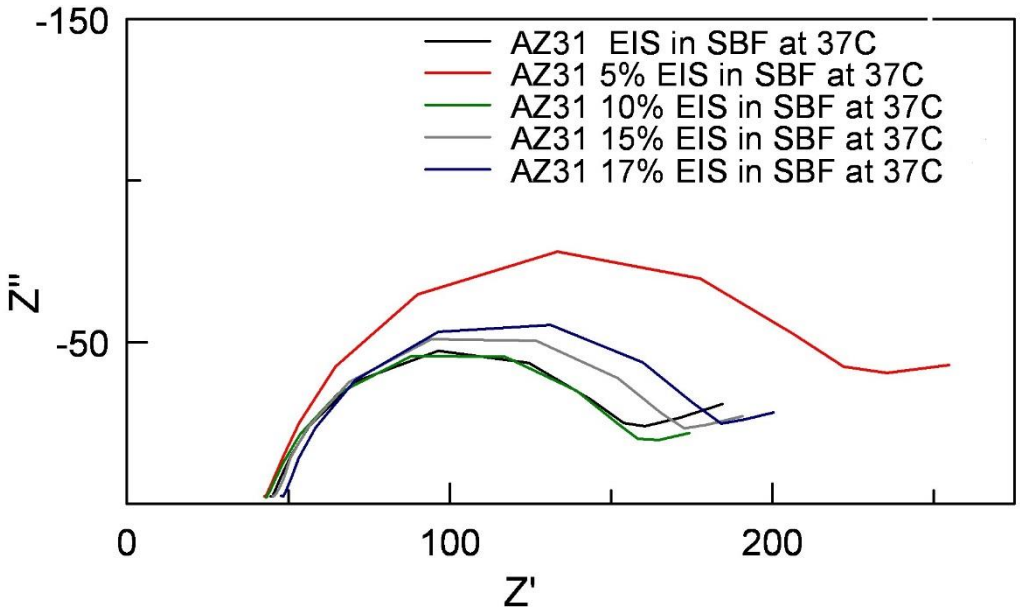

Figure (4-14) Nyquist test result for AZ31 alloy

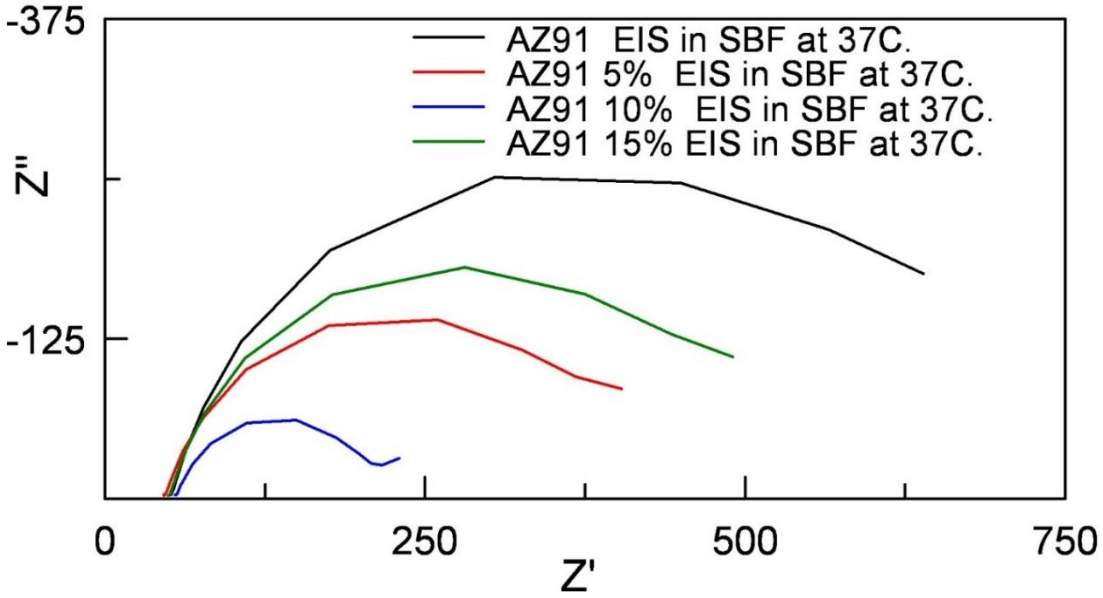

Figure (4-15) Nyquist test result for AZ91 alloy

4.5.3.2 Bode test

It is the relationship between the resistance and frequency. As shown in figure (4-16), (4-17)

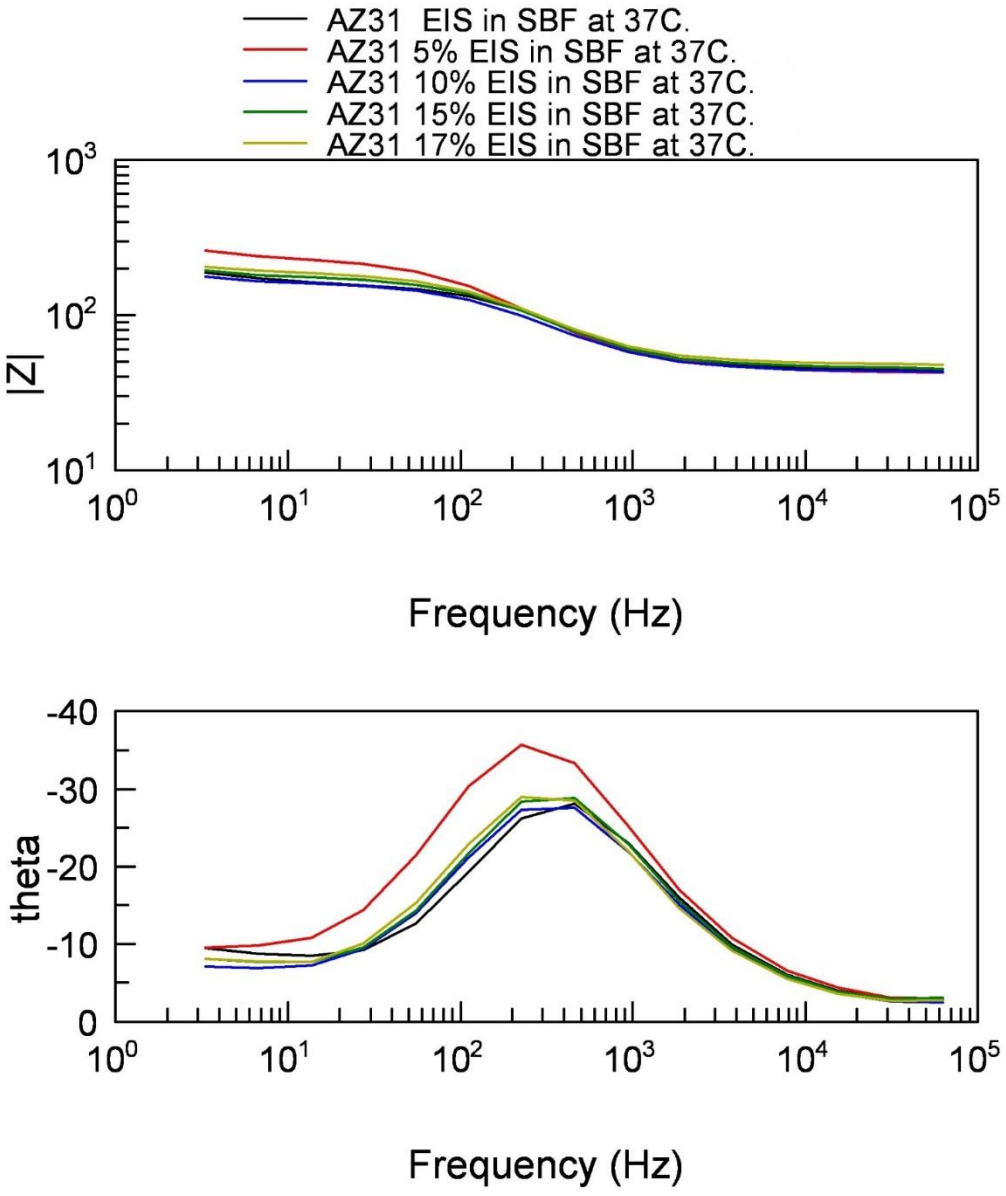

Figure (4-16) Bode test result for AZ31 alloy

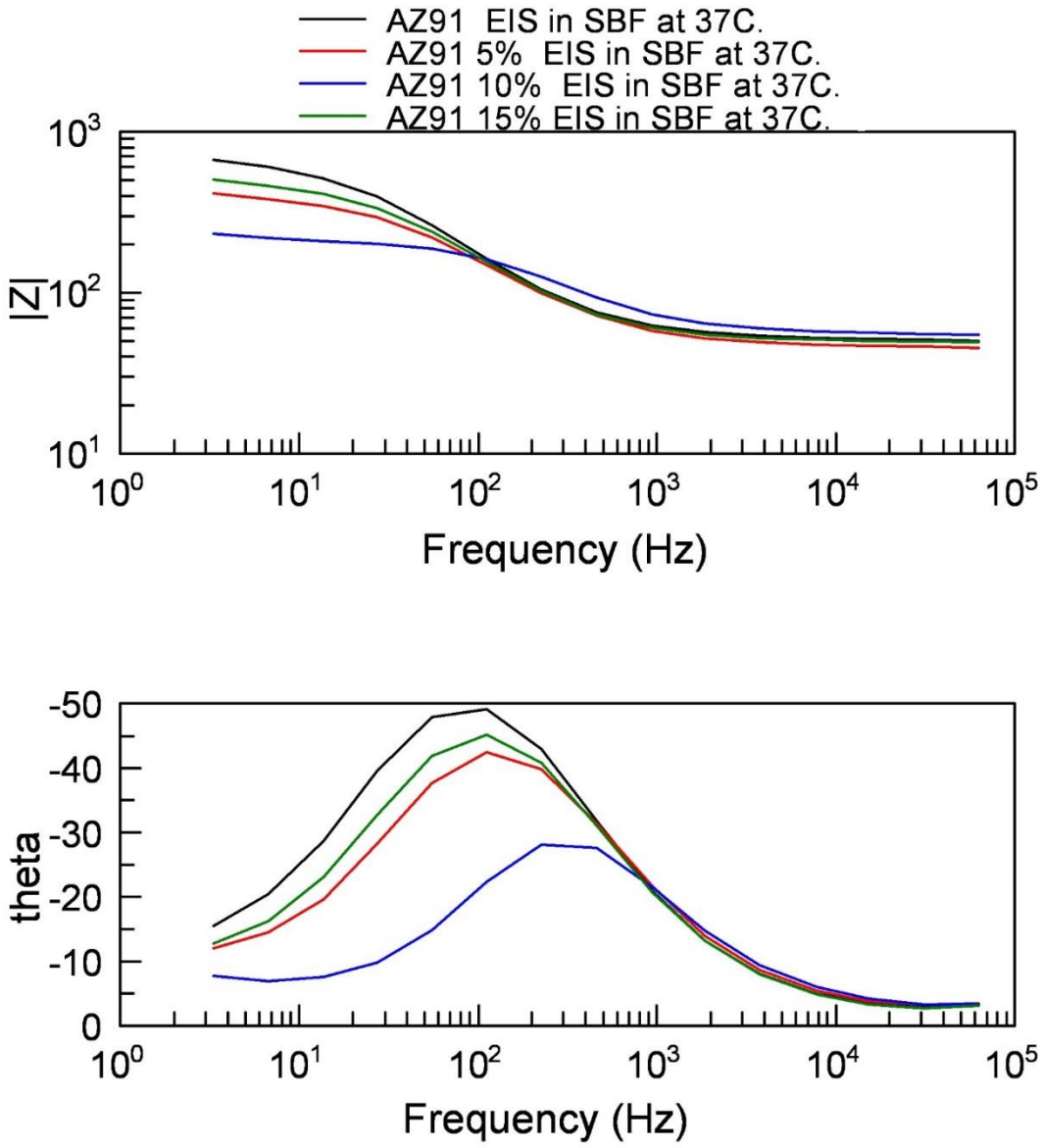

Figure (4-17) Bode test result for AZ91 alloy

4.5.4 The simple immersion

4.4.4.1 First Immersion test

According to ISO 16428 standard the weight loss value of alloys sample in different cold work percentage immersion in (SBF) at 37°C recording in the table (4-3). The value of corrosion rate for alloys various with cold work percentage for both alloys samples as in table (4-3). This diversity came from the method of interaction of magnesium alloys with the corrosion environment, where magnesium alloys are affected by the variables of temperature, the pH number of the solution and the type of ions, as well as the distribution of the second phase in the alloy and the flow of the fluid. These variables directly affect the rate of corrosion and the formation of insulating layers on the surface of the alloy. The study added the variable of internal stresses and deformation with the microstructure of the alloy.

Table (4-3) weight change to immersion AZ31 and AZ91 alloy samples

Sample	weight change in grams
AZ31	0.0175
AZ31 5%	0.0152
AZ31 10%	0.0189
AZ31 15%	0.0201
AZ31 17%	0.018
AZ91	0.008
AZ91 5%	0.0063
AZ91 10%	0.0051
AZ91 15%	0.0061

By use the equation [133]:-

$$MR = \Delta m/A.t$$

Where

MR: The mass loss rate

Δm : The mass losses (g)

A: the exposed area (m^2)

t: the exposure time (days)

Calculated the mass loss rate as in the table (4-4)

Table (4-4) the mass loss rate of AZ31 and AZ91 sample

Sample	MR (g / m^2 day)
AZ31	5
AZ31 5%	4.3429
AZ31 10%	5.4
AZ31 15%	5.7429
AZ31 17%	5.1429
AZ91	2.2858
AZ91 5%	1.8
AZ91 10%	1.457
AZ91 15%	1.7429

4.4.4.2 Second Immersion test

According to (Yufeng Zheng) [116], the weight loss value of alloys sample in different cold work percentage immersion in SBF for 21 days without change the SBF recording in the table (4-5). Continuing the test, it found that the samples of AZ91 alloys completely disappeared within a period of five to seven months. While the samples of AZ31 alloys continued to be present. This is because of the pH degree. As the increase in the pH leads to the stability of the layer formed on alloy AZ31. Which consisting of (AL_2O_3, MgO, $Mg(OH)_2$) and not to be broken like what happens in alloy AZ91,figure (4-18) and (4-19), which, due to the high content of particles of the second phase and its interaction with chlorides, acts as cathodic corrosion.

Based on the microstructure characteristics of the AZ31 and AZ91 Mg alloys, the different effects of cold rolling on their corrosion resistance can explained as follow. The AZ31 alloy was mainly composed of a-Mg matrix. Therefore, the corrosion resistance of AZ31 alloy depended largely on α-Mg matrix. After cold rolling, the α-Mg grains were refined to severe plastic deformations. The nanostructure had larger specific surface area and higher surface activity [134, 135] that plentiful grain boundaries were likely to improve the corrosion resistances of ultrafine-grained Mg alloys by accelerating the passivation kinetics or/and lowering micro-galvanic corrosion between grain interior and grain boundary. This confirmed that the surface layer of cold rolling AZ31 alloy would be quickly passivated with the formation of a relatively stable and compact passive film as exposed to corrosive solution [136]. The immediate passivation could effectively reduce the corrosion rate of alloy specimen in corrosion solution, and thus improve the corrosion resistance of AZ31 alloy.

The AZ91 alloy was consisted of α-Mg and β-phases. When the sample was immersed in corrosion medium, the passive film forming on a nano-layer, displayed better corrosion resistance than that on the as-received one. However, the corrosion resistance of AZ91 alloy depended, to a great extent, on the size, distribution and fraction of β-phases [137]. Although β-phases at some sites were capable of impeding corrosion advance, the isolated coarse β-phase in AZ91 alloy preferentially served as an effective cathode to accelerate corrosion of the α-Mg matrix [138]. Cold rolling did not change the shape and distribution of β-phases. As a result, the improvement of the corrosion resistance, resulting from passive film, was limited [139].

Table (4-5) weight change to immersion AZ31 and AZ91 samples

Sample	weight change in grams
AZ31	+0.012
AZ31 5%	+0.008
AZ31 10%	+0.021
AZ31 15%	+0.012
AZ31 17%	+0.019
AZ91	- 0.305
AZ91 5%	-0.199
AZ91 10%	-0.098
AZ91 15%	-0.168

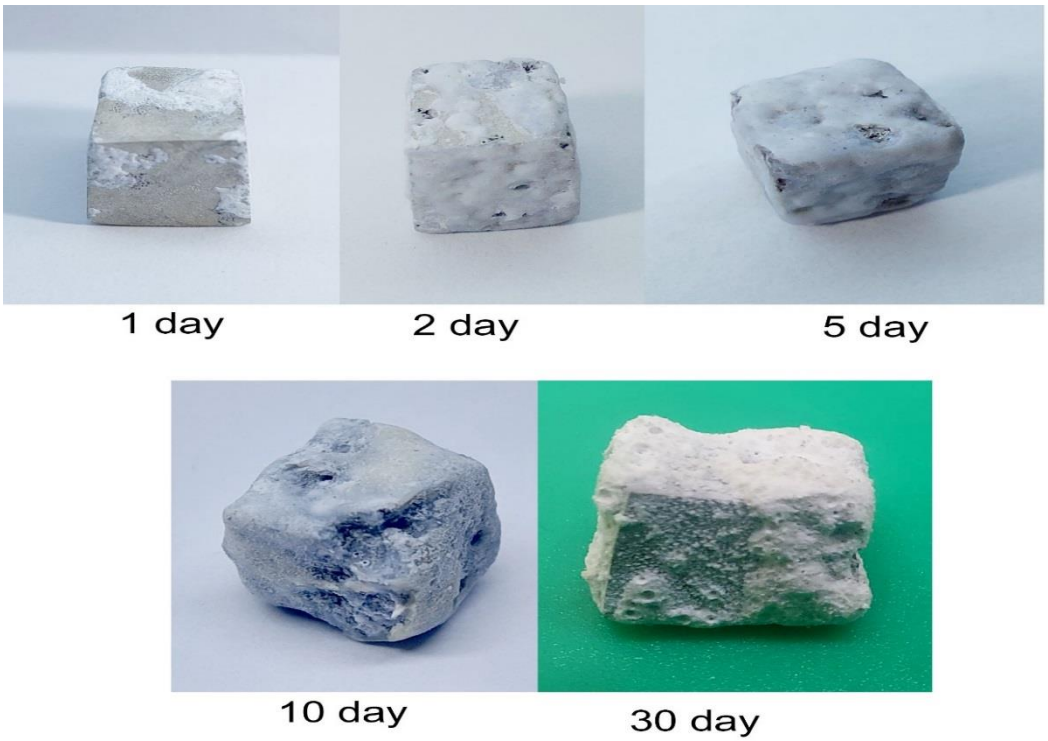

Figure (4-18) AZ31 alloy sample after different immersion time.

Figure (4-19) AZ91 alloy sample after different immersion time.

4.5.5 Ion released

AZ91 and AZ31 samples are stored in plastic containers with tight lids and expose to the physiological medium (SBF) for seven days. The solutions held at 37 °C with the use of a thermostatic bath. After that, examination the solution and record the result in table (4-6) for AZ31 and AZ91 alloy.

For AZ31 alloy, remarked that the increase in liberated ions coincides with the increase in the percentage of cold forming, and then decreases again with a percentage of formation of 17%,but in the 5% cold forming there is drop in liberated ions. In contrast, in AZ91 alloy, with an increase in the percentage of formation, the amount of liberated ions increases, but in the 10% cold forming, there is drop in liberated ions. As mentioned, the result of ion released are same with immersion test results according ISO 16428 standard.

Table (4-6) AZ31 and AZ91 ion released

Sample	Mg :flam eCont Actual
AZ31	248.158 ppm
AZ31 5%	227.202 ppm
AZ31 10%	252.040 ppm
AZ31 15%	258.433 ppm
AZ31 17%	248.957 ppm
AZ91	125.736 ppm
AZ91 5%	141.952 ppm
AZ91 10%	111.700 ppm
AZ91 15%	140.231 ppm

4.5.6 PH-Measurement results

After 7 days in the solution, the pH levels are determined at each sample (Tables 4-7). The SBF solution pH is (7.4). It showed that all samples caused a rise in pH due to the presence of alkaline breakdown products. There is a general tendency for the pH value to rise before it leveled out as the deterioration progressed.

Table (4-7) pH changes of SBF solution

No.	Alloys	Initial PH	Final PH
1	AZ31	7.4	8.7
2	AZ31 5%	7.4	8.7
3	AZ31 10%	7.4	8.7
4	AZ31 15%	7.4	8.7
5	AZ31 17%	7.4	8.7
6	AZ91	7.4	10
7	AZ91 5%	7.4	10
8	AZ91 10%	7.4	10
9	AZ91 15%	7.4	10

4.5.7 Hydrogen evaluate Measurement results

A relative long-term corrosion behavior of Mg alloys evaluate by hydrogen evolution test. Hydrogen collection performed by placing the entire specimen surface (6 cm^2) into the SBF solution under inverted burette systems. Hydrogen gas evolution observed produced by Mg alloy corrosion [111]:

$$Mg(s) + 2H_2O\ (aq) \rightarrow Mg\ (OH)_2\ (s) + H_2\ (g)$$

The resulted calculated in table (4-8). In the AZ31 alloy section of the table (4-8), can noted that the quantity of free hydrogen grows as the percentage of cold forging rises, but that it settles back down to the same value at the formation rate of 17% as in the base alloy. Except the sample AZ31 5%. The table (4-8) shows that after five days of immersion, all of the models stabilized at the same value. As for the AZ91 alloy, we notice a increase in the amount of rising hydrogen with the increase in the formation rate, except the lowest value at the formation rate of AZ91 5%, as shown in Tables (4-8).

Table (4-8) Hydrogen evaluate for AZ31, AZ91 alloys

alloys	Day 1 in ml	Day 2 in ml	Day 3 in ml	Day 4 in ml	Day 5 in ml	Day 6 in ml	Day 7 in ml	Total
AZ31	3.2	2.9	2.8	2.8	3	2.5	2.5	19.7
AZ31 5%	3.2	3	2.2	2.5	2.5	2.3	2.5	18.2
AZ31 10%	3.1	3.1	3.2	3	2.9	2.5	2.5	20.3
AZ31 15%	3.4	3.3	3.4	2.9	3.3	2.5	2.5	21.3
AZ31 17%	3.1	3	2.7	2.9	3.1	2.5	2.5	19.8
AZ91	16	17.1	20.1	17	15.2	12	12	109.4
AZ91 5%	16	18.2	23.3	20	19.2	19	19	134.7
AZ91 10%	12.4	15	17	16.8	14.6	12	12	100.8
AZ91 15%	14.4	25.2	20.2	19.8	19	19	19	136.6

4.6 Antibacterial test

After culturing the samples for bacteria and incubating them for 24 hours in the College of Science laboratories, it is found that all samples exhibited the same behavior in the growth of bacteria, indicating that the rolling process had no effect on the results.

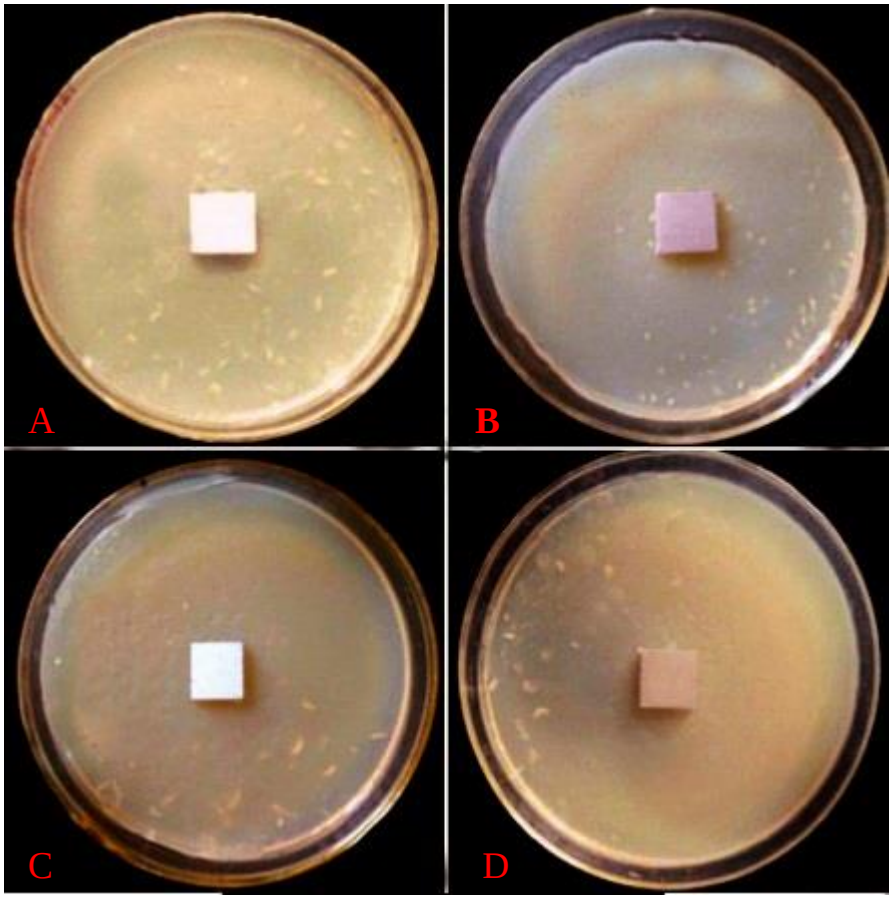

Figure (4-20) Antibacterial test for AZ91
A) AZ91 as received. B)AZ91 5% C)AZ91 10% D) AZ91 15%

4.7 Wear testes results

A sample of alloys subjected to wear testing, which done at a constant speed (350rpm), distance (197.82 m), load (5N), and duration (30 min). The wear test conducted in SBF at room temperature. For AZ31 alloys sample from figure (4-22) to (4-26). Moreover, for AZ91 alloys sample from figure (4-27) to (4-30). The sample weight record before and after test and the weight change calculated in table (4-9). In general, increasing the cold formation led to an increase in the wear resistance of the used alloys. AZ31 alloy, by increasing the forming percentage, increased the wear resistance to 10%, and it has the highest wear resistance. Then the resistance decreased, reaching 17%. This can be attribute to the stress hardening of the surface of the sample, as it reached the highest resistance at this ratio. As for the AZ91 alloy, it had the highest wear resistance at a 5% forming percentage, and it declined to 15%, but it remained higher than the base alloy.

Table (4-9) wear test results

Sample	weight change in mg	Volume loss (mm^3)	Specific rate (mm^3/Nm)
AZ31	4.3	2.443	$2.469*10^{-3}$
AZ31 5%	2.8	1.59	$1.607*10^{-3}$
AZ31 10%	1.9	1.08	$1.091*10^{-3}$
AZ31 15%	3.1	1.76	$1.779*10^{-3}$
AZ31 17%	3.7	2.10	$2.123*10^{-3}$
AZ91	4.4	2.44	$2.466*10^{-3}$
AZ91 5%	2.4	1.33	$1.344*10^{-3}$
AZ91 10%	3.6	2	$2.022*10^{-3}$
AZ91 15%	3.7	2.05	$2.072*10^{-3}$

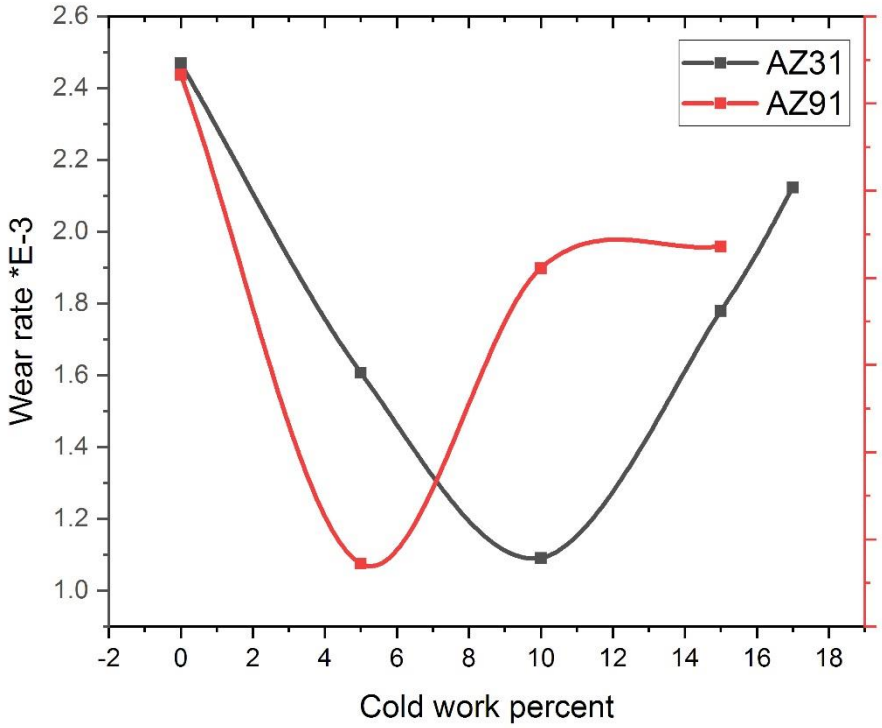

Figure (4-21) Wear rate for AZ31 and AZ91

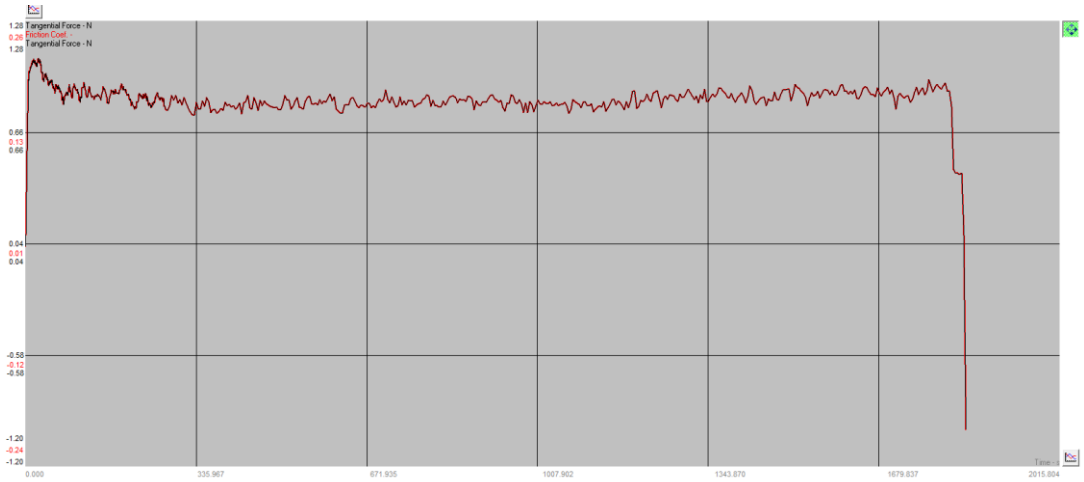

Figure (4-22) Wear test for AZ31

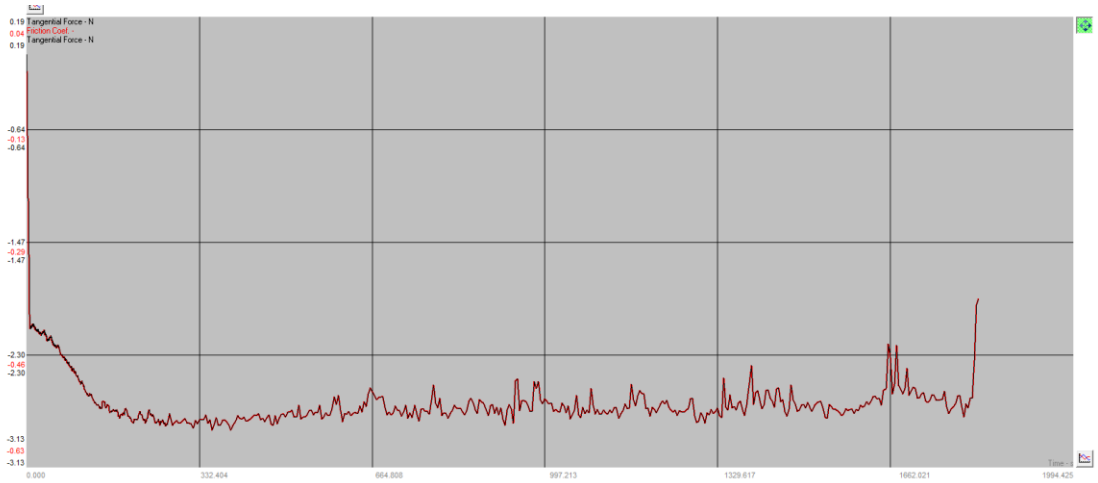

Figure (4-23) Wear test for AZ31 5%

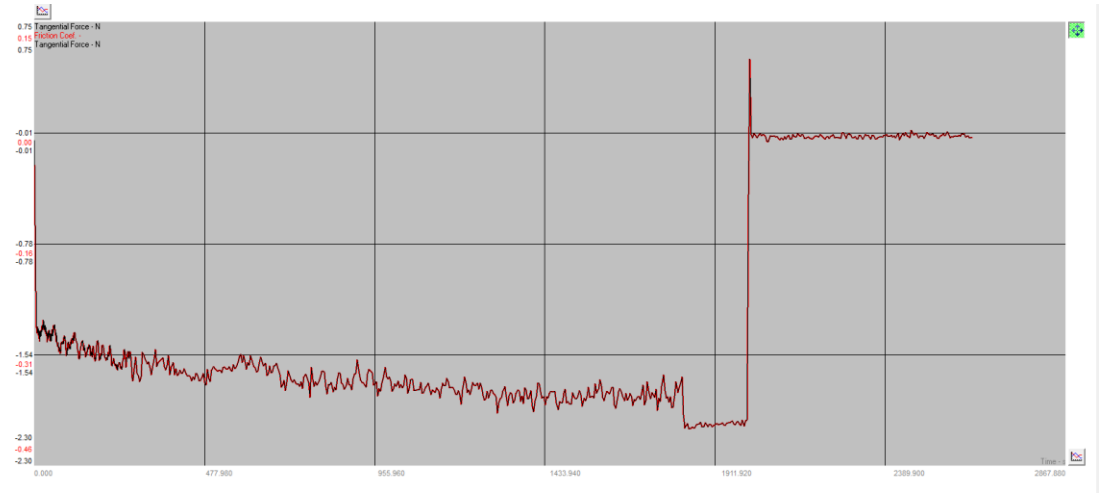

Figure (4-24) Wear test for AZ31 10%

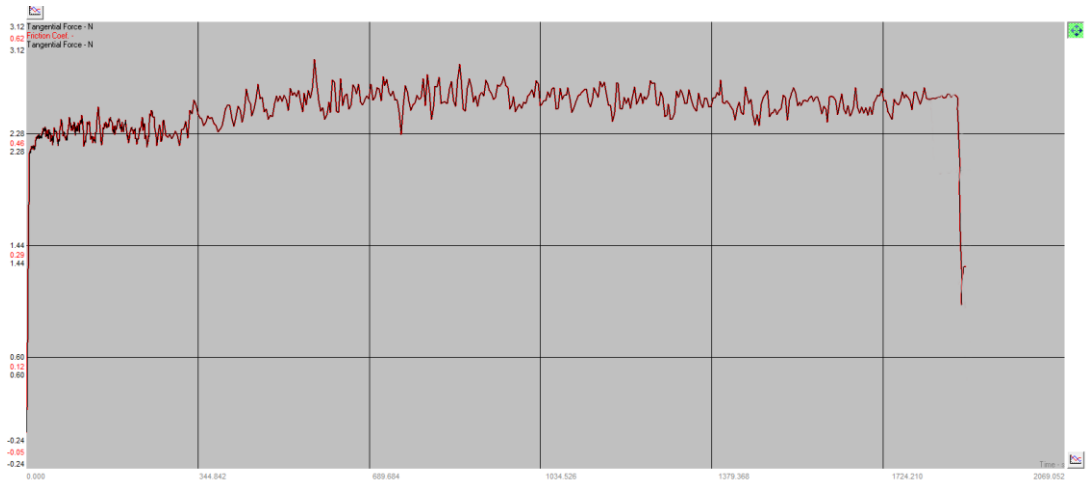

Figure (4-25) Wear test for AZ31 15%

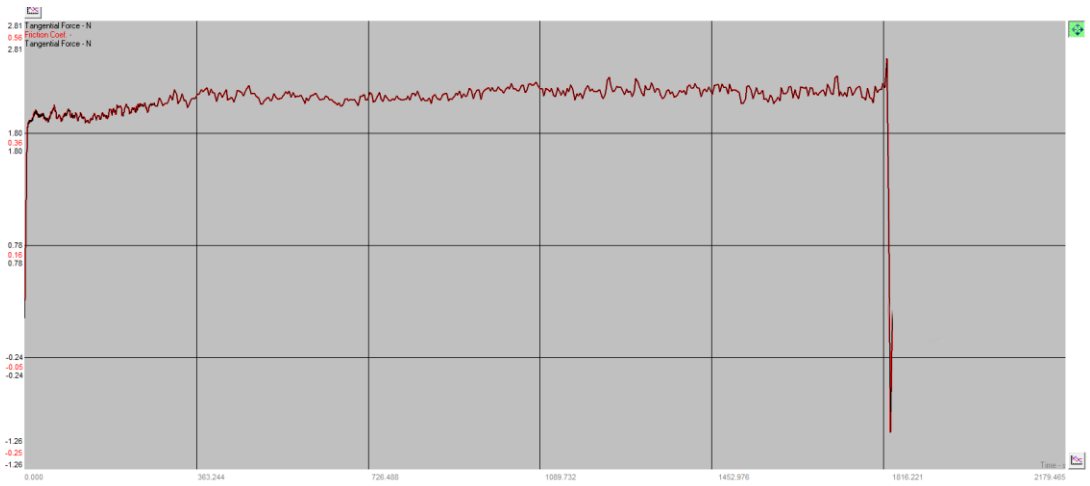

Figure (4-26) Wear test for AZ31 17%

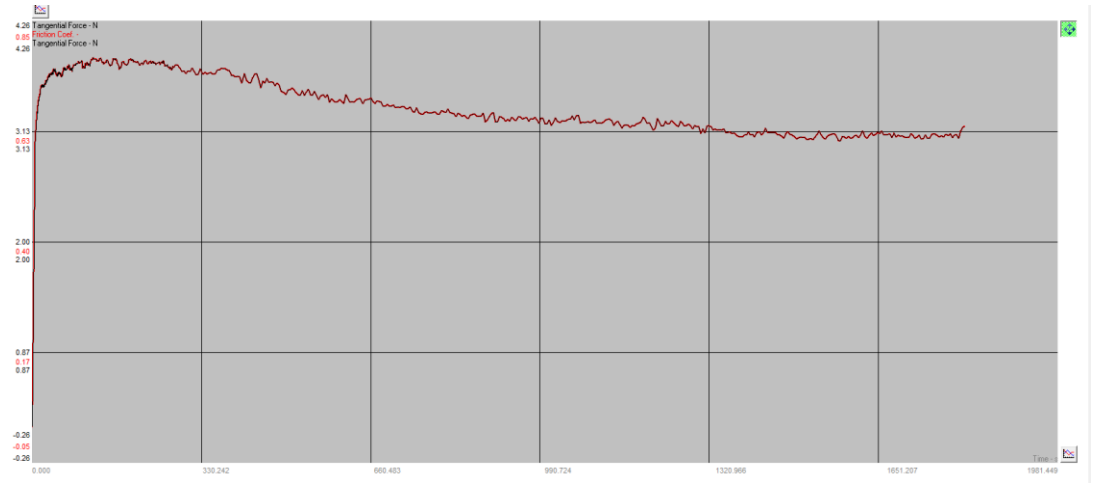

Figure (4-27) Wear test for AZ91

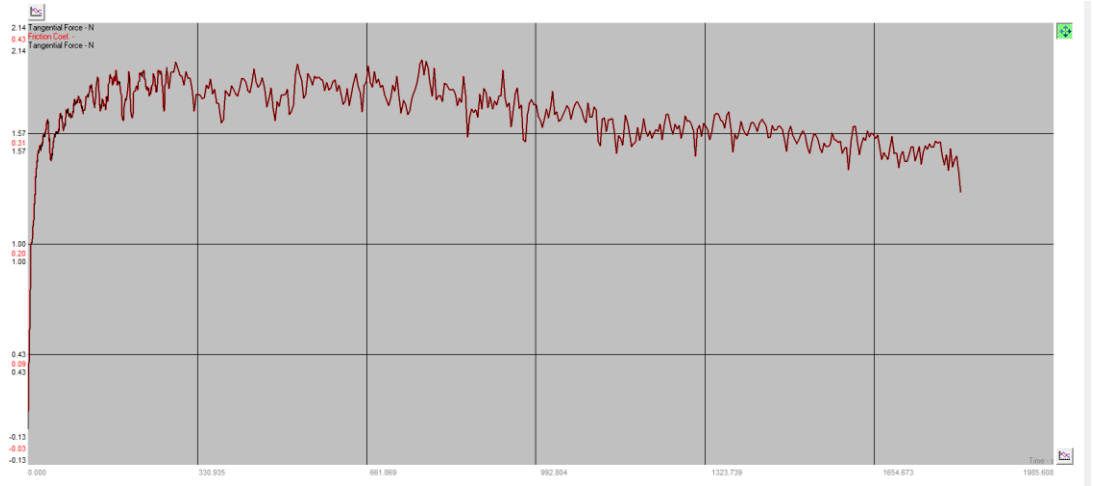

Figure (4-28) Wear test for AZ91 5%

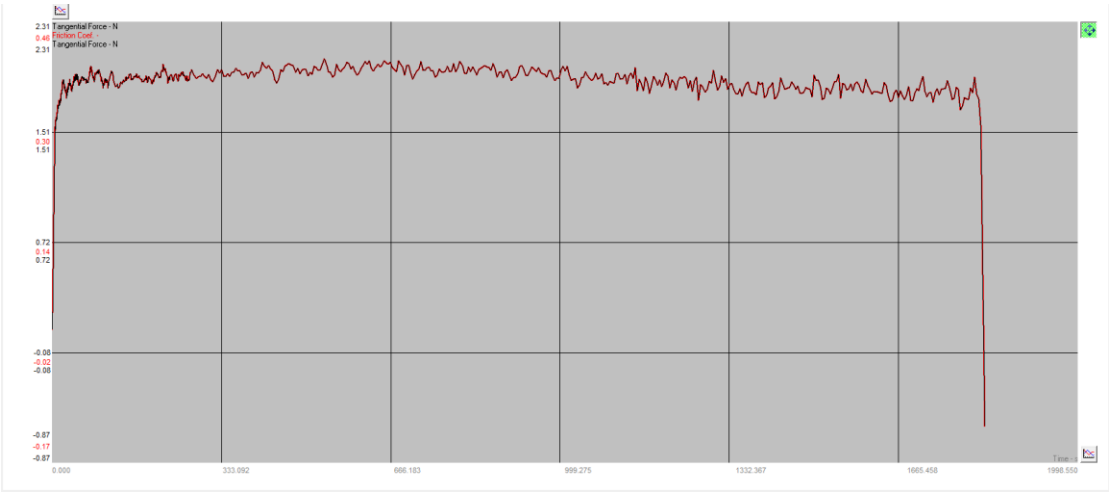

Figure (4-29) Wear test for AZ91 10%

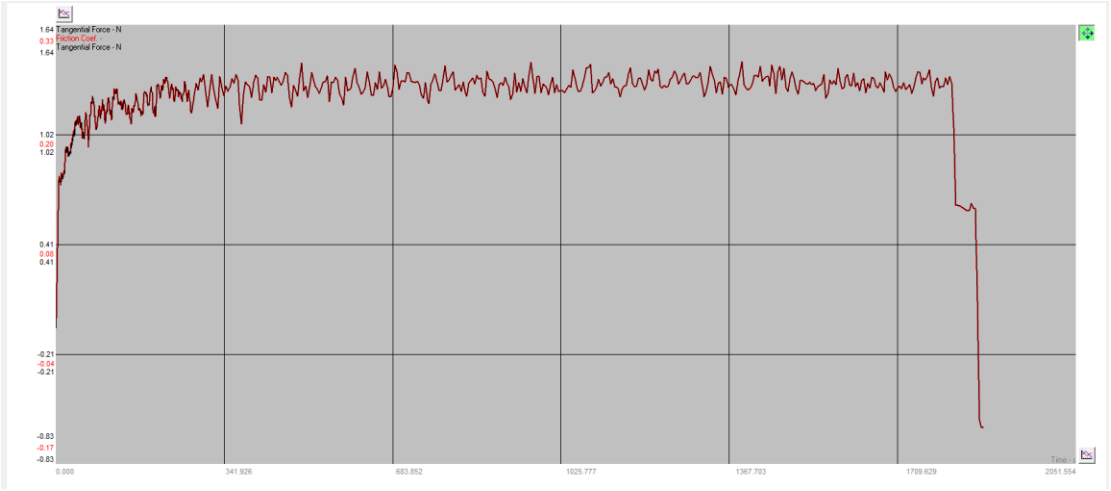

Figure (4-30) Wear test for AZ91 15%

Chapter

Five

Chapter Five

Conclusions and Suggestions

5.1 Conclusions

The study are arrives at the following conclusions:-

1- From the SEM and optical microscope, we note that the microstructure of both alloys (AZ31) and (AZ91) change after cold work. The microstructure evolution mechanicals twins and the orientation of grains.
2- The hardness of the alloys increased with increasing cold work due to the increase in surface compressibility and stress generation.
3- The potential dynamic polarization shows that there is a shift toward lower current densities for AZ91 with increasing cold work. While in other hand increase in current densities for AZ31 with increasing cold work.
4- In general, the hydrogen evolution test shows that the samples of AZ31 have almost the same performance. While the AZ91 alloy Performance contrast, where 5% of the formation recorded the least hydrogen liberation.
5- The ion released test shows that the samples of AZ31 have almost the same performance except 5% samples. While the AZ91 alloy Performance contrast, where 10% of the formation recorded the least.

6- In the immersion test, the behavior of magnesium alloys is observed in a variable manner according to the environment, temperature variables, and the pH degree. It varied from the formation of a protective layer in alloys AZ31 to rapid corrosion.
7- Wear resistance for AZ31 and AZ91 alloys in the as received sample is lower wear resistance than cold work samples. Where the wear resistance increased with cold work percentage.

5.2 Suggestions

Based on the conclusions drawn, the study comes out with the following suggestion for future research:-

1- Investigating the influence of cold work (rolling) with heat treatment on the corrosion and wear behaver of Mg alloys.
2- Investigating the influence of cold work (rolling) with heat treatment on the Tribe-corrosion behaver of Mg alloys.
3- Investigating the influence of hot work (rolling) on the corrosion and wear behaver of Mg alloys.

Refernces

References

[1] K. U. Kainer, "Magnesium alloys and technology", Wiley online library, 22Jun. 2004.

[2]Gaurav Gautam, Sanjeev Kumar, Kamal Kumar. Processing of biomaterials for bone tissue engineering: State of the art. Material today. Volume 50, Part 5, 2022, Pages 2206-2217

[3] Prof. Giordano Emanuele Domenico Boghi Caterina. SVILUPPO E CARATTERIZZAZIONE REOLOGICA DI SOSPENSIONI A BASE DI IDROSSIAPATITE PER LA REALIZZAZIONE DI IMPIANTI PER LA RIGENERAZIONE DEL TESSUTO OSSEO. 2018

[4] H. Wang , Y. Estrin , H. M. Fu , G.L. Song ,and Z. Zúberová "The effect of pre-processing and grain structure on the bio corrosion and fatigue resistance of magnesium alloy AZ31", Advanced Engineering Materials, vol. 9, , pp. 967-972, Nov. (2007).

[5] W. Sietsema, "Animal models of cortical porosity". Bone 17, pp.297–305, (1995).

[6] J.M. Ramirez, and W.C. Hurt, "Bone remodeling in periodontal lesions". J. Periodontol, 48, pp. 74–77 (1977)

[7] M.P. Staiger, A.M. Pietak, J. Huadmai, and G. Dias, Magnesium and its alloys as orthopedic biomaterials: a review. Biomaterials 27, pp.1728–1734, (2006).

[8] P. Trumbo, S. Schlicker, A.A. Yates, and M. Poos,"Dietary reference intakes for energy, carbohydrate, fiber, fat, fatty acids cholesterol, protein and amino acids", J. Am. Diet. Assoc. 102, pp.1621–1630 (2002).

[9] K.F. Farraro, K.E. Kim, S.L. Woo, J.R. Flowers, and M.B. McCullough, "Revolutionizing orthopedic biomaterials: the potential of biodegradable and bio resorbable magnesium-based materials for functional tissue engineering", J. Bio mech. 47, pp.1979–1986, (2014)

[10] R. Martin," Porosity and specific surface of bone", Crit. Rev. Biomed. Eng. 10, pp.179–222, (1983).

References

[11] P. Prendergast, R. Huiskes, "Micro damage and osteocyte-lacuna strain in bone: a microstructural finite element analysis", J. Bio mech. Eng. 118, pp. 240–246, (1996).

[12] Gupta, Manoj, Meenashisundaram, and Ganesh Kumar, "Insight into Designing Biocompatible Magnesium Alloys and Composites", Springer Briefs in Materials January 14 (2015).

[13] Frank Czerwinski, "magnesium alloys - properties in solid and liquid states", In Tech, Chapters published November 05, (2014).

[14] Q. Chen and G. A. Thouas, "Metallic implant biomaterials," Materials Science and Engineering: R: Reports, vol. 87, pp. 1-57, 2015.

[15] Mano, J.F., et al., Bioinert, biodegradable and injectable polymeric matrix composites for hard tissue replacement: state of the art and recent developments. Composites Science and Technology, 2004. 64(6): p. 789-817.

[16] Takayoshi Nakano, Metals for Biomedical Devices (Second Edition) Woodhead Publishing Series in Biomaterials 2019.

[17] Ibrahim, H., et al., In Vitro Corrosion Assessment of Additively Manufactured Porous NiTi for Bone Fixation Applications. Metals, 2018. 8(3): p. 164.

[18] Wei, S.; Ma, J.X.; Xu, L.; Gu, X.S.; Ma, X.L. Biodegradable materials for bone defect repair. Mil. Med. Res. 2020, 7, 54.

[19] Magnesium alloys corrosion and surface treatments, Edited by Frank Czerwinski, Published by InTech, and JanezaTrdine 9, 51000 Rijeka, Croatia (2011).

[20] F. Mansfeld and U. Bertocci, "Electrochemical Corrosion Testing", STP 727, American Society for Testing and Materials, West Conshohocken, PA, (1979).

[21] R. Cottis and S. Turgoose, NACE International, "Electrochemical Impedance and Noise".

References

[22] Lu Q, Han WJ, Choi HJ. Smart and functional conducting polymers: application to electrorheological fluids. Molecules. 2018;23(11):2854.

[23] Chung JJ, Fujita Y, Li S, Stevens MM, Kasuga T, Georgiou TK, et al. Biodegradable inorganic-organic hybrids of methacrylate star polymers for bone regeneration. Acta Biomater. 2017;54:411–8.

[24] Salgado AJ, Coutinho OP, Reis RL. Bone tissue engineering: state of the art and future trends. Macromol Biosci. 2004;4(8):743–65.

[25] Garric X, Nottelet B, Pinese C, Leroy A, Coudane J. Biodegradable synthetic polymers for the design of implantable medical devices: the ligamentoplasty case. Med Sci (Paris). 2017;33(1):39–45.

[26] Hench LL. The story of bioglass. J Mater Sci Mater Med. 2006;17(11):967–78.

[27] Fiume E, Barberi J, Verné E, Baino F. Bioactive glasses: from parent 45s5 composition to scaffold-assisted tissue-healing therapies. J Funct Biomater. 2018;9(1):24.

[28] Montazerian M, Dutra ZE. History and trends of bioactive glass-ceramics. J Biomed Mater Res A. 2016;104(5):1231–49.

[29] Fu Q, Rahaman MN, Fu H, Liu X. Silicate, borosilicate, and borate bioactive glass scaffolds with controllable degradation rate for bone tissue engineering applications. I. Preparation and in vitro degradation. J Biomed Mater Res A. 2010;95(1):164–71.

[30] Kamrani S, Fleck C. Biodegradable magnesium alloys as temporary orthopaedic implants: a review. Biometals. 2019;32(2):185–93.

[31] Purnama A, Hermawan H, Couet J, Mantovani D. Assessing the biocompatibility of degradable metallic materials: state-of-the-art and focus on the potential of genetic regulation. Acta Biomater. 2010;6(5):1800–7.

[32] Seitz JM, Durisin M, Goldman J, Drelich JW. Recent advances in biodegradable metals for medical sutures: a critical review. Adv Healthc Mater. 2015;4(13):1915–36.

References

[33] Myrissa A, Agha NA, Lu Y, Martinelli E, Eichler J, Szakács G, et al. In vitro and in vivo comparison of binary mg alloys and pure mg. Mater Sci Eng C Mater Biol Appl. 2016;61:865–74.

[34] Wang H, Zheng Y, Liu J, Jiang C, Li Y. In vitro corrosion properties and cytocompatibility of Fe-Ga alloys as potential biodegradable metallic materials. Mater Sci Eng C Mater Biol Appl. 2017;71:60–6.

[35] Drelich AJ, Zhao S, Guillory RJ 2nd, Drelich JW, Goldman J. Long-term surveillance of zinc implant in murine artery: surprisingly steady biocorrosion rate. Acta Biomater. 2017;58:539–49.

[36] Zheng, Y., X. Gu, and F. Witte, Biodegradable metals. Materials Science and Engineering: R: Reports, 2014. 77: p. 1-34.

[37] Li, H., Y. Zheng, and L. Qin, Progress of biodegradable metals. Progress in Natural Science: Materials International, 2014. 24(5): p. 414-422.

[38] Berglund, I.S., et al., Synthesis and characterization of Mg-Ca-Sr alloys for biodegradable orthopedic implant applications. Journal of Biomedical Materials Research Part B: Applied Biomaterials, 2012. 100(6): p. 1524-1534.

[39]. Schinhammer, M., et al., Design strategy for biodegradable Fe-based alloys for medical applications. Acta biomaterialia, 2010. 6(5): p. 1705-1713.

[40]. Liu, B. and Y. Zheng, Effects of alloying elements (Mn, Co, Al, W, Sn, B, C and S) on biodegradability and in vitro biocompatibility of pure iron. Acta biomaterialia, 2011. 7(3): p. 1407-1420.

[41]Bowen, P.K., J. Drelich, and J. Goldman, Zinc exhibits ideal physiological corrosion behavior for bio absorbable stents. Advanced Materials, 2013. 25(18): p. 2577-2582.

[42]H.F. Li , X.H. Xie, K. Zhao, Y.B. Wang, Y.F. Zheng, W.H. Wang, L. Qin, In vitro and in vivo studies on biodegradable CaMgZnSrYb high-entropy bulk metallic glass. Acta biomaterialia, 2013. 9 (10): p. 8561-8573.

References

[43] Moravej, M. and D. Mantovani, Biodegradable metals for cardiovascular stent application: interests and new opportunities. International journal of molecular sciences, 2011. 12(7): p. 4250.

[44] Engineering, N.A.o. and I.o. Medicine, Adviser, teacher, role model, and friend: On being a mentor to students in science and engineering. 1997: Natl Academy Pr.

[45] Kim, M., C.V. Carman, and T.A. Springer, Bidirectional transmembrane signaling by cytoplasmic domain separation in integrins. Science, 2003. 301(5640): p. 1720-1725.

[46] Willumeit, R., F. Feyerabend, and N. Huber, Magnesium degradation as determined by artificial neural networks. Acta biomaterialia, 2013. 9(10): p. 8722-8729.

[47] Kirkland, N.T., N. Birbilis, and M. Staiger, Assessing the corrosion of biodegradable magnesium implants: a critical review of current methodologies and their limitations. Acta biomaterialia, 2012. 8(3): p. 925-936.

[48] Rude, R., Magnesium. In 'Modern nutrition in health and disease'. 10th edn (Eds ME Shils.) pp. 223–247. 2006, Lippincott Williams & Wilkins: Baltimore, MD, USA.

[49] Rude, R. and F. Singer, Magnesium deficiency and excess. Annual review of medicine, 1981. 32(1): p. 245-259.

[50] Brandt, J., et al., Nanocrystalline hydroxyapatite for bone repair: an animal study. Journal of Materials Science: Materials in Medicine, 2010. 21(1): p. 283-294.

[51] Wolf, F.I. and A. Cittadini, Chemistry and biochemistry of magnesium. Molecular aspects of medicine, 2003. 24(1): p. 3-9.

[52] Ghosh, P., M. Mezbahul-Islam, and M. Medraj, Critical assessment and thermodynamic modeling of Mg–zn, Mg–sn, Sn–Zn and Mg–Sn–Zn systems. Calphad, 2012. 36: p. 28-43.

References

[53] Bakhsheshi-Rad, H., et al., Mechanical and bio-corrosion properties of quaternary Mg–Ca–Mn–Zn alloys compared with binary Mg–Ca alloys. Materials & Design, 2014. 53: p. 283-292.

[54] Kirkland, N.T. and N. Birbilis, Magnesium Biomaterials: Design, Testing, and Best Practice. 2014: Springer.

[55] Groves, E.W.H., Some Clinical and Experimental Observations on the operative treatment of fractures, With Especial Reference to the Use of Intra-Medullary Pegs. British medical journal, 1912. 2(2704): p. 1102.

[56] Wang, H., Y. Estrin, and Z. Zuberova, Bio-corrosion of a magnesium alloy with different processing histories. Materials Letters, 2008. 62(16): p. 2476-2479.

[57] Mezbahul-Islam, M., A.O. Mostafa, and M. Medraj, Essential magnesium alloys binary phase diagrams and their thermochemical data. Journal of Materials, 2014.

[58] Scully, Silverman, and Kendig, "Electrochemical Impedance: Analysis and Interpretation", STP 1188, ASTM.

[59] Nie, J. and B. Muddle, Precipitation hardening of (Mg-Ca-Zn) alloys. Scripta Materialia, 1997.

[60] Sachin Kumar Sharma, Kuldeep Kumar Saxena, Vinayak Malik, Kahtan A. Mohammed, Chander Prakash, Dharam Buddhi, Saurav Dixit. Significance of Alloying Elements on the Mechanical Characteristics of Mg-Based Materials for Biomedical Applications Crystals 2022, 12(8), 1138.

[61]Feng Ge, Jiaxuan Yin, Yue Liu, Wenjun Leng, Xin Wang, Zhongyu Cui, Roles of pH in the NH4+-induced corrosion of AZ31 magnesium alloy in chloride environment. Journal of Magnesium and Alloys Volume 10, Issue 11, November 2022, Pages 3167-3178

[62] Witte, F., Reprint of the history of biodegradable magnesium implants: A review. Acta biomaterialia, 2015. 23: p. S28-S40.

References

[63]Sankalp Agarwal, James Curtin, Brendan Duffy, Swarna Jaiswal Biodegradable magnesium alloys for orthopaedic applications: A review on corrosion, biocompatibility and surface modifications. Materials Science and Engineering: C Volume 68, 1 November 2016, Pages 948-963

[64] UANGLING SONG, ANDREJ ATRENS, XIANLIANG WU, and BO ZHANG. Corrosion behaviour of AZ21, AZ501 and AZ91 in Sodium Chloride; October 1998. Corrosion Science 40(10):1769-1791

[65] Baker, H.; Okamoto, H. Alloy Phase Diagrams, 9th ed; ASM International: Geauga County, OH, USA, 1995; Volume 3

[66] Modeling the precipitation processes and strengthening mechanisms in a Mg-Al-(Zn) AZ91 alloy August 2005 Metallurgical and Materials Transactions A 36(8):2093-2105

[67] Gusieva, K.; Davies, C.H.J.; Scully, J.R.; Birbilis, N. Corrosion of magnesium alloys: The role of alloying. Int. Mater. Rev. 2015, 60, 169–194.

[68] Hermann, F.; Sommer, F.; Jones, H.; Edyvean, R.G.J. Corrosion inhibition in magnesium-aluminum-based alloys induced by rapid solidification processing. J. Mater. Sci. 1989, 24, 2369–2379.

[69] Lunder, O.; Lein, J.E.; Aune, T.K.;Nisancioglu, K. The Role of Mg 17 Al 12 Phase in the Corrosion ofMgAlloyAZ91.Corrosion 1989, 45, 741–748.

[70] Winzer, N.; Atrens, A.; Song, G.; Ghali, E.; Dietzel, W.;Kainer, K.U.; Hort, N.; Blawert, C. A critical review of the Stress Corrosion Cracking (SCC) of magnesium alloys. Adv. Eng. Mater. 2005, 7, 659–693.

[71] Domingo, J.L. Reproductive and developmental toxicity of aluminum: A review. Neurotoxicol. Teratol. 1995, 17, 515–521.

[72]Venugopal, B.; Luckey, T.D. Metal Toxicity in Mammals. Volume 2. Chemical Toxicity of Metals and Metalloids; Plenum Press: Berlin, Germany, 1978.

References

[73]Flaten, T.P. Aluminum as a risk factor in Alzheimer's disease, with emphasis on drinking water. Brain Res. Bull.2001, 55, 187–196.

[74]El-Rahman, S.S.A. Neuropathology of aluminum toxicity in rats (glutamate and GABA impairment).Pharmacology. Res. 2003, 47, 189–194.

[75] Hanawalt, J.D.; Nelson, C.E.; Peloubet, J.A. Corrosion studies of magnesium and its alloys. Trans AIME 1942, 47, 273–299.

[76]Robinson, H.A.; George, P.F. Effect of Alloying and Impurity Elements in Magnesium Alloy Cast Anodes. Corrosion 1954, 10, 182–188.

[77]Culotta, V.C.; Yang,M.; Hall,M.D.Manganese Transport and Trafficking: Lessons Learned from Saccharomyces cerevisiae. Eukaryot. Cell 2005, 4, 1159–1165.

[78] Zhang, L.-N.; Hou, Z.-T.; Ye, X.; Xu, Z.-B.; Bai, X.-L.; Shang, P. The effect of selected alloying element additions on properties of Mg-based alloy as bioimplants: A literature review. Front. Mater. Sci. 2013, 7, 227–236.

[79] Brandt, E.G.; Hellgren, M.; Brinck, T.; Bergman, T.; Edholm, O. Molecular dynamics study of zinc binding to cysteines in a peptide mimic of the alcohol dehydrogenase structural zinc site. Phys. Chem. Chem. Phys. 2009, 11, 975–983.

[80] Prasad, A.S. Zinc in human health: Effect of zinc on immune cells. Mol. Med. 2008, 14, 353–357.

[81] Hanawalt, J.D.; Nelson, C.E.; Peloubet, J.A. Corrosion studies of magnesium and its alloys. Trans AIME 1942, 47, 273–299.

[82]Song, G.-L.; Atrens, A. Corrosion Mechanisms of Magnesium Alloys. Adv. Eng. Mater.1999, 1, 11–33.

[83] Shaw, B.A. Corrosion Resistance of Magnesium Alloys. In ASM Handbook; ASM International Handbook Committee: Metals Park, OH, USA, 2003; Volume 13A.

[84] Zhang, S.; Zhang, X.; Zhao, C.; Li, J.; Song, Y.; Xie, C.; Tao, H.; Zhang, Y.; He, Y.; Jiang, Y.; et al. Research on an Mg–Zn alloy as a degradable biomaterial. Acta Biomater.2010, 6, 626–640.

[85] Persaud-Sharma, D.; McGoron, A. Biodegradable Magnesium Alloys: A Review of Material Development and Applications. J. Biomim. Biomater. Tissue Eng. 2012, 12, 25–39.

[86] Zberg, B.; Uggowitzer, P.J.; Löffler, J.F. MgZnCa glasses without clinically observable hydrogen evolution for biodegradable implants. Nat. Mater.2009, 8, 887–891.

[87] Hofstetter, J.; Becker, M.; Martinelli, E.;Weinberg, A.M.; Mingler, B.; Kilian, H.; Pogatscher, S.; Uggowitzer, P.J.; Löffler, J.F. High-strength low-alloy (HSLA) Mg-Zn-Ca alloys with excellent biodegradation performance. JOM 2014, 66, 566–572.

[88] Jiao, W.; Li, H.F.; Zhao, K.; Bai, H.Y.; Whang, Y.B.; Zheng, Y.F.; Wang, W.H. Development of Ca Zn based glassy alloys as potential biodegradable bone graft substitute. J. Non-Cryst. Solids 2011, 357, 3830–3840.

[89] Rad, H.R.B.; Idris, M.H.; Kadir, M.R.A.; Farahany, S. Microstructure analysis and corrosion behavior of biodegradable Mg–Ca implant alloys. Mater. Des.2012, 33, 88–97.

[90] Zhang, E.; Yang, L. Microstructure, mechanical properties and bio-corrosion properties of Mg–Zn–Mn–Ca alloy for biomedical application. Mater. Sci. Eng. A 2008, 497, 111–118.

[91] Kirkland, N.T.; Birbilis, N.; Walker, J.; Woodfield, T.; Dias, G.J.; Staiger, M.P. In-vitro dissolution of magnesium-calcium binary alloys: Clarifying the unique role of calcium additions in bio resorbable magnesium implant alloys. J. Biomed. Mater. Res. Part B Appl. Biomater. 2010, 95, 91–100.

[92]M. Bornapour, M. Celikin, M. Cerruti, M. Pekguleryuz. Magnesium implant alloy with low levels of strontium and calcium: The third element effect and phase selection improve bio-corrosion resistance and

mechanical performance. Materials Science and Engineering Volume 35, 1 February 2014, Pages 267-282

[93] Hector, B. Heiss, W.: „Magnesium Die-Castings as Structural Members of the New Mercedes-Benz Roadster“, SAE-Technical Paper Series no. 900798 (1990).

[94] Breuer, H. Dolfen, E.: "Magnesium", KU Kunststoffe, Carl Hanser Verlag, Jahrgang 89, pp. 64-66, (1999).

[95] Rozak, G. A.; Purgert, R. E.; Thomas, J.; Hale R.: „Metal Compression Forming [MCF]“, IMA 99 Annual World Magnesium Conf. IMA, McLean, USA, Toronto pp. 55-57, (1997).

[96]S. Virtanen, I. Milošev, E. GomezBarrena, R. Trebše, J. Salo, Y.T. K onttinen ‘Special modes of corrosion under physiological and simulated physiological conditions’ Acta Biomater, 4 (2008), pp. 468-476

[97] M. Esmaily , J.E. Svensson , S. Fajardo ,c , N. Birbilis , G.S. Frankel , S. Virtanen , R. Arrabal , S. Thomas , L.G. Johansson ‘Fundamentals and advances in magnesium alloy corrosion’ progress in Materials Science, August 2017, volume 89, Pages 92-193

[98] A.H.M. Sanchez, B.J.C. Luthringer, F. Feyerabend, R. Willumeit

Mg and Mg alloys: how comparable are in vitro and in vivo corrosion rates? A review Acta Biomater, 13 (2015), pp. 16-31

[99] S. Hiromoto, M. Inoue, T. Taguchi, M. Yamane, N. Ohtsu “In vitro and in vivo biocompatibility and corrosion behaviour of a bioabsorbable magnesium alloy coated with octacalcium phosphate and hydroxyapatite” Acta Biomater, 11 (2015), pp. 520-530

[100] J. Koike, T. Kobayashi, T. Mukai, H. Suzuki, K. Maruyama, K. Higashi, The activity of non-basal slip systems and dynamic recovery at room temperature in fine-grained AZ31B magnesium alloys, Acta Mater.51 (2003) 2055-2065.

[101] H. Wang, B. Clausen, L. Capolungo, I.J. Beyerlein, J. Wang, C.N. Jomé, Stress and strain relaxation in magnesium AZ31 rolled plate: In-situ

neutron measurement and elastic viscoplastic polycrystal modeling, Int. J. Plasticity 79 (2016) 275-292.

[102] Q. Miao, L.X. Hu, G.J. Wang, E. Wang, Fabrication of excellent mechanical properties AZ31 magnesium alloy sheets by conventional rolling and subsequent annealing, Mater. Sci. Eng. A 528 (2011) 6694-6701

[103] H.Wang, Y.EstrinZ, and Zúberová, "Bio-corrosion of a magnesium alloy with different processing histories", Materials Letters, vol. 62, pp. 2476-247915, June (2008).

[104]Bo Song, Renlong Xin, Gang Chen, Xiyan Zhang, Qing Liu, Improving tensile and compressive properties of magnesium alloy plates by pre-cold rolling Author links open overlay panel" Scripta Materialia Volume 66, Issue 12, June 2012, Pages 1061-1064.

[105] Seyed Mohammad Arab, Abbas Akbarzadeh, On the cold rolling of AZ31 Mg alloy after Equal Channel Angular Pressing. Journal of Magnesium and Alloys Volume 2, Issue 3, September 2014, Pages 203-207

[106] Sean Johnston, Zhiming Shi, Andrej Atrens, The influence of pH on the corrosion rate of high-purity Mg, AZ91 and ZE41 in bicarbonate buffered Hanks' solution Corrosion Science Volume 101, December 2015, Pages 182-192

[107] Sultan Alsagabi, Jakraphan Ninlachart, Krishnan S. Raja & Indrajit Charit . Passivity and Localized Corrosion of AZ31 Magnesium Alloy in High pH Electrolytes. Journal of Materials Engineering and Performance volume 25, pages2364–2374 (2016)

[108] Ebrahim Tolouie and Roohollah Jamaati. Effect of asymmetric cold rolling on the microstructure, texture, and mechanical properties of the AZ91 alloy. Materials Research Express, Volume 6, Number 3. 2018.

[109] Cancan Liu, Hui Zheng, Xin Gu , Bailing Jiang , Jun Liang, Effect of severe shot peening on corrosion behavior of AZ31 and AZ91

magnesium alloys. Journal of Alloys and Compounds Volume 770, 5 January 2019, Pages 500-50

[110] R Vaira Vignesh, R Padmanaban & M Govindaraju , Study on the corrosion and wear characteristics of magnesium alloy AZ91D in simulated body fluids. Bulletin of Materials Science volume 43, Article number: 8 (2020)

[111] Ebrahim Tolouie, Roohollah Jamaati. Effect of rolling reduction on the microstructure, texture, and mechanical behavior of AZ91 alloy. Journal of Materials Research and Technology Volume 26, September–October 2023, Pages 7947-7957

[112] Ming-Tarng Yeh, Ching-Tang Chang, Jian-Yih Wang and Hsin-Chih Lin, "Mechanical Properties & Material Processing of Magnesium aluminum Alloys", Amli Materials Technology Co. LTD. Taiwan, November 9, (2012).

[113] Bensu Tuncaa , E.Erkan Aşıkb , G.İpek Nakaş c , Şakir Bord " Recrystallization of AZ31 Alloy" Middle East Technical University, Department of Metallurgical and Materials Engineering, Ankara, Turkey, 2015.

[114] Ju Hyun Won, Hyun Woo Lee, Seok Hong Min, Tae Kwon Ha . Effect of Aging Treatment on Mechanical Properties of Non-Flammable AZ91D Mg Alloy. International Journal of Materials and Metallurgical Engineering Vol:9, No:8, 2015

[115] Litzy Lina Choquechambi Catorceno, Hamilton Ferreira Gomes de Abreu, Angelo Fernando Padilha ‘Effects of cold and warm cross-rolling on microstructure and texture evolution of AZ31B magnesium alloy sheet’ Journal of Magnesium and Alloys Volume 6, Issue 2, June 2018, Pages 121-133

References

[116] Yufeng zheng “magnesium alloys as degradable biomaterials” 2016.

[117] T. Kokubo and H. Takadama, Biomaterials, 2006, 27

[118] R. Cottis and S. Turgoose, NACE International, "Electrochemical Impedance and Noise.

[119] Asma Ghanbari1 · Hassan Jafari2 · Faramarz Ashenai Ghasemi1 Asma Ghanbari1 · Hassan Jafari2 · Faramarz Ashenai Ghasemi1. Wear Behavior of Biodegradable Mg–5Zn–1Y–(0–1)Ca Magnesium Alloy in Simulated Body Fluid. The Korean Institute of Metals and Materials 2019.

[120] Yavuz Kaplan, Role of Reinforcement materials on mechanical and Tribological properties of PTFE composites. The polymer sociely of Korea 2020; 44(4): p 436-444.

[121] G. Ben Hamua, D. Eliezer, L. Wagner, The relation between severe plastic deformation microstructure and corrosion behavior of AZ31 magnesium alloy. Journal of Alloys and Compounds 2009 468(1):222-229.

[122] Y.N. Wang, J.C. Huang, Acta Mater. 55 (2007) 897–905.

[123] S.H. Park, J.H. Lee, H. Yu, J. Yoon, B.S. You, Mater. Sci. Eng. A 612 (2014) 197–201

[124] C. Lv, T. Liu, D. Liu, S. Jiang, W. Zeng, Mater. Des. 33 (2012) 529–533.

[125] A. Chapuis, J.H. Driver, Acta Mater. 59 (2011) 1986–1994.

References

[126] Q. Huo, X. Yang, J. Wang, H. Sun, J. Guo, L. Jiang, Mechanical behavior and deformation mechanisms of AZ31 Mg alloy at liquid nitrogen temperature, Mater. Lett. 109 (2013) 78–82.

[127] X.F. Zhang, G.H. Wu, W.C. Liu, W.J. Ding, Trans. Nonferrous Met. Soc. China (English Ed. 22 (2012) 2883–2890.

[128] Y.B. Chun, C.H.J. Davies, Mater. Sci. Eng. A 556 (2012) 253–259.

[129] G.E. Dieter, Mechanical Metallurgy, SI Metric, McGraw-Hill, London, 1988.

[130] M. Haghshenas, V. Bhakhri, R. Oviasuyi, R.J. Klassen, MRS-Materials Research Society 5 (2015) Pages 513–518.

[131] Weigui Zhang a, Kun Li , Runqiang Chi, Susheng Tan, Peijie Li, Insights into microstructural evolution and deformation behaviors of a gradient textured AZ31B Mg alloy plate under hypervelocity impact. Journal of Materials Science & Technology Volume 91, 20 November 2021, Pages 40-57

[132] Zhiming Shi, Ming Liu, Andrej Atrens, Measurement of the corrosion rate of magnesium alloys using Tafel extrapolation. Corrosion Science Volume 52, Issue 2, February 2010, Pages 579-588

[133] Emmanuel Mena-Morcillo, Lucien Veleva “Degradation of AZ31 and AZ91 magnesium alloys in different physiological media: Effect of surface layer stability on electrochemical behavior” Journal of Magnesium and Alloys Volume 8, Issue 3, September 2020

[134] G.R. Argade, S.K. Panigrahi, R.S. Mishra, Effects of grain size on the corrosion resistance of wrought magnesium alloys containing neodymium, Corrosion Sci. 58 (2012).

[135] N. Birbilis, K.D. Ralston, S. Virtanen, H.L. Fraser, C.H.J. Davies, Grain character influences on corrosion of ECAPed pure magnesium, Corrosion Eng. Sci. Technol. 45 (2010).

[136] L.P. Wang, Y.M. Lin, Z.X. Zeng, W.M. Liu, Q.J. Xue, L.T. Hu, J.Y. Zhang, Electrochemical corrosion behavior of nanocrystalline Co coatings explained by higher grain boundary density, Electrochim. Acta 52 (2007).

[137] G.L. Song, A. Atrens, M. Dargusch, Influence of microstructure on the corrosion of diecast AZ91D, Corrosion Sci. 41 (1999).

[138] R. Ambat, N.N. Aung, W. Zhou, Evaluation of microstructural effects on corrosion behavior of AZ91D magnesium alloy, Corrosion Sci. 42 (2000).

[139] Y.J. Ko, C.D. Yim, J.D. Lim, K.S. Shin, Effect of Mg17Al12 precipitate on corrosion behavior of AZ91D magnesium alloy, Mater. Sci. Forum 419 (2003).

Appendixes

Sample Name: **AZ31** Date of Receipt: 13/02/2022
Description: 1 Date of Evaluation: 13/02/2022

Average Atomic Number: 0.00 Loss of Ignition: 1.0000%

Z	Symbol	Element	Concentration		Abs.Error	
11	Na	Sodium	0.003	%	(0.0)	%
12	Mg	magnesium	92.38	%	(0.0)	%
13	Al	Aluminum	3.25	%	(0.0)	%
14	Si	Silicon	0.08	%	0.046	%
15	P	Phosphorus	> 0.098	%	0.024	%
16	S	Sulfur	0.079	%	(0.0)	%
21	Ca	Calcium	> 0.003	%	0.0087	%
22	Ti	Titanium	0.09	%	(0.0)	%
23	V	Vanadium	0.00089	%	(0.0)	%
24	Cr	Chromium	0.14	%	0.034	%
25	Mn	Manganese	0.15	%	0.11	%
26	Fe	Iron	0.004	%	0.067	%
27	Co	Cobalt	0.065	%	0.033	%
28	Ni	Nickel	0.0942	%	0.024	%
29	Cu	Copper	0.04	%	0.084	%
30	Zn	Zinc	1.23	%	(0.0)	%
40	Zr	Zirconium	< 0.050	%	(0.0)	%
41	Nb	Niobium	< 0.00371	%	(0.0)	%
42	Mo	Molybdenum	< 0.07	%	0.32	%
47	Ag	Silver	0.057	%	0.11	%
48	Cd	Cadmium	> 0.033	%	0.079	%
50	Sn	Tin	0.09	%	0.077	%
51	Sb	Antimony	0.092	%	0.12	%
74	W	Tungsten	< 0.0072	%	(0.0)	%
82	Pb	Lead	0.89	%	0.064	%

Sum of concentration 99.00 %

Sample Name: **AZ91**
Description: 2

Date of Receipt: 13/02/2022
Date of Evaluation: 13/02/2022

Average Atomic Number: 0.00
Loss of Ignition: 1.0000%

Z	Symbol	Element	Concentration		Abs.Error	
11	Na	Sodium	0.003	%	(0.0)	%
12	Mg	magnesium	87.34	%	(0.0)	%
13	Al	Aluminum	< 9.3	%	(0.0)	%
14	Si	Silicon	0.01	%	0.045	%
15	P	Phosphorus	> 0.04	%	0.024	%
16	S	Sulfur	> 0.0965	%	0.0071	%
22	Ti	Titanium	0.0044	%	0.011	%
23	V	Vanadium	< 0.00080	%	(0.0)	%
24	Cr	Chromium	0.098	%	0.029	%
25	Mn	Manganese	0.1	%	(0.0)	%
26	Fe	Iron	0.004	%	0.058	%
27	Co	Cobalt	0.08	%	0.020	%
28	Ni	Nickel	0.0977	%	0.071	%
29	Cu	Copper	0.025	%	0.25	%
30	Zn	Zinc	< 1	%	(0.0)	%
40	Zr	Zirconium	< 0.013	%	(0.0)	%
41	Nb	Niobium	< 0.0043	%	(0.0)	%
42	Mo	Molybdenum	0.19	%	0.28	%
47	Ag	Silver	0.159	%	0.057	%
48	Cd	Cadmium	> 0.206	%	0.033	%
50	Sn	Tin	0.08	%	0.067	%
51	Sb	Antimony	0.08	%	0.096	%
74	W	Tungsten	< 0.0063	%	(0.0)	%
82	Pb	Lead	0.062	%	0.054	%

Sum of concentration 99.00 %

		Sample ID	Mg:FlameCont Actual	Mg:FlameCont Actual C
1	1	AZ31	248.158	ppm
2	2	AZ31 5%	227.202	ppm
3	3	AZ31 10%	252.040	ppm
4	4	AZ31 15%	258.433	ppm
5	5	AZ31 17%	248.957	ppm
6	6	AZ91	125.736	ppm
7	7	AZ91 5%	141.952	ppm
8	8	AZ91 10%	111.700	ppm
9	9	AZ91 15%	140.231	ppm

الخلاصة

المواد المعدنية القابلة للتحلل ذات أهمية خاصة في التطبيقات الطبية. ان اختيار المغنيسيوم كأحد المواد الحيوية المستقبلية يرجع إلى خصائص الميكانيكية، والوزن المنخفض، ومعامل المرونة الأقرب للعظام والتوافق الحيوي. مع الجسم البشري.

يشمل هذا البحث دراسة تأثير العمل على البارد (الدرفلة) على التآكل في بيئة محاكيه للبيئة الحيوية وكذلك خصائص البلى لسبائك المغنسيوم (AZ31)و(AZ91) .

تبدأ الدراسة بأول خطوات العمل عن طريق تسخين العينات إلى (250 و400 درجة مئوية) لمدة ساعة ثم تبريدها في الفرن. ثم تتم عملية الدرفلة للعينات بنسب مختلفة (5%، 10%، 15%، 17%). وبعدها تمت عملية تحليل البنية المجهرية للعينة باستخدام المجهر الضوئي والمجهر الالكتروني لملاحظة تأثير الدرفلة على البارد على البنية المجهرية.

تم كذلك إجراء اختبار مقاومة البلى للعينات؛ حيث تم هذا الاختبار عن طريق الانزلاق على سطح العينات في سائل الجسم المحاكي (SBF) .

يتحقق اختبار التآكل الحيوي للعينات عن طريق غمر العينات في سائل الجسم المحاكي (SBF) وقياس قيمة معدل التآكل لكل عينة عن طريق اختبار تافل، والتحليل الطيفي للمقاومة الكهروكيميائية (EIS) ، ودرجات الأس الهيدروجيني ، وتحرر الهيدروجين ، وتحرر الأيونات ، و اختبار الاستنبات البكتيري.

أظهرت نتائج اختبار التآكل أن مقاومة التآكل للعينات الاساسية كانت الأقل مقارنةً بالعينات المدرفلة على البارد. أظهرت نتائج اختبار التآكل قيمة عالية لمعدل التآكل للعينة الأساس مقارنة مع قيمة معدل تآكل منخفضة للعينات المدرفلة على البارد لسبائك AZ91 ، في حين أن قيمة معدل التآكل منخفض للعينة الأساس مقارنة مع قيمة معدل التآكل لعينات المدرفلة على البارد لسبائك AZ31.

وزارة التعليم العالي والبحث العلمي

جامعـــــــــــــــة بابـــــــــل

كليـــــــة هندســـــــة المـــواد

قســـــــــم هندســـــــة المعـادن

تأثير التشكيل على البارد على سلوك التآكل والبلى لسبيكة المغنيسيوم الحيوية

رسالة

مقدمة الى قسم المعادن في كلية هندسة المواد / جامعة بابل

وهي جزء من متطلبات نيل درجة الماجستير في

هندسة المواد / المعادن

من قبل

زيد علي هادي عباس

(بكالوريوس هندسة معادن -2003)

بإشراف

أ. د زهير طالب خليف

2023/م 1444/هـ